4-23-2014

The Ionothermal Syntheses of Metal Thiophosphates

Grant Christian Bos Alexander
Lake Forest College, alexagc@lakeforest.edu

The Ionothermal Syntheses of Metal Thiophosphates

Abstract
The development of new materials is integral for the advancement of science and technology. However, before new materials can be applied, they must be synthesized and characterized. Here, the synthesis and characterization of five novel metal thiophosphates of Ni, Cr, Mo, and Mn are presented: $[EMIM]_2[Ni^{II}(P_2S_8)_2]$ and $[EMIM]_3[Ni^{II}(P_3S_9)(P_3S_9)]$ (EMIM = 1-ethyl-3-methyl- imidazoilum), $[EMIM]_3[Cr^{III}(P_3S_9)_2]$, and $[EMIM]_2[M(P_2S_8)_2]$ ($M = Mn^{II}$, Mo^{II}). The synthesis of a new salt of the thioselenate anion, $[P_2Se_8]^{2-}$, is also reported. Additionally, the computational characterization and simulation of the infrared spectra of the nickel thiophosphates $[EMIM]_7[(NiP_3S_8)_4(PS_4)]$, $[EMIM]_4[Ni^{II}(P_3S_9)_2]$, $[EMIM]_2[Ni^{II}(P_2S_8)_2]$, $[EMIM]_3[Ni^{II}(P_3S_9)(P_3S_9)]$ is given.

Document Type
Thesis

Distinguished Thesis
yes

Degree Name
Bachelor of Arts (BA)

Department or Program
Chemistry

First Advisor
Jason A. Cody

Second Advisor
Dawn C. Wiser

Third Advisor
Michael M. Kash

Keywords
novel metal thiophosphates, synthesis, salts

Subject Categories
Chemistry

LAKE FOREST COLLEGE

Senior Thesis

The Ionothermal Syntheses of Metal Thiophosphates

by

Grant Christian Bos Alexander

April 23rd, 2014

The report of the investigation undertaken as a
Senior Thesis, to carry one course of credit in
the Department of Chemistry

Michael T. Orr Krebs Provost and Dean of the Faculty	Jason A. Cody, Chairperson
	Dawn C. Wiser
	Michael M. Kash

Abstract

The development of new materials is integral for the advancement of science and technology. However, before new materials can be applied, they must be synthesized and characterized. Here, the synthesis and characterization of five novel metal thiophosphates of Ni, Cr, Mo, and Mn are presented: $[EMIM]_2[Ni^{II}(P_2S_8)_2]$ and $[EMIM]_3[Ni^{II}(P_3S_9)(P_3S_9)]$ (EMIM = 1-ethyl-3-methyl-imidazoilum), $[EMIM]_3[Cr^{III}(P_3S_9)_2]$, and $[EMIM]_2[M(P_2S_8)_2]$ ($M = Mn^{II}$, Mo^{II}). The synthesis of a new salt of the thioselenate anion, $[P_2Se_8]^{2-}$, is also reported. Additionally, the computational characterization and simulation of the infrared spectra of the nickel thiophosphates $[EMIM]_7[(NiP_3S_8)_4(PS_4)]$, $[EMIM]_4[Ni^{II}(P_3S_9)_2]$, $[EMIM]_2[Ni^{II}(P_2S_8)_2]$, $[EMIM]_3[Ni^{II}(P_3S_9)(P_3S_9)]$ is given.

To the Chemistry Department for fostering my curiosity;

to Dr. Cody for his direction and patience;

to those who lent their support;

Katelyn, Trevor, Dr. Fischer,

Thank you

Table of Contents

Chapter 1: Introduction

The advancement of science and technology depends upon the development and implementation of materials that exhibit useful properties. Once prepared and understood, these materials can then be applied in devices to expand and augment our ability to build, compute, produce, generate electrical energy, etc. Therefore, the research and discovery of such materials is of both of great importance and interest to physicists, material scientists, and chemists alike. Discoveries such as the semiconductor spurred the information age and the explosion of ever-smaller portable electronic devices such as tablets and smartphones.[1] Now there is an ever-growing interest in ever-smaller quantum computing that demands new materials to facilitate the requisite complex interactions needed for the next "quantum" leap in technology.[1] Similarly, the emergence of high-efficiency photovoltaic and thermoelectric materials has promised a future of green energy, generating great interest in developing new and more efficient materials for solar and thermal energy harvesting.[1]

However, it is not only the materials for electronics and renewable energy (Figure 1.1) that have gathered momentum. Novel syntheses of new magnetic materials, gas storage solids, catalysts, superconductors, and nanoparticles have all developed significantly in the 21st century to the point that it seems that when a material of a certain character is required there is little that stands between the initial desire and the acquisition -- only time and funding.[1]

Figure 1.1. Examples of novel materials that have been instrumental in the development of science and technology. A) silicon wafer. B) photovoltaic cell. C) thermoelectric cell.

Unfortunately, effortlessly designing a specific material with a desired property is not a reality. There is much more complexity in the chemistry, synthesis, and the composition of a material needs to be understood in order to have the "on-demand" materials of tomorrow.

Materials, and specifically crystalline materials, are all composed of unit cells; the single repeating unit of the solid that is characterized by size, shape, symmetry, and contents. These unit cells can contain both individual atoms and molecules depending on the complexity of the material at hand. They are the repeating structure of the solid that continues infinitely in all directions. Even the smallest crystal of NaCl visible to the naked eye (a cube of dimensions 0.1 mm) contains over 5 quadrillion unit cells. With the advent of X-ray crystallography (XRD) chemists were able probe at the chemical composition of materials, from the unit cell of simple table salt (Figure 1.2a), to the atomic structures of the silicon wafer (Figure 1.2b), or the more complicated materials that will be discussed in a following section.

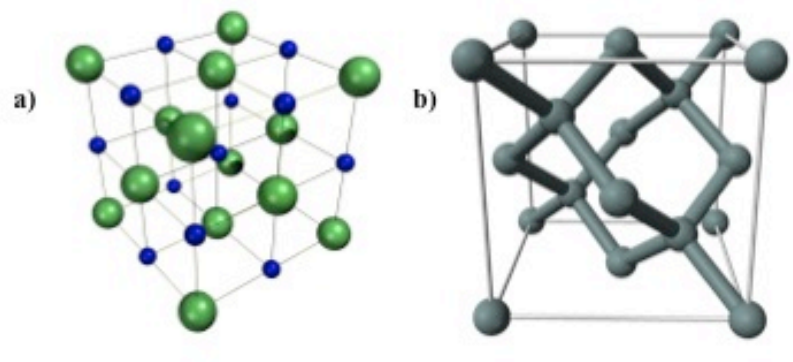

Figure 1.2. **a**) The unit cell of NaCl (Key: Cl; green. Na; blue) **b**) The unit cell of a silicon crystal with adamantine structure (Key: Si; gray)

When speaking of materials on the molecular level, they are better referred to as extended solids. Extended solids, like pure Si or NaCl, can be best considered as very large single molecules even though they are defined as discrete repeating units. The discrete unit cells that are defined by XRD only describe the most basic repeating unit. When developing materials, this discrete and infinite nature of extended solids adds a significant layer of difficulty for preparing new compounds at the atomic level. The coordination environment of reagents must be controlled consistently to form products large enough to observe and characterize.

As the ability to "look" inside materials using XRD to see the chemical composition of materials was established in the early 20th century, other routes of materials development dependent on already existing products were being explored. With the increase in computing power over the last decade, simulations of the chemistry of materials to elucidate novel properties by using computational chemistry are slowly becoming more viable.[1] These simulated materials can then be synthesized in a laboratory and characterized by XRD and other means to assess whether or not the established theories have correctly predicted the chemistry of the material, thereby demonstrating the theoretically driven route to material

discovery and development. This computational element of the field of chemistry has consistently grown in both use and applicability since its advent, but is still limited by breadth of chemical understanding as theory continues to develop. It is in this gap that the continued synthesis of new materials remains a foundation of the development of new chemical theories.

Synthetic chemistry, specifically exploratory synthetic chemistry, strives to discover new properties by the convention of "make then measure," where novel materials are prepared and the properties are then characterized. While not as theory-driven as the method of "simulation then synthesis," the benefits of "make then measure" lie in the circumvention of the limitations of established theory, allowing for serendipity in the discovery of new materials that can lead to the observation of unpredicted, desirable properties. This thesis is based upon this principle, and demonstrates both the use of new synthetic techniques and the discovery of new materials.

Materials and Properties

While materials have already been described in general, there are a wide variety of crystalline materials that are under investigation for their novel and useful properties. The general understanding of these materials, including zeolites, coordination polymers, metal-organic frameworks, and polyoxometallates, is helpful in understanding the overall goal of this thesis.

Zeolites

Zeolites are a class of aluminosilicate anions that have the representative composition of $Al_xSi_yO_z$ stabilized by group I and II cations.[2] Zeolites are a class of extended solids that do not form discrete molecular units, instead forming large expanded structures that include their most notable feature as shown in Figure 1.3: their open channels. Being porous allows zeolites to selectively adsorb many different molecules such as H_2O, CO_2, methanol, and other hydrocarbons.[2]

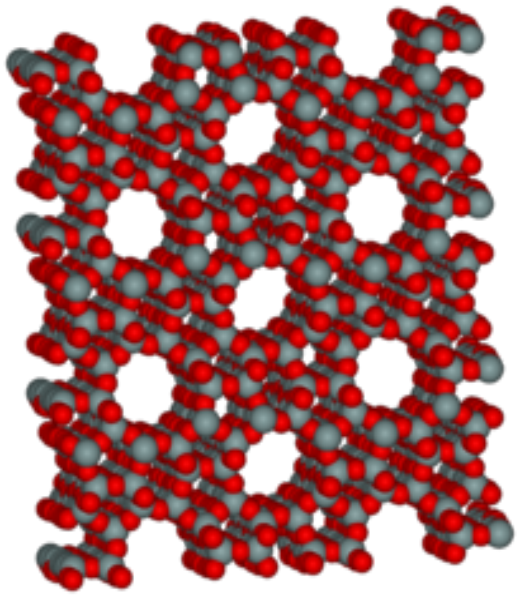

Figure 1.3. A simplified structural representation of the synthetic ZSM-5 zeolite $Na_n[Al_nSi_{96-n}O_{192}]\cdot 16H_2O$ (n <27) used for catalysis (Key: Al,Si; gray, O; red). Na and H_20 are not shown. Note the pores within the extended structure that can accommodate the reaction materials.

Within zeolites, the aluminum and silicon ratios also vary quite widely and these variations also play a large role in the properties of the material.[3] A greater amount of Al present in a zeolite facilitates greater hydrophilicity; however if the synthetic zeolite is Si-rich the resulting zeolite is hydrophobic.[3] Hydrophobic zeolites are already being used for their ability to adsorb organic solvents and volatile chlorinated hydrocarbons.[2] Hydrophilic zeolites are commonly seen as laboratory

desiccants and drying agents.[3] Additionally, zeolites such as ZSM-5 are highly catalytically active when coordinated cations are displaced by protonation, where the channels lead to the catalytic reduction of methanol into longer alkanes, alkenes, and aromatic compounds.[3] The catalytic and adsorptive properties of zeolites remain a great interest and are continually being developed.[1]

Coordination Polymers

Like zeolites, coordination polymers (CPs) are large, extended molecular frameworks that rely on metal-ligand coordination as the main structure-determining agent.[4] CPs are diverse in composition, as both metal and ligand can be varied in composition to include metals such as Fe,[5] Ni,[6] Cu,[7] Cd,[8] and many others. Ligands, the organic portions of the framework, are also diverse ranging from simple diatomic molecules such as cyanide anions to larger aromatic groups of biphenyls and bipyridines.[4] As seen in Figure 1.4, CPs are also able to accommodate other molecules in their porous frameworks, where the size of these pores can be augmented by the size of the bridging ligands between metal atom sites. Like zeolites, this was then exploited to adsorb various gases.[4] While this is a notable property, CPs gain most of their importance from their "metamorphosis" into 3D metal-organic frameworks.[4]

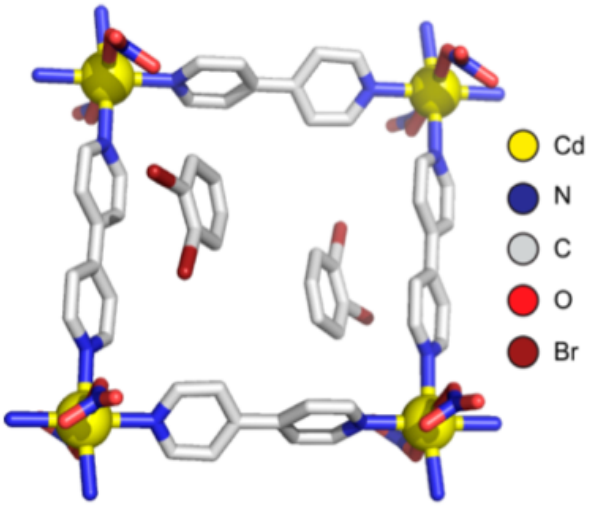

Figure 1.4. The repeating unit of the coordination polymer [Cd(4,4'-bpy)$_2$(NO$_3$)$_2$] (bpy = bipyridine) with *o*-dibromobenze as an example of an accommodated molecule.[4,8]

Metal-Organic Frameworks

The progression from the discovery of coordination polymers is the metal-organic framework (MOF). MOFs are large extended solids that have a wide array of notable properties in addition to the gas adsorption of CPs.[4] Like CPs, MOFs are based around the interaction between transition metals such as Zn, Mn, and Cu and organic ligands, but they differ in the nature as the metal centers being polyatomic clusters such as ZnO$_4$ rather than single atoms (see Figure 1.5).[9] MOF porosity is significantly more permanent than CPs as framework stability is greatly facilitated by the bridging organic ligands between large centers.[9] Their properties are rather adaptable to include energy storage,[10] chemical sensing,[11] and chemical purification.[12] With the adaptability in polyatomic metal center composition MOFs have also been synthesized to contain catalytic sites that, in tandem with the adjustable porosity based on ligand size, allow for size-, shape-, stereo-, and chemically-exclusive catalysts.[13]

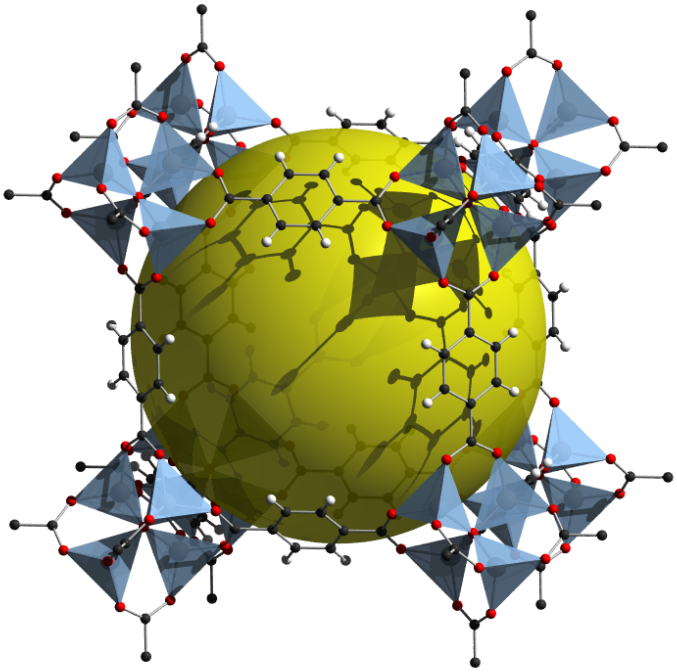

Figure 1.5. The simplest representation of the MOF $Zn_4O(BDC)_3$ (MOF-5). (BDC = 1,4-benzenedicarboxylate) The large yellow sphere demonstrates the porous area of the structure. Zn atoms are contained within the blue tetrahedra. (Key: O; red. C; gray. H; white.)[14]

Polyoxometalates

Deviating from the extended structures of the coordination polymers and MOFs, polyoxometalates (POMs) are discrete anionic metal-oxygen clusters.[15] POMs are based upon blocks of MO_x polyhedra where M = V, Mo, or W in a high oxidation state of 4+ to 6+.[15] Figure 1.6 shows a simple POM $[PW_{12}O_{40}]^{3-}$ as a discrete anion, that is composed of twelve octahedrally coordinated tungsten atoms surrounding a centrally located, tetrahedral phosphorus atom.[16] POMs are similar to the metal complexes as seen in MOFs, however they are not seen as MOF subunits, but occasionally as catalysts inserted into the MOF framework.[17,18] Beyond catalytic activity, POMs are also found active in magnetic materials[19,20], electrochemistry[21], and medicine[22,23].

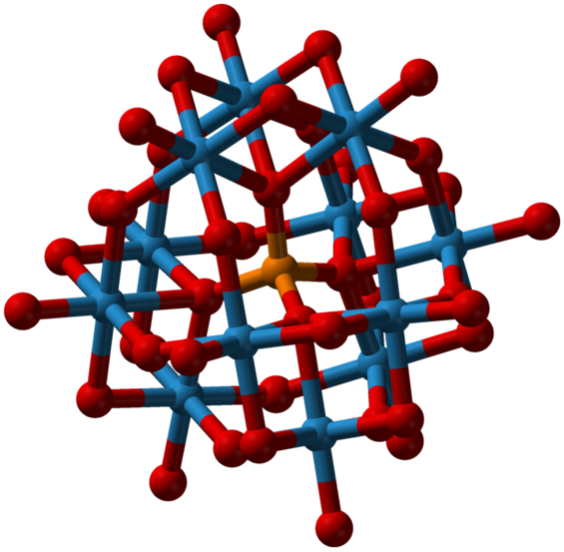

Figure 1.6. The POM anion $[PW_{12}O_{40}]^{3-}$. Note the octahedral coordination environment of all W atoms and the tetrahedral coordination of P at the center. (Key: P; orange. W; blue. O; red)[16]

Synthetic Methods

While the structure of a material is a fundamental part of its character, the route by which it was synthesized is also of great importance because of the constraints and possible reactivity of the product. Additionally, not all materials can be approached with the same synthetic method, thus leading to the relative diversity of methods used today. Moreover, the development of both more economically viable and environmentally friendly approaches to synthesis are desirable for lower temperature synthesis, solvent recycling, and/or the possibility of successive batch syntheses.

The most basic of synthesis methods for materials is that of high temperature synthesis, requiring the combination of reagents together under high heat to facilitate atomic diffusion throughout the melting solid reagents and thereby generate new products.[1] High-temperature synthesis allows for little control other

than thermodynamic; the most stable product is always favored. However, the inclusion of metal fluxes expands the more traditional method by conducting syntheses in primarily inert molten metals such as Al, Ga, Ir, Sn, or Pb to allow for both thermodynamic and kinetic control.[1] Similarly, molten salt methods also allow for reactive flux-like control of kinetics and thermodynamics, but added the ability for salt inclusion into the product allowing for further variation in the synthetic method with the wide range of salts available for use.[1]

As the methods of high-temperature, metal flux, and molten salt synthesis evolved to generate numerous new compounds, there were other lower-temperature routes that were desirable for greater control of reaction conditions. Using water, hydrothermal methods were developed demanding high-pressure vessels that could withstand the vapor pressures exerted during mild syntheses over 100°C. The lower temperatures allow for greater thermodynamic and kinetic control beyond what is offered by high-temperature methods. Additionally, significant pressures were exerted upon the reaction system within the synthesis to allow for additional measures of control and variability within the hydrothermal experiment. Unsurprisingly, this method was then adapted for use with other common solvents to develop solvothermal methods that allow for solvent choice to add an additional structure-determining factor to possible synthetic products.

Ionic Liquids

Ionic liquids, first reported as early as 1914,[24] have developed significantly since in the last twenty years with the growth of interest in their novel properties and their promising uses in synthesis.[25] Ionic liquids (ILs), or more specifically, room-temperature ionic liquids (RTILs), are defined as semi-organic molecular salts that are liquids below 298K at 1 atm.[26] RTILs are known for high thermal stability, wide ranges of liquidity, low vapor pressures at moderate temperatures, high boiling points, and adaptability as solvents for many materials and reagents.[26,27]

RTILs are built around a two-fold selection process, one being the organic cation (Figure 1.7), and the other being the organic/inorganic anion (Figure 1.8). There is a wide range of degree of variability in RTILs, the organic cation core selected; the length and composition of the requisite R groups that can further

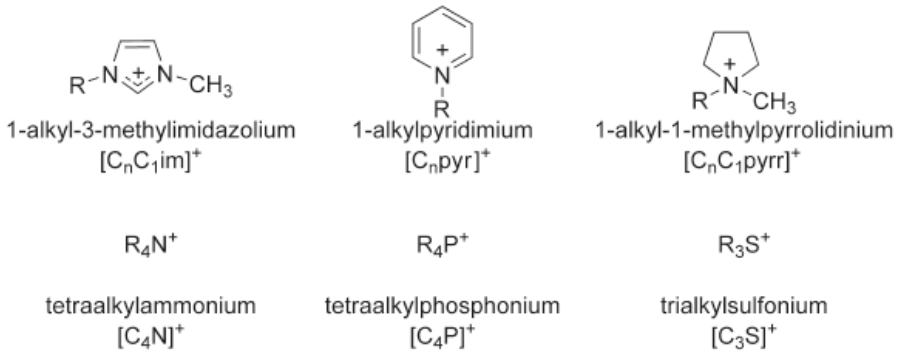

Figure 1.7. A collection of common IL organic cations.[28]

enhance RTIL character. Variations of R group length and composition on many of these common cores has been subject to investigation to examine the how well ionic liquids can be "tuned" to meet desired properties.[29,30,31] Similarly, the anionic portion of the RTIL can also be varied to enhance desired properties depending on

size and anion polarity.[28,31] Between these two variables, RTILs have been adapted for use in many different syntheses and industrial methods.

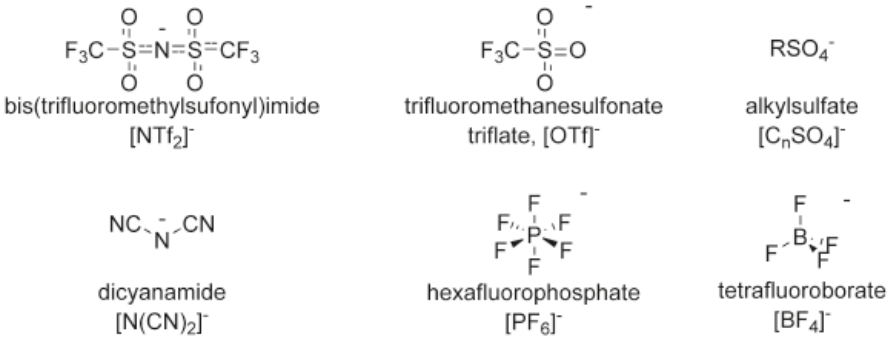

Figure 1.8. A collection of common RTIL organic/inorganic anions.[28]

Advantages and Applications of RTILs in Synthesis

As noted, RTILs have a wide variability in characteristics,high thermal stability, wide ranges of liquidity, low vapor pressures at moderate temperatures, high boiling points, and adaptability as solvents, that can be exploited for use in synthesis and industrial methods. The ability for RTILs to withstand elevated temperatures has allowed for the synthesis of many solids at moderate temperatures (~200^{0}C) with out fear of solvent polymerization or degradation.[28] This lack of degradation and polymerization also give RTILs the possibility to be re-used after products are withdrawn, whereas common organic solvents must be distilled and reclaimed, or worse, evaporated into the atmosphere. Additionally, the vast range of liquidity for RTILs allows for viable liquid phases down to approximately -80°C, further allowing the possible application of ILs as solvents in highly exothermic reactions that can be better controlled at decreased temperatures where common solvents freeze.[32]

While the high temperature stability and liquidity favor the use of RTILs, the real hallmarks of RTIL applicability is evident in their low vapor pressures, high boiling points, and solubility properties.

With conventional solvents, solvothermal methods require the reaction vessels to be increasingly strong as pressure builds up within the vessel as the solvent boils. These vessels are also expensive and difficult to clean and reuse, so the time between successive trials under solvothermal methods is also extended. As RTILs have low vapor pressures below their boiling points, substituting RTILs for the conventional organic solvents has given rise to a new solvothermal method, aptly deemed ionothermal synthesis that circumvents for strong pressure vessel to carry out syntheses as heating RTILs generates little to no vapor. Additionally, the high boiling point of RTILs relative to other solvents allows for greater synthesis temperatures to be reached while still maintaining low-pressure reaction environments.

As the role of high-temperature synthesis was the need to cause diffusion of molecules throughout the reaction melt, ionothermal synthesis employs the ionic and polar natures of ionic liquids to solvate reagents that are often insoluble in conventional polar solvents.[33] This has allowed for a wide range of applicability in the synthesis of previously mentioned materials such as zeolites,[34] coordination polymers,[35,36] metal-organic frameworks,[27,37] and polyoxometalates,[38] Like conventional solvents, the ability for ionic liquids to solvate reagents also increases greatly with heat, further increasing the advantage of employing RTILs for use in synthesis.

Another of the notable uses of RTILs or ILs in synthesis is the nature of the organic cation to act as a structure-determining agent (SDA) of the final product in solution.[27,31] In the case of RTILs, the organic cation can act as both SDA and part of the end product as well, balancing out any anionic charge on the product if the product is indeed anionic. This method has been found useful in the synthesis of porous zeolites, MOFs, and organic-inorganic hybrid structures.[27,31]

The Current Project

The aim of this research is to investigate metal thiophosphate synthesis by ionothermal methods. As the advantages and applications of RTILs in synthesis are already known, they are now being implemented and developed for use in exploratory synthetic inorganic chemistry. Considering that there are many facets of the discipline, chalcogenide (compounds containing S, Se, Sb, Te) synthesis was of interest because of the novel properties of chalcogenides possibly applicable in thermoelectric[39,40] and photovoltaic[41] devices. Of more interest, however, was the possibility of forming zeolite-like materials that could be catalytically active. When chalcogenides are prepared by molten flux routes with phosphorus, common products include structural features such as tetrahedral $[PS_4]^{3-}$ and ethane-like $[P_2S_6]^{4-}$ anions (Figure 1.9).[42] The ionothermal route would provide a new method of attempting thiophosphate synthesis, and was thought to be able to uncover new thiophosphate anions that would otherwise been unseen by conventional synthesis routes.

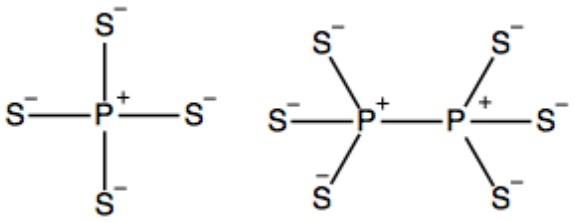

Figure 1.9. The unexciting $[PS_4]^{3-}$ and $[P_2S_6]^{4-}$ thiophosphate anions that are commonly found in molten flux methods.[42]

However, it was not strictly thiophosphate anions that were of great interest upon the project's inception. The simple nickel thiophosphate $KNiPS_4$ was found to be rather interesting due not only to its extended infinite structure of the $[Ni^{II}PS_4]^-$ subunit (Figure 1.10a) where Ni adopts a square planar coordination environment and $[PS_4]^{3-}$ acts as a bridging ligand.[43] More interestingly, when the chains of the $[Ni^{II}PS_4]^{3-}$ were dissolved in N,N'-dimethylformamide (DMF) they passed through a liquid-crystalline phase and ultimately formed cyclic $[Ni^{II}_3P_3S_{12}]^{3-}$ rings that were isolated and characterized as salts of organic cations, (Figure 1.10b).[44]

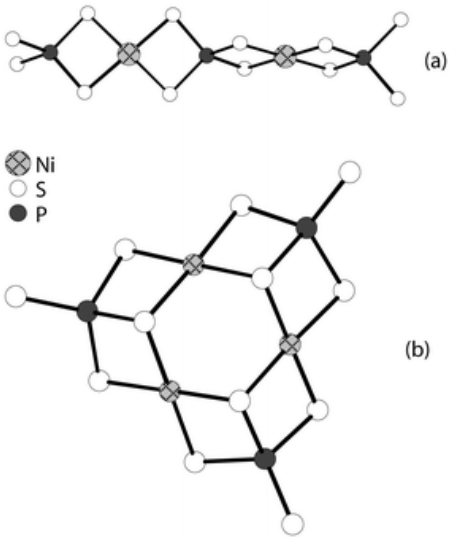

Figure 10. a) The repeating $NiPS_4^-$ anionic units. Note how PS_4^{3-} bridges the square planar Ni^{II} atoms to form the extended string structure. b) the isolated $[Ni_3P_3S_{12}]^{3-}$ anion. Note the square planar coordination environment of Ni^{II} and the tetrahedral coordination of P persist in the ring-like structure as well.[44]

It was these rings that led to the project of investigating the synthesis of new metal thiophosphates using ionothermal routes. RTILs are able to solubilize readily the elemental Ni, P, and S, add an organic cation to allow for product crystallization, and open the door to variation and of the SDA as also governed by the organic cation.[45]

Project Status

Prior to this senior thesis, five previous students worked on this project. From these five, two new thiophosphate compounds, $[EMIM]_7[(Ni^{II}P_3S_8)_4(PS_4)]$ (Figure 1.11a) and $[EMIM]_4[Ni^{II}(P_3S_9)_2]$ (Figure 11b), were isolated from ionothermal syntheses using $[EMIM]BF_4$ (EMIM = 1-ethyl-3-methyl-imidazoilum) and the requisite elements. $[EMIM]_7[(Ni^{II}P_3S_8)_4(PS_4)]$ was first isolated as fine black needles in 2007 and was incredibly difficult to recreate.[46] In subsequent attempts of recreation, the method of RTIL synthesis was investigated to find a new synthesis route, molar ratios of the Ni : P : S were varied, and the RTIL was varied.[47,48,49] In 2011 the other nickel thiophosphate salt, $[EMIM]_4[Ni^{II}(P_3S_9)_2]$, was discovered in the continued attempt to recreate the original $[(Ni^{II}P_3S_8)_4(PS_4)]^{7-}$ anion.[50]

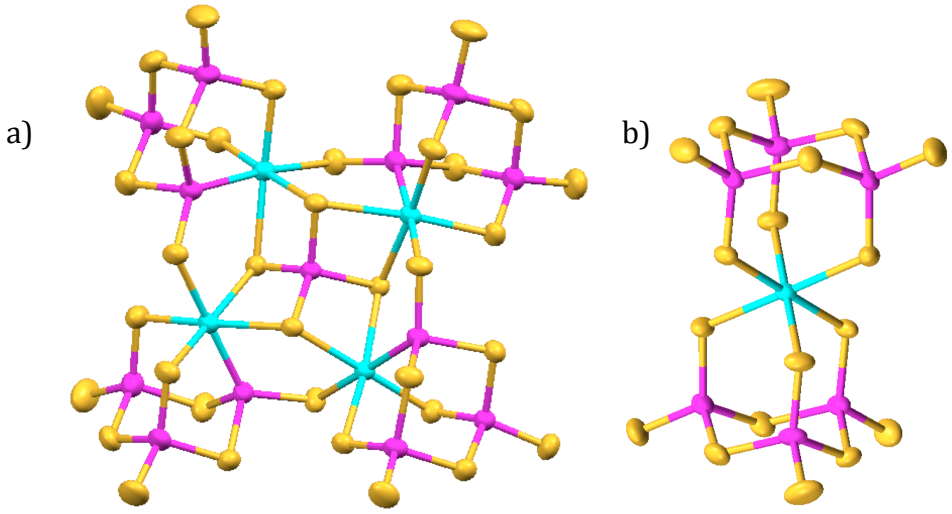

Figure 1.11. a) The isolated $[(Ni^{II}P_3S_8)_4(PS_4)]^{7-}$ anion. b) The isolated $[Ni^{II}(P_3S_9)_2]^{4-}$ anion. (Key: Ni; cyan. P; Pink. S; yellow)[45,46,50]

This senior thesis presents the synthesis and characterization of five novel metal thiophosphates of Ni, Cr, Mo, and Mn; $[EMIM]_2[Ni^{II}(P_2S_8)_2]$ and $[EMIM]_3[Ni^{II}(P_3S_9)(P_3S_9)]$ (see Chapter 3), $[EMIM]_3[Cr^{III}(P_3S_9)_2]$ (see Chapter 4), and $[EMIM]_2[M(P_2S_8)_2]$ (M = Mn^{II}, Mo^{II}) (see Chapter 6) using the RTILs. The ionothermal synthesis of the known $[P_2Se_8]^{2-}$ anion is reported in Chapter 5. Additionally, the infrared characterization and simulation of the nickel thiophosphates $[EMIM]_7[(NiP_3S_8)_4(PS_4)]$, $[EMIM]_4[Ni^{II}(P_3S_9)_2]$, $[EMIM]_2[Ni^{II}(P_2S_8)_2]$, $[EMIM]_3[Ni^{II}(P_3S_9)(P_3S_9)]$ is investigated to determine thiophosphate stretches in Chapter 7. Chapter 8 presents a summary of the major research discoveries and proposes possible future steps for this project.

Chapter 2: Reaction Setup, Synthetic Scheme & Product Characterization

As this thesis presents a number of different compounds that have been synthesized and characterized by similar methods, this chapter serves as the general experimental procedure for each of the following chapters (3 - 7). The specifics of reaction, procedure, and characterization will be described within the product chapter as necessary.

Reaction Preparation

Synthesis of RTIL [EMIM]BF_4

[EMIM]BF_4 was synthesized according to the literature.[51] (Scheme 2.1)

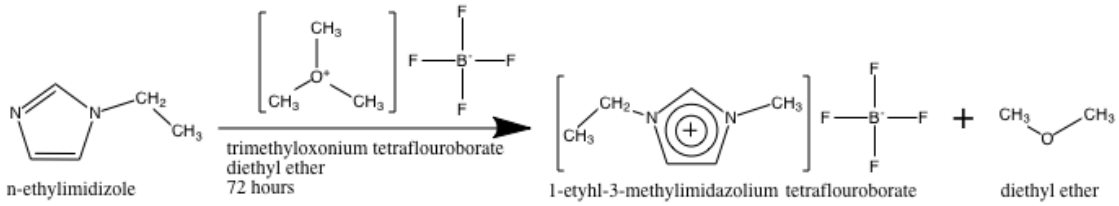

Scheme 2.1. The synthesis of [EMIM]BF4

A volume of 80 ml of anhydrous diethyl ether was added to a 250 mL three-neck round bottom flask suspended in an ice bath over a stir motor. To the central neck of this flask a water condenser capped with stopcock valve with a hose to a vacuum / nitrogen line was attached; a thermometer was inserted in the left neck to monitor reaction temperature. A stir bar was added to the flask. A rubber septum cap was loosely placed in the remaining neck. A gentle flow of nitrogen was sent through the system to lessen reagent oxidation.

Prior to November 14th, 2013, only 13 mL of n-ethylimidazole (EIM) was added to the stirring diethyl ether though the right neck via autopipet, followed by 20 g (typically two 10 g bottles) of [OMe_3]BF_4 added slowly by spatula to limit the relative exothermic nature of the methylation reaction (Scheme 2.1) and reduce

dimethylation. After 11/14/13 when new 25 g bottles of $[OMe_3]BF_4$ were acquired, it was found that the all the reactions prior had been adjusted to have EIM as the limiting reagent instead of the volatile $[OMe_3]BF_4$. This was corrected for a 1.2 : 1 molar ratio of EIM to $[OMe_3]BF_4$ for 19 mL EIM to 25 g of $[OMe_3]BF_4$. These reactions had noticeably more yield than reactions of previous molar ratios as expected.

Following complete $[OMe_3]BF_4$ addition, the ice bath was removed, the water condenser and the nitrogen flow were stopped. The solution was stirred for 72 hours, with the longer stirring time yielding marginally more product. After stirring, two transparent, immiscible layers were seen: a layer of the clear, colorless diethyl ether and another of the lightly yellow product. Using a separatory funnel the $[EMIM]BF_4$ was isolated and washed with four aliquots of approximately 20 mL of anhydrous diethyl ether. The resultant $[EMIM]BF_4$ was transferred to a Schlenk flask and evacuated on the vacuum line equipped with liquid nitrogen trap to remove the a majority of the remaining diethyl ether. Warm water was used to facilitate this process once significant amounts of bubbling had stopped. Once bubbling had ceased, the flask was backfilled with nitrogen, closed, and transferred to a vacuum oven where further removal of diethyl ether and water was conducted in at 120 °C under vacuum for 24 - 72 hours. While in the oven the flask was opened. The oven was then backfilled with nitrogen and Schlenk flask with product quickly removed and closed. Upon returning to the laboratory, the flask was once again evacuated and backfilled with nitrogen.

The resultant [EMIM]BF_4 occasionally appeared slightly darker after the vacuum oven treatment. It is thought that this is due to slight EMIM polymerization, however, NMR showed little / no evidence of this.

Synthesis of RTIL [EMIM]CF_3SO_3

[EMIM]CF_3SO_3 was synthesized according to the literature.[52] (Scheme 2.2)

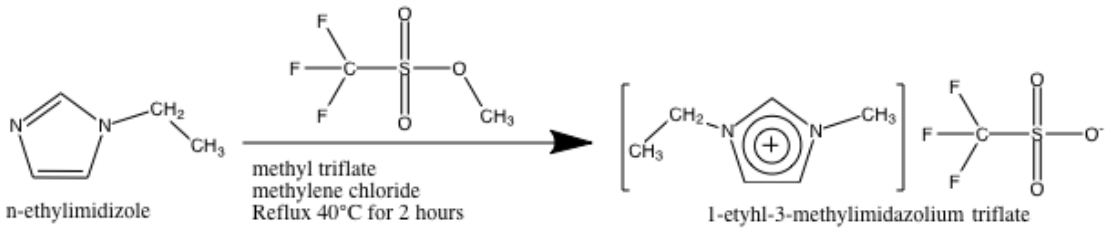

Scheme 2.2. The synthesis of [EMIM]CF_3SO_3

A volume of 60 mL of CH_2Cl_2 was substituted for the now-banned 1,1,1-trichloroethane (due to it being classified as ozone-depleting) found in the literature preparation. The same apparatus was used as in [EMIM]BF_4 synthesis, save for the ice bath being replaced by a heated sand bath. Under nitrogen flow, 5.7 mL of EIM was dispensed into the stirring CH_2Cl_2, followed by a drop-wise addition of 5.0 g of CF_3SO_3Me over 30 minutes to an hour. The addition is very exothermic. Nitrogen flow was stopped and the sand bath set to keep the reaction refluxing at 40 °C for two hours with a glass stopper in the right-neck to prevent vapor escape. After two hours, the contents of the flask were poured into a 150 mL round bottom flask and placed on the rotatory evaporator at to isolate the [EMIM]CF_3SO_3 and recollect the CH_2Cl_2 solvent. The RTIL was then placed in the vacuum oven for 24 hours at a moderate temperature to remove any remaining CH_2Cl_2. The resultant RTIL is a light yellow color and less viscous than the [EMIM]BF_4.

Pre-mixed Elemental Ratios

Pre-mixed elemental ratios were prepared in 1.250 g batches for each experiment in the MBraun Lab Master 130 glove box. In each case the M : P : C (M = metal, P = phosphorus, C = chalcogenide) molar ratio was determined, then the 1.250 g mass proportion of each component was weighed on an analytical balance in the glove box separately and deposited into a mortar. The elements were then ground together using the mortar and pestle until the elemental mixture was visibly homogeneous. Each 1.250 g batch was used for between 8 and 10 trials.

Reaction Vessel Preparation

Reaction tubes were prepared from 1.2 m long Pyrex tubes with a wall width of 2 mm. These tubes were cut into three pieces, and then further halved by methane/oxygen torch into six closed-end tubes. The tubes were not dried before reactions, and an investigation of dried tubes showed no change in product outcome.

General Synthetic Scheme

The reaction scheme is as follows, and is also described in reference 45.

Reaction tubes were labeled and brought into the nitrogen atmosphere MBraun Lab Master 130 glove box. 125.0 mg portions of the appropriate pre-mixed elemental ratio were weighed on the analytic balance and deposited via funnel into the reaction tube. Reaction tubes were then sealed with stoppers and transferred to a nitrogen-filled glove bag that was then purged 4 times with nitrogen before solvent was added. 1250 μL of the appropriate RTIL (as described above) was

dispensed into the reaction tube using an autopipet. The reaction tubes were sealed again by rubber stopper and were removed from the glove bag and were mixed using a vortex mixer. The reaction tubes then were transferred to a vacuum line, evacuated, and sealed using a methane/oxygen torch.

The reactions were carried out in a Precision Scientific model 18EM mechanical convection oven with Therm-O-Watch© Model RS-1200A temperature controller at 150 °C for varying amounts of time. Reactions were then either cooled slowly over a number of days or pulled immediately out of the oven at the appropriate moment. Heating profiles will be provided in the following chapters. A general heating scheme is displayed below in Figure 2.1. After reactions were complete solid products were isolated by vacuum filtration and washed using dry acetone before being stored in a petri dish and placed in a desiccator prior to characterization.

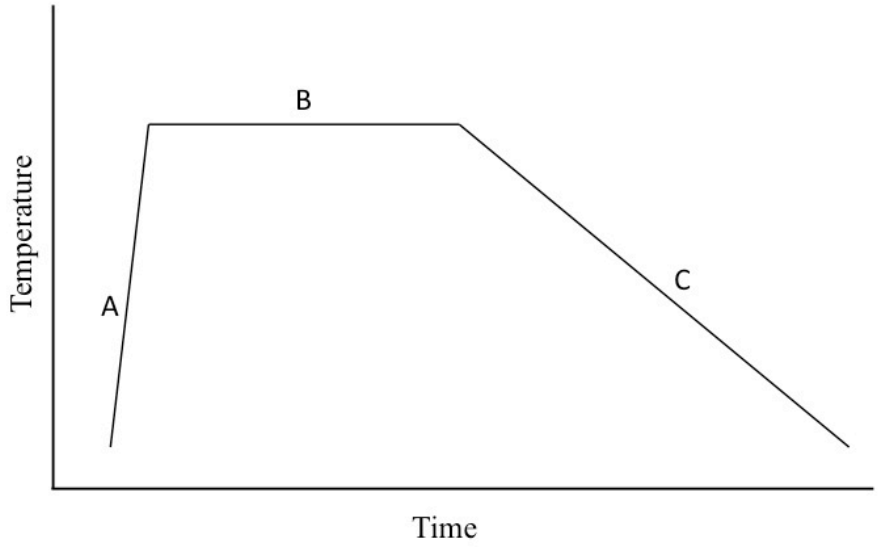

Figure 2.1. General Heating profile for all reaction sets. **A**: Initial ramp time from the room temperature reaction vessels to the hold temperature. **B**: The hold time of the reaction set at 150 °C. **C**: The cooling duration and rate for the given product.

Product Characterization

An essential part of inorganic synthesis is the characterization of the reaction products. Depending on the type of product, there are numerous methods of structure and composition investigation. The project employed a number of methods noted below and data is provided in the corresponding chapters

Single Crystal X-Ray Diffraction (XRD)

XRD was used to evaluate all solid products for structure analysis. Most often, preliminary unit cells were found using Lake Forest College's Enraf Nonius CAD4 Diffractometer. Full data collections for structure solutions were completed at other institutions in Germany, France, and the United States.

Energy Dispersive Analysis by X-Ray (EDAX)

EDAX was completed at Northwestern University's EPIC NUANCE center on a Hitachi S-3400N-II Scanning Electron Microscope (SEM) using double-sided conductive tape on aluminum stubs. EDAX was used to assess the metal content of single crystals to determine the need for XRD or not. M : P : C ratios (experimental; M = metal, C = chalcogenide (S or Se)) were also used to determine the possible product structure relative to known product M : P : C ratios at the time.

Fourier Transform Infrared Spectroscopy (FT-IR)

FT-IR spectroscopy was used for simple Ni^{II} product identification due to characteristic thiophosphate stretching bands in the IR range of 1000 - 400 cm^{-1}. Samples were prepared in KBr disks and analyzed on the Thermo Nicolet Avatar

360 FT-IR spectrometer system. By 2013, a new Thermo Scientific Nicolet iS-50 FT-IR spectrometer with ATR attachment with diamond anvil was available for use and KBr disks were no longer necessary.

^{31}P Nuclear Magnetic Resonance (NMR)

NMR was used to investigate the environments of ^{31}P atoms for one Ni^{II} product. A Varian Inova 400MHz Fourier Transform (FT)-NMR with multinuclear variable-temperature probe was used with deuterated dimethylsulfoxide (DMSO-d_6) as the solvent.

Commercial Elemental Analysis

Ni^{II} compounds were sent to ALS Environmental in Tucson, AZ for carbon, hydrogen, and nitrogen elemental analysis. The reported experimental compositions were then compared to the calculated values for the structures obtained from crystallographic structure determination.

Chapter 3: The Nickel Thiophosphates $[Ni^{II}(P_2S_8)2]^{2-}$ and $[Ni^{II}(P_3S_9)(P_2S_8)]^{3-}$

This chapter reports the discovery of two new nickel thiophosphate anions isolated as salts of the $[EMIM]^+$ cations. Both title compounds were isolated in the summer of 2011 and published in *Inorganic Chemistry* in November of 2012 with two other compounds that were created prior to this senior thesis. See reference 45 or Appendix 1.

$[EMIM]_2[Ni^{II}(P_2S_8)_2]$

Synthesis

Two crystalline forms of the salt $[EMIM]_2[Ni^{II}(P_2S_8)_2]$ were synthesized from several different Ni : P : S molar ratios: both 1 : 6 : 18 and 1 : 4 : 16 in $[EMIM]BF_4$ and both 1 : 6 : 18 and 1 : 3.25 : 9 in $[EMIM]CF_3SO_3$. The general synthesis scheme described in Chapter 2 was used for all reactions. Reaction vessels were heated at 150 °C for 72 hours then dropped to 70 °C as rapidly as possible to continue cooling at 0.5 °C/h down to 20 °C. The product was initially isolated from the 1 : 6 : 18 molar ratios, however isolation of larger amounts of product were accomplished in the direct molar ratio of 1 : 4 : 16 in $[EMIM]BF_4$. Isolated crystals were predominantly the α-form (orange needles) from both RTILs, however with thermal cycling due to power outage, a different packing of the same ions was isolated in a β-form (orange cubes) from $[EMIM]BF_4$. Yield calculated based on Ni recovery gave 44% (62 mg) from $[EMIM]BF_4$ and 35.9% (92.1 mg) from $[EMIM]CF_3SO_3$.

Characterization

XRD. XRD was originally completed using the Enraf Nonius CAD4 to determine the unit cell. The full structure solution for $[EMIM]_2[Ni^{II}(P_2S_8)_2]$ was completed in Germany using Imaging Plate Diffraction System from STOE & CIE using graphite-monochromatic Mo Kα radiation. Figure 3.1 shows the thermal ellipsoid diagram of the novel $[Ni^{II}(P_2S_8)_2]^{2-}$ anion. Details of this full structure solution are given in Table 3.1. Full geometrical elements are shown in Table 3.2.

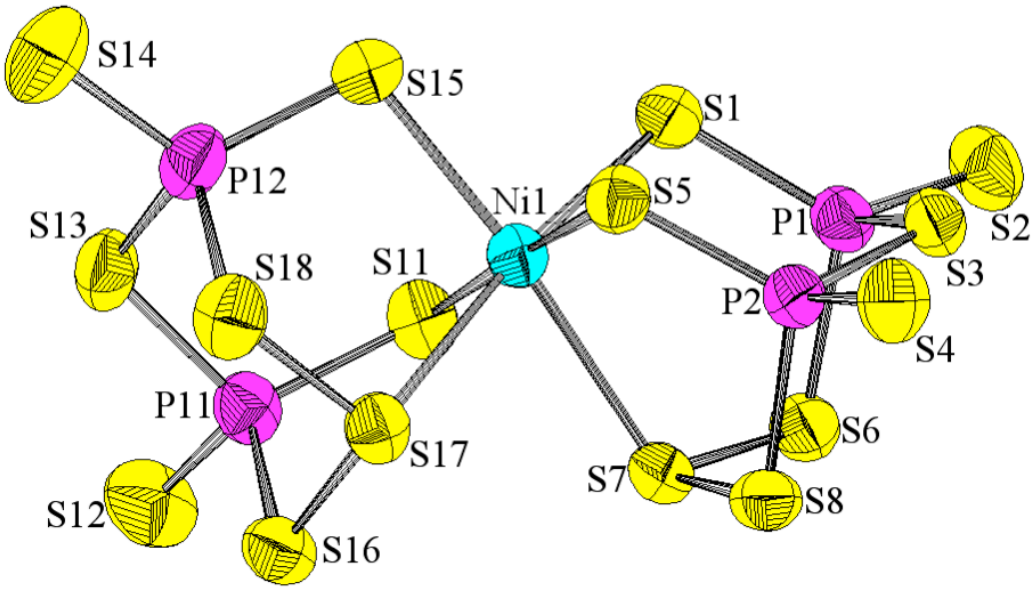

Figure 3.1. Thermal ellipsoid sketch of the $[Ni^{II}(P_2S_8)_2]^{2-}$ anion (Ni: cyan; P: magenta; S: yellow).

Table 3.1. Crystal Parameters for the α- and *β*- forms of $[EMIM]_2[Ni^{II}(P_2S_8)_2]$.

Chemical formula	α-$[EMIM]_2[Ni^{II}(P_2S_8)_2]^{2-}$	β-$[EMIM]_2[Ni^{II}(P_2S_8)_2]^{2-}$
a, Å	22.5477(9)	7.2317(5)
b, Å	7.2491(2)	17.7138(9)
c, Å	24.0143(9)	13.4488(9)
α, °	90	90
β, °	116.410(3)	93.637(8)
γ, °	90	90
V, $Å^3$	2515.9(2)	1719.33(19)
Z	4	2
Formula weight, g mol^{-1}	917.89	917.89
Space group	P $2_1/n$	P 2_1
T, °C	20	–73
l, Å	0.71073	0.71073
D_{calcd}	1.734	1.773
μ, mm^{-1}	1.701	1.739
R1(F_o)	0.0356	0.0478
wR2(F_o^2)	0.0838	0.1194

Table 3.2. Bond Distances (Å) and Angles (°) for the inorganic portion of both crystalline forms of $[EMIM]_2[Ni^{II}(P_2S_8)_2]$.

Chemical formula	α-$[EMIM]_2[Ni^{II}(P_2S_8)_2]^{2-}$	β-$[EMIM]_2[Ni^{II}(P_2S_8)_2]^{2-}$
Ni–S	2.3538(8) – 2.5821(8)	2.3692(19) – 2.5543(15)
P–S	1.9313(12) – 2.1369(10)	1.945(3) – 2.130(2)
S–S	2.0556(11) – 2.0641(11)	2.060(2) – 2.068(3)
Cis S – Ni – S	78.01(2) – 95.34(3)	80.44(5) – 95.90(6)
Trans S – Ni – S	172.82(3) – 177.78(3)	175.94(7) – 176.80(6)
S – P – S	102.94(5) – 118.08(5)	103.50(10) – 119.83(13)
P – S – P	109.89(4) – 110.82(4)	109.94(10) – 110.18(10)
P – S – S	99.64(4) – 101.60(4)	99.85(9) – 101.62(9)
S – S – S	106.20(4) – 106.75(5)	105.19(10) – 106.10(10)

FT-IR. FT-IR on needles isolated from [EMIM]BF: (See Chapter 7 Figure 7.3)

$\tilde{\nu}$(EMIM$^+$) = 960 (w), 916 (w), 798 (w), 772.98 (vw), 699 (w), 667 (sh), 642 (s), 618 (m), 592 (vw), 522 (w) cm^{-1}.

$\tilde{\nu}$([Ni(P$_2$S$_8$)$_2$]$^{2-}$) = 824 (m), 751 (w), 741 (w), 691 (m), 675 (s), 574 (m), 548 (m), 500 (m), 467 (m), 461 (m), 457 (w) cm^{-1}.

FT-IR on needles isolated from [EMIM]CF_3SO_3: (See Chapter 7 Figure 7.3)

$\tilde{\nu}$(EMIM$^+$) = 953 (w), 916 (w), 798 (w), 700 (w), 667 (sh), 644 (s), 618 (s), 596 (vw) cm^{-1}.

$\tilde{\nu}$([Ni(P$_2$S$_8$)$_2$]$^{2-}$) = 825 (m), 751 (w), 741 (w), 690 (m), 676 (s), 575 (s), 548 (m), 502 (m), 468 (m), 463 (m), 457 (w) cm^{-1}.

^{31}P NMR. (400MHz, DMSO–d_6, 20 °C) δ = 82.38 ppm.

Elemental Analysis. Elemental analysis quantities (See Table 3.3.) show reasonable agreement. As the RTIL is rather viscous crystals are difficult to isolate without mild contamination from the RTIL itself, thus C, H, and N values deviate slightly from the expected values.

Table 3.3. Experimental and calculated elemental analysis results for $[Ni^{II}(P_2S_8)_2]^{2-}$.

Analysis	%C	%H	%N
Elemental Analysis	15.3	2.91	5.89
Calculated	15.7	2.42	6.10

Discussion

The novel $[Ni^{II}(P_2S_8)_2]^{2-}$ anion appears in two crystalline polymorphs, α-$[EMIM]_2[Ni^{II}(P_2S_8)_2]$ and *β*-$[EMIM]_2[Ni^{II}(P_2S_8)_2]$, where the anion is isostuctural and bond distances (Table 3.2) compare well to other nickel thiophosphate compounds.[53,54,55] $[Ni^{II}(P_2S_8)_2]^{2-}$ is found as a octahedral Ni^{II} atom with two tridentate 1,3–$(P_2S_8)^{2-}$ ligands chelating to the metal in a *cis* fashion rather than *trans* orientation to give the molecule very low symmetry (C_2). Chelation occurs from the central sulfur of the trisulfide bridge to the metal and two sulfur atoms from each of the two bridged PS_4 groups contained in the moiety.

The 1,3-$(P_2S_8)^{2-}$ anion has previously been reported, first in 1997 as a PPh_4^+ salt then as a ligand to Ti in $[(TiCl_2)(P_2S_8)]_2$ in 2009 where each 1,3-$(P_2S_8)^{2-}$ moiety is tetradentate with coordination from terminal S atoms only; the trisulfide bridge does not participate in coordination.[53]

$\underline{[EMIM]_3[Ni^{II}(P_3S_9)(P_2S_8)]}$

Synthesis

$[EMIM]_2[Ni^{II}(P_3S_9)(P_2S_8)]$ was synthesized from Ni : P : S molar ratios of 1 : 3.25 : 9 in $[EMIM]BF_4$. The general synthesis scheme was used for all reactions. Reaction vessels were heated at 150 °C for 72 hours then quickly dropped to 70 °C in the oven before slow cooling at 0.5 °C/hr down to 20 °C. Isolated crystals were orange hexagonal tubes encasing the RTIL. Yield calculated based on Ni recovery: 38% (115.9 mg).

Characterization

XRD. XRD was completed in the same method that was used for the previous compound, $[EMIM]_2[Ni^{II}(P_2S_8)_2]$. Figure 3.2 shows the thermal ellipsoid diagram of the $[Ni^{II}(P_3S_9)(P_2S_8)]^{3-}$ anion. Details of this full structure solution are given in Table 3.4. Select geometrical elements are shown in Table 3.5.

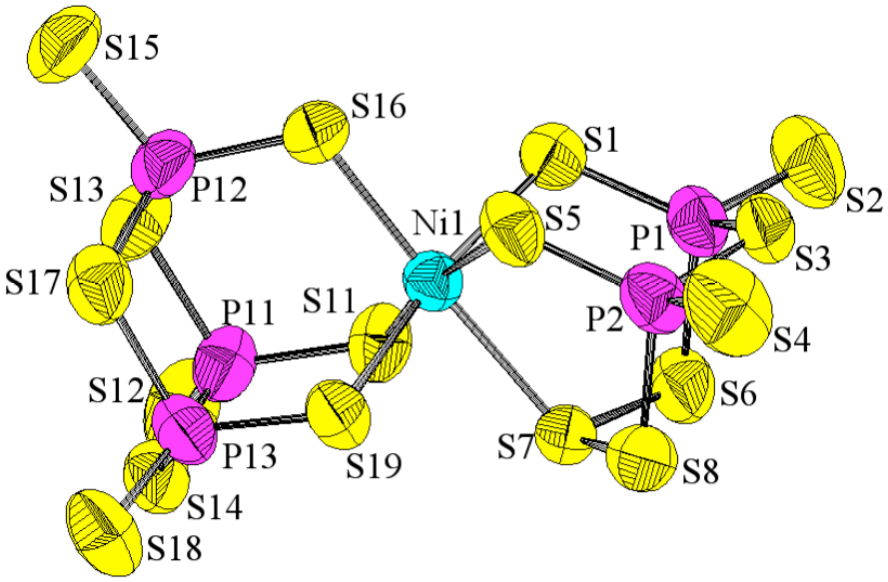

Figure 3.2. Thermal ellipsoid sketch of the $[Ni^{II}(P_3S_9)(P_2S_8)]^{3-}$ anion (Ni: cyan; P: magenta; S: yellow).

Table 3.4. Crystallographic Data for $[Ni(P_3S_9)(P_2S_8)]^{3-}$.

Chemical formula	$[EMIM]_3[Ni(P_3S_9)(P_2S_8)]$
a, Å	11.8394(2)
b, Å	20.0693(3)
c, Å	56.7194(13)
α, °	90
β, °	90
γ, °	90
V, Å^3	13476.8(4)
Z	12
Formula weight, g mol^{-1}	1092.08
Space group	P 2_1 2_1 2_1
T, °C	20
l, Å	0.71073
D_{calcd}	1.615
μ, mm^{-1}	1.425
R1(F_o)	0.0444
wR2(F_o^2)	0.1222

Table 3.5. Selected Bond Distances (Å) and Angles (°) for $[Ni(P_3S_9)(P_2S_8)]^{3-}$.

Ni–S	2.369(3) – 2.564(3)
P–S	1.936(4) –2.127(4)
S–S	2.057(4) – 2.063(4)
Cis S – Ni – S	78.91(10) – 101.48(11)
Trans S – Ni – S	169.37(11) – 179.23(10)
P – S – P	102.69(17) – 120.05(19)
P – S – S	109.17(17) – 110.46(16)
S – S – S	99.69(15) – 100.94(15)
Ni – P – S	106.08(16) – 106.70(16)

FT-IR. FT-IR from sample isolated from $[EMIM]BF_4$. (Chapter 7 Figure 7.4)

$\tilde{\nu}(EMIM^+)$ = 956 (br), 798 (w), 699 (w), 668 (sh), 646 (s), 617 (s) cm^{-1}.

$\tilde{\nu}([Ni(P_3S_9)(P_2S_8)]^{3-})$ = 983 (br), 924 (br), 818 (m), 741 (w), 730 (w), 686 (m), 666 (s), 656 (s), 607 (m) 590 (m), 579 (m), 556 (m), 544 (w), 493 (s), 464 (m), 460 (m), 458 (m) cm^{-1}.

Elemental Analysis. As for $[EMIM]_2[Ni^{II}(P_2S_8)_2]$, remaining IL on and within the crystals of $[EMIM]_3[Ni^{II}(P_3S_9)(P_2S_8)]$contributed to variations between the calculated and experimental values (See Table 3.6). However, this still allowed distinction between this salt and the one described previously.

Table 3.6. Experimental and calculated elemental analysis results for $[Ni^{II}(P_3S_9)(P_2S_8)]^{3-}$

Analysis	C	H	N
Elemental Analysis	21.9	3.74	8.43
Structure	19.8	3.05	7.69

Discussion

The $[Ni^{II}(P_3S_9)(P_2S_8)]^{3-}$ contains both the 1,3-$(P_2S_8)^{2-}$ moiety seen previously and the nonathiocyclotriphosphate $(P_3S_9)^{3-}$ moiety giving the anion C_s symmetry. The cyclic $(P_3S_9)^{3-}$ chelates to the octahedral Ni^{II} in a tridentate manner with terminal S atoms in axial positions of the $(P_3S_9)^{3-}$ chair–like conformation. The geometry of the $(P_3S_9)^{3-}$ moiety does not change significantly with coordination to the metal center when compared between the ligand form and isolated salt of the $(P_3S_9)^{3-}$.[54]

Like 1,3-$(P_2S_8)^{2-}$, the $(P_3S_9)^{3-}$ moiety is not new: it was first published in 1982 from a reaction of liquid ammonia and P_4S_{10}.[56] The crystal structure was not completed until 1992 when $(P_3S_9)^{3-}$ was prepared from elemental reactions in organic solvents, however in 2007 the $[pyH]_3[P_3S_9]$ salt was isolated (pyH = pyridinium).[54,55]

The $(P_3S_9)^{3-}$ moiety has previously been isolated as a metal-coordinating ligand in neutral molecular species, coordination polymers, and as a nickel thiophosphate. The $(t\text{-}Bu)_6Ga^{I}_3P_3S_9$ species, prepared from pentane and *t*-Bu_3Ga and P_4S_{10} at room temperature, contains $(P_3S_9)^{3-}$ as a dentate ligand to three alkylated gallium atoms to form a large ring structure, facilitating the coordination of all terminal sulfur atoms.[57] Additionally, $K_2[Cu^{I}P_3S_9]$, prepared from K_2S, P_2S_5, and Cu by reactive flux, is a coordination polymer with $(P_3S_9)^{3-}$ groups coordinated to Cu^{I} in both tridentate and monodentate modes, one on each side of the Cu^{I}.[58] This coordination scheme creates a propagating chain of $[CuP_3S_9]^{2-}$ with K^+ present for charge balance. The salt $[EMIM]_4[Ni^{II}(P_3S_9)_2]$ was isolated in 2011 by Gilbert J. Reynders III, a previous Senior Thesis student, by the same methods as the compounds described in this chapter.[50] However, all attempts to remake this compound have been unsuccessful.

Chapter 4: The Chromium Thiophosphate $[Cr^{III}(P_3S_9)_2]^{3-}$

This chapter reports the discovery of the novel chromium thiophosphate anion isolated as a molecular salt of the $[EMIM]^+$ cation. The compound was originally synthesized at the end of the summer of 2012, but was not characterized until 2013 when J. A. Cody was on sabbatical in Nantes, France. The manuscript for this compound has been completed and is in process of being submitted to *Acta Crystallographica, Section E*: *Structural Reports Online* for publication.

Synthesis

$[EMIM]_3[Cr^{III}(P_3S_9)_2]$ was synthesized from Cr : P : S molar rations of 1 : 4 : 16 in $[EMIM]CF_3SO_3$. The general synthesis scheme was used as outlined in Chapter 2. Reaction vessels were heated at 150 °C for 96 hours then slow cooled at 0.5 °C/h to 30 °C. The product was isolated as small orange plates separated from surrounding black solid. Yield calculations based of Cr were not implemented as the product amount was so minute.

Characterization

XRD. Characterization of $[EMIM]_3[Cr^{III}(P_3S_9)_2]$ was carried out using a Nonius CCD Diffractometer with graphite-monochromatic Mo Kα radiation. Figure 4.1 shows the thermal ellipsoid diagram of the novel $[Cr^{III}(P_3S_9)_2]^{3-}$ anion. Details of the full structure solution are given in in Table 4.1. Full geometrical details are shown in Tables 4.2 and 4.3

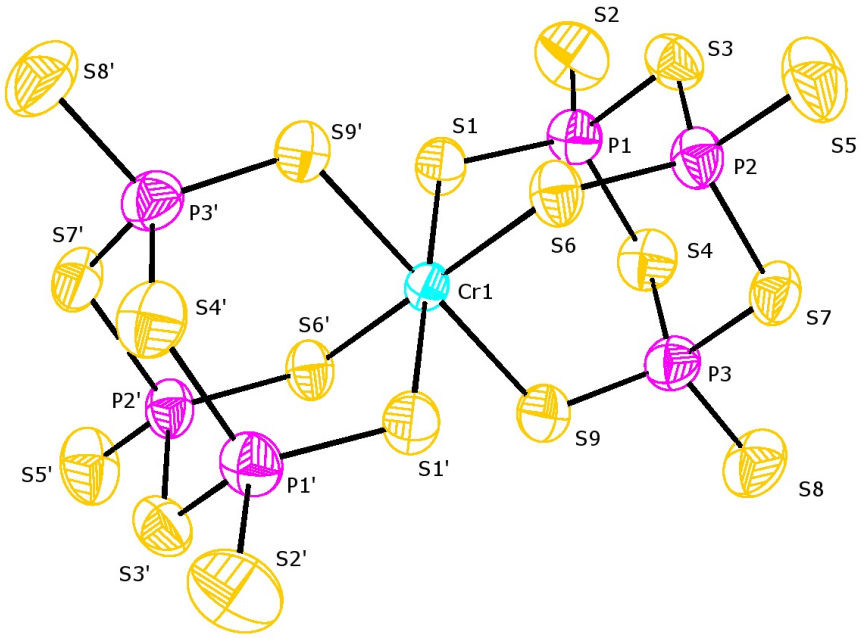

Figure 4.1. Thermal ellipsoid sketch of the $[Cr^{III}(P_3S_9)_2]^{3-}$ anion (Cr: cyan, P: magenta, S: yellow).

Table 4.1. Crystallographic Data for the $[Cr^{III}(P_3S_9)_2]^{3-}$ Anion

Chemical formula	$[EMIM]_3[Cr^{III}(P_3S_9)_2]^{3-}$
a, Å	12.735(3)
b, Å	10.150(2)
c, Å	18.316(4)
α, °	90
β, °	100.80(3)
γ, °	90
V, Å^3	2325.6(8)
Z	2
Formula weight, g mol^{-1}	1148.4
Space group	P 2_1/c
T, °C	20
l, Å	0.71073
D_{calcd}	1.64
μ, mm^{-1}	1.29
R1(F_o)	0.069
wR2(F_o^2)	0.211

Table 4.2. Bond Distances (Å) for the $[Cr^{III}(P_3S_9)_2]^{3-}$ Anion.

Cr1–S1	2.4082 (15)	S3–P1	2.111 (2)
Cr1–S1^{i}	2.4082 (15)	S4–P3	2.098 (3)
Cr1–S6	2.4105 (15)	S4–P1	2.101 (3)
Cr1–S6^{i}	2.4106 (15)	S5–P2	1.951 (2)
Cr1–S9^{i}	2.4108 (17)	S6–P2	1.989 (2)
Cr1–S9	2.4108 (17)	S7–P3	2.106 (2)
S1–P1	1.993 (2)	S7–P2	2.116 (2)
S2–P1	1.951 (3)	S8–P3	1.965 (3)
S3–P2	2.110 (2)	S9–P3	1.970 (3)

Symmetry Code: i = −*x*+1, −*y*+1, −*z*.

Table 4.3. Bond Angles (°) for the $[Cr^{III}(P_3S_9)_2]^{3-}$ Anion.

S1–Cr1–S1^{i}	180	P3–S9–Cr1	117.68 (10)
zS1–Cr1–S6	95.50 (6)	S2–P1–S1	114.59 (12)
S1^{i}–Cr1–S6	84.50 (6)	S2–P1–S4	104.40 (12)
S1–Cr1–S6^{i}	84.50 (6)	S1–P1–S4	113.30 (11)
S1^{i}–Cr1–S6^{i}	95.50 (6)	S2–P1–S3	105.01 (12)
S6–Cr1–S6^{i}	180	S1–P1–S3	112.56 (10)
S1–Cr1–S9^{i}	82.26 (6)	S4–P1–S3	106.13 (11)
S1^{i}–Cr1–S9^{i}	97.74 (6)	S5–P2–S6	113.99 (11)
S6–Cr1–S9^{i}	82.09 (6)	S5–P2–S3	104.66 (12)
S6^{i}–Cr1–S9^{i}	97.91 (6)	S6–P2–S3	114.04 (10)
S1–Cr1–S9	97.74 (6)	S5–P2–S7	104.58 (11)
S1^{i}–Cr1–S9	82.26 (6)	S6–P2–S7	113.81 (10)
S6–Cr1–S9	97.91 (6)	S3–P2–S7	104.71 (9)
S6^{i}–Cr1–S9	82.09 (6)	S8–P3–S9	115.98 (13)
S9^{i}–Cr1–S9	180	S8–P3–S4	104.61 (12)
P1–S1–Cr1	117.16 (8)	S9–P3–S4	112.64 (11)
P2–S3–P1	108.11 (9)	S8–P3–S7	104.20 (11)
P3–S4–P1	109.24 (9)	S9–P3–S7	112.05 (11)
P2–S6–Cr1	116.21 (8)	S4–P3–S7	106.50 (10)
P3–S7–P2	109.28 (10)		

Symmetry Code: i = −*x*+1, −*y*+1, −*z*.

Discussion

The $[Cr^{III}(P_3S_9)_2]^{3-}$ is analogous in structure to the $[Ni^{II}(P_3S_9)_2]^{4-}$ reported in reference 45 with pseudo-D_{3h} symmetry. Structurally, the Cr – S bonds are shorter then the Ni – S bonds as expected for the change in metal center from Ni^{II} to Cr^{III}, an average of 2.4458 Å to 2.4099 Å respectively. (See Table 4.2) P – S bonds in both anions are comparable considering the difference in data collection temperatures: 20 °C for the chromium thiophosphate and -100 °C for the nickel analog. *Cis* S – M – S bond angles vary slightly with an increase to 97.91° at maximum and 82.09° at the minimum in $[Cr^{III}(P_3S_9)_2]^{3-}$ compared to 97.04° and 82.96° in $[Ni^{II}(P_3S_9)_2]^{4-}$. A similar trend of decreased minimum and increased maximum is seen in both the S – P – S angles and P – S – P angles of the ligands. Because the anion sits on an inversion center, the *trans* S – Cr – S angles are 180°.

As the $(P_3S_9)^{3-}$ anion has already been discussed in Chapter 3, there are few comparisons to make to $[Cr^{III}(P_3S_9)_2]^{3-}$ beyond similarities to its nickel analog. However, in the case of Cr^{III} the type of ligand is unusual. The literature has not shown the discovery of any other chromium thiophosphate compounds, that may mark $[Cr^{III}(P_3S_9)_2]^{3-}$ as the first of its kind in the literature when published.[59] Additionally, Cr with tridentate ligands is also not seen in the literature. Cr^{III} is commonly seen either coordinated to bidentate organic sulfur-containing ligands such as $S_2CC_6H_6$ or $S_2COC_2H_5$, or in highly coordinated metallocubane structures such as $[Cp_6Cr_8S_8\{C(S)NEt_2)_2\}]$.[60, 61, 62]

Chapter 5: The Thioselenate Salt $[EMIM]_2[P_2Se_8]$

This chapter reports the isolation and characterization of the $[EMIM]_2[P_2Se_8]$ molecular salt. This compound was also synthesized at the end of the summer of 2012 like that of the chromium compound of Chapter 4. The sample was characterized in Nantes, France while J. A. Cody was on sabbatical. The structure of the salt was published in *Acta Crystallographica, Section E*: *Structural Reports Online* in August of 2013. See reference 63 or Appendix 2.

Synthesis

$[EMIM]_2[P_2Se_8]$ was synthesized from a reaction of elemental Ni, P, and Se in a 1 : 4 : 16 ratio. The general synthesis scheme was used as outlined in Chapter 2. The reaction tube was heated at 150 °C for 96 hours then cooled to room temperature at a rate of 0.5 °C/h to30 °C. Crystals were isolated as both red blocks and yellow plates where morphology was not an indication of a different unit cell. Color was variable probably due to absorption effects of the different thickness of crystals.

Characterization

XRD. Characterization of $[EMIM]_2[P_2Se_8]$ was carried out using a Nonius CCD Diffractometer with graphite-monochromatic Mo Kα radiation. Figure 5.1 shows the thermal ellipsoid diagram of the novel $[P_2Se_8]^{2-}$ anion. Details of the full structure solution are given in in Table 5.1. Full geometrical elements are shown in Tables 5.2 and 5.3.

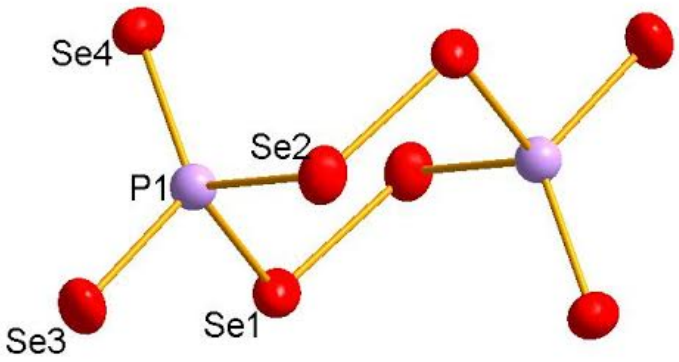

Figure 5.1. Thermal ellipsoid sketch of the $[P_2Se_8]^{2-}$ anion (P: purple, Se: red).

Table 5.1. Crystallographic Data for the $[P_2Se_8]^{2-}$ anion.

Chemical formula	$[EMIM]_2[P_2Se_8]$
a, Å	7.8885(4)
b, Å	9.3783(4)
c, Å	9.8039(5)
α, °	110.390(3)
β, °	96.395(4)
γ, °	102.992(5)
V, Å^3	648.00(5)
Z	1
Formula weight, g mol^{-1}	915.96
Space group	$P\bar{1}$
T, °C	20
l, Å	0.71073
D_{calcd}	2.347
μ, mm^{-1}	11.41
R1(F_o)	0.029
wR2(F_o^2)	0.063

Table 5.2. Bond Distances (Å) for the $[P_2Se_8]^{2-}$ anion.

P1–Se4	2.1104 (8)
P1–Se3	2.1334 (8)
P1–Se1	2.2794 (9)
P1–Se2^i	2.2809 (8)
Se1–Se2	2.3442 (5)
Se2–P1^i	2.2809 (8)

Symmetry code for equivalent atoms: i = 1 - x, - y, - z.

Table 5.3. Bond Angles (°) for the $[P_2Se_8]^{2-}$ anion.

Se4–P1–Se3	122.19 (4)
Se4–P1–Se1	113.49 (4)
Se3–P1–Se1	100.04 (3)
Se4–P1–Se2^{i}	113.90 (4)
Se3–P1–Se2^{i}	100.49 (3)
Se1–P1–Se2^{i}	104.32 (3)
P1–Se1–Se2	102.89 (2)
P1^{i}–Se2–Se1	102.37 (2)

Symmetry code for equivalent atoms: i = 1 - x, - y, - z.

Discussion

The $[P_2Se_8]^{2-}$ anion was first reported in 1992 used in the synthesis of $[Fe_2(CO)_4(PSe_5)_2]^{2-}$, however the anion has not been isolated as a salt of the [EMIM] cation before.[64] The $[EMIM]_2[P_2Se_8]$ complex crystallizes such that the $[P_2Se_8]^{2-}$ anions form around a column of the [EMIM] captions such that Z = 1 as seen in Figure 5.2. Despite having nickel in the reaction in an effort to prepare a thioselenate analog of $[Ni^{II}(P_2S_8)_2]^{2-}$, no Ni-containing products were obtained from the trials containing Se.

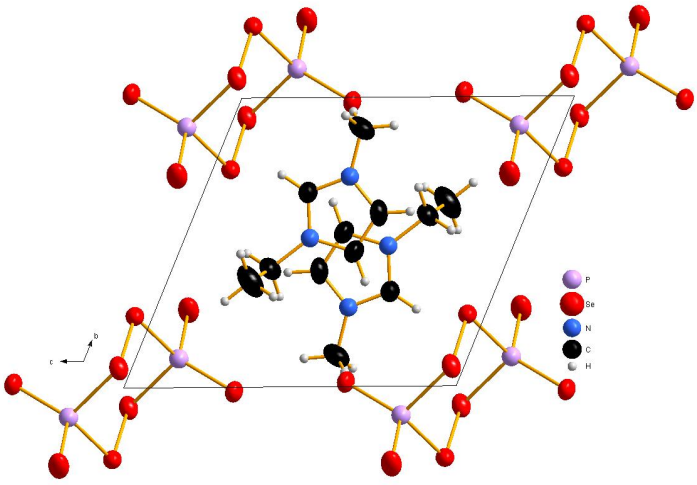

Figure 5.2. The crystal packing of the $[EMIM]_2[P_2Se_8]$ salt viewed along the *a* axis. (P: pink, Se: red, N: blue, C: black, H: white).

Compared to Rotter et al.'s study in 2008, the $P_2Se_8^{2-}$ anion presented here agrees well with $P_2Se_8^{2-}$ observed in the salt $[(n\text{-}Bu)_4N]_2[P_2Se_8]\cdot 2MeCN$.[65] P1 – Se1 bond length of the $[EMIM]_2[P_2Se_8]$ and $[(n\text{-}Bu)_4N]_2[P_2Se_8]\cdot 2MeCN$ are 2.2794(9) Å and 2.279(1) Å respectively. Similarly, $P1^i$ – Se2 bond distances agree at 2.2809(8) Å and 2.280(1) Å. Terminal P – Se bonds also agree with lengths of 2.108(1) Å and 2.135(1) Å in the ammonium salt to 2.1104(8) Å and 2.1334(8) Å in the imidazolium version. However, packing effects are evident in the remaining Se1 – Se2 bond as it is elongated from 2.336(1) Å in $[(n\text{-}Bu)_4N]_2[P_2Se_8]\cdot 2MeCN$ to 2.3442(5) Å in the $[EMIM]^+$ salt.

Chapter 6: The Manganese and Molybdenum Analogs of $[Ni^{II}(P_2S_8)_2]^{2-}$

This chapter reports the probable isolation of the Mn and Mo analogs of the $[Ni^{II}(P_2S_8)_2]^{2-}$ anion synthesized by simple metal substitution. (Figure 6.1) This work was also completed during the summer of 2012 and initial characterization was completed in Nantes, France.

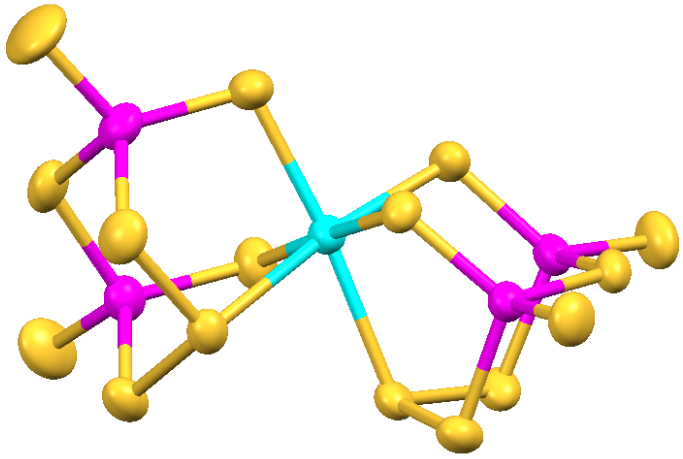

Figure 6.1. Thermal ellipsoid sketch of the $[M^{II}(P_2S_8)_2]^{2-}$ anion (M = Ni, Mn, Mo: cyan; P: magenta; S: yellow).

Synthesis

The $[EMIM]_2[M(P_2S_8)_2]$ (M = Mn^{II}, Mo^{II}) analogs were synthesized from M : P : S molar ratios of 1 : 4 : 16 in $[EMIM]BF_4$. The general synthesis scheme was used as outlined in Chapter 2. Reactions tubes were heated at 150°C for 96 hours then slow cooled at 0.5°C/hr to 30°C. The initial products were isolated as yellow needles of each metal compound after a significant amount of curing time was allowed. Upon further investigation it was found that the solubility point for the complexes in solution was below that of ambient temperature, unlike the Ni^{II} anions that precipitated at approximately 35°C. Attempts at slowing cooling using refrigeration and a water medium to facilitate quasi-uniform cooling succeeded in growing crystals of the anionic Mn^{II} and MoII species.

Characterization

XRD. Characterization of the $[EMIM]_2[M(P_2S_8)_2]$ (M = Mn, Mo) compounds was carried out using a Nonius CCD Diffractometer with graphite-monochromatic Mo Kα radiation. Only the unit cells (Table 6.1) were determined as both compounds were highly air sensitive and the cyrocooling apparatus was unavailable for use to combat rapid oxidation of the product.

Table 6.1. Preliminary Unit Cell Parameters of $[Mn^{II}(P_2S_8)_2]^{2-}$ and $[Mo^{II}(P_2S_8)_2]^{2-}$ compared to the known β-form of the $[Ni^{II}(P_2S_8)_2]^{2-}$ anion. Percent differences in geometry are calculated relative to β-form $[Ni^{II}(P_2S_8)_2]^{2-}$ for each analog.

Chemical formula	$[Ni^{II}(P_2S_8)_2]^{2-}$	$[Mn^{II}(P_2S_8)_2]^{2-}$	$[Mo^{II}(P_2S_8)_2]^{2-}$	Mn^{II} % Difference	Mo^{II} % Difference
a, Å	7.2317	7.268	7.259	0.5	0.4
b, Å	17.7138	18.01	17.909	1.7	1.1
c, Å	13.4488	13.633	13.548	1.4	0.7
α, °	90	90	90		
β, °	93.637	95.6	93.8	2.1	0.2
γ, °	90	90	90		
V, $Å^3$	1719.33	1784.51	1761.25	3.8	2.4

Discussion

Without full structure solutions there is no definite knowledge of actual Mn^{II} and Mo^{II} containing analogs to β-$[EMIM]_2[Ni^{II}(P_2S_8)_2]$, however the similarity in unit cell parameters gives the preliminary assumption significant merit. Between the Mn^{II} and Mo^{II} species, there is little difference in the values of the unit cell parameters. Relative to β-$[EMIM]_2[Ni^{II}(P_2S_8)_2]$, the Mn^{II} analog geometry is at most 1.7% longer on the *a*, *b*, and *c* axes and 2.1% on the β angle. Unit cell volume is 3.8% larger as expected from the larger cell axes. With Mo^{II}, a similar trend is found with analog geometry is at most 1.1% longer on the *a*, *b*, and *c* axes and but only 0.2% on

the β angle. Again, Unit cell volume is 2.4% larger as expected from the larger cell axes.

An examination of the Shannon radii shows that between $[Ni^{II}(CN)_6]^{4-}$ and $[Mn^{II}(CN)_6]^{4-}$ the ionic radius of the complex increases from 0.69Å to 0.83Å respectively.[66] The relative increase in ionic radius may be one of the contributing factors in the enlargement of the unit cell to accommodate the possibly larger Mn^{II} thiophosphate anion. Data for Mo^{II} was not included for hexa-coordinate systems.

Additional support of the Mn^{II} and Mo^{II} analogs also is evident in the relative air sensitivity. β-$[EMIM]_2[Ni^{II}(P_2S_8)_2]$ is relatively air stable, but the Mn^{II} and Mo^{II} compounds had oxidized within fifteen minutes of being exposed to air. This significant difference in chemistry serves as further evidence of the analog preparation.

Mn^{II} coordinated to S – P structural features are not unheard of, however compounds do not appear in the same fashion of homoleptic metal thiophosphates. Products include Mn^{II} containing P, S, N heterocycles or thiophosphate containing ligands as seen in Figure 6.2a and 6.2b with either alkoxy groups or aryl groups bonded to an uncharged phosphorus atom.[67,68] Mo^{II} with S – P structural features is less common; they appear in similar arrangements to the Mn^{II} complexes with alkoxy groups and also in complex multi-metal center systems (Figure 6.2c and 6.2d).[69,70]

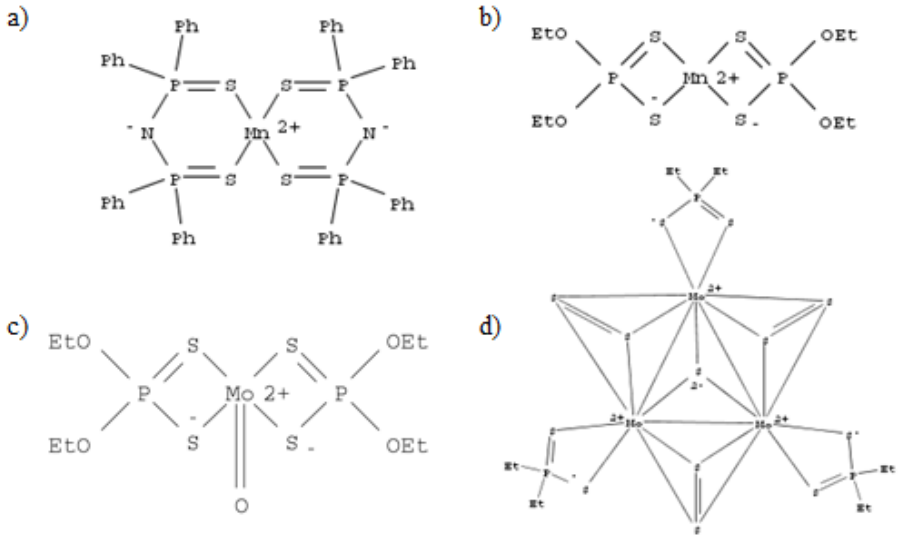

Figure 6.2. Examples of Mn^{II} (a,b) and Mo^{II} (c,d) thiophosphate-like compounds.[67,68,69,70]

Chapter 7: The Computational Modeling of Nickel Thiophosphate IR Spectra

During the spring of 2013 under the direction of Dr. Wiser, a computational study was undertaken to reproduce the FT-IR spectra all four nickel thiophosphates (Figure 7.1) published in *Inorganic Chemistry* (reference 45, Appendix 1). This independent study project combined both personal interests in the molecular vibration as observed by spectroscopy and the use of computational chemistry to model the vibrational frequencies of inorganic anions from their crystal structures. Due to the significant difference in the subject matter of this project a separate introduction is included.

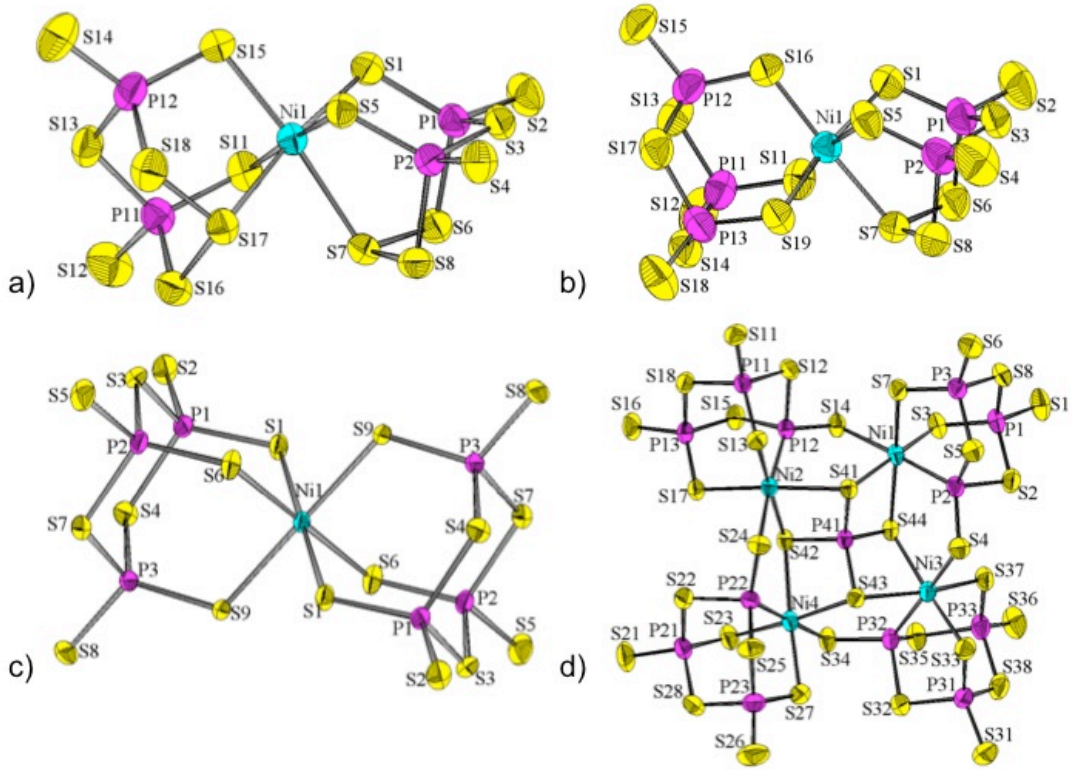

Figure 7.1. Thermal ellipsoid plots of the structures of nickel thiophosphate anions: a) $[Ni^{II}(P_2S_8)2]^{2-}$; b) $[Ni^{II}(P_3S_9)(P_2S_8)]^{3-}$; c) $[Ni^{II}(P_3S_9)_2]^{4-}$, d) $[(Ni^{II}P_3S_8)_4(PS_4)]^{7-}$ (Ni: cyan, P: magenta, S: yellow).

Introduction

When synthesizing multiple compounds that are visibly similar, a method of rapid characterization to distinguish between products is incredibly useful. For organic synthesis the use of FT-NMR or FT-IR is a prime example, however with the inorganic synthesis of solid, air-sensitive materials such convenient methods are not always as prevalent. When the four compounds, $[EMIM]_2[Ni^{II}(P_2S_8)_2]$, $[EMIM]_3[Ni^{II}(P_2S_8)(P_3S_8)]$, $[EMIM]_4[Ni^{II}(P_3S_8)_2]$, and $[EMIM]_7[(Ni^{II}P_3S_8)_4(PS_4)]$ (EMIM = 1-ethyl-3-methylimidazolium) were first prepared, XRD was the only method of characterization that could be completed on site.[45] FT-IR characterization was then tested and found to be a surprisingly useful method of quick characterization. Consequently, this led to a great curiosity: what parts of the anion structure gave rise to the specific FT-IR absorbances? At this point, neither synthesis nor spectroscopy could elucidate an answer; computational modeling was the next step.

Computational methods provide the ability to model complex systems that would otherwise be unobservable using conventional analytical methods. The calculation of FT-IR frequencies is useful for predictive spectra, but what is more revealing is the ability to visualize and animate the intramolecular vibrations that give rise to the spectrum's peaks. However as the size of atoms and number of electrons in a model grows, calculation times increase and the question arises of whether or not results will be viable. When considering the simulation of transition metal compounds there is ample literature providing support and use for their modeling.[71,72] Unfortunately, much of this literature pertains to properties other than vibrational frequency such as bond nature and ligand coordination.[73,74]

The calculation of infrared frequencies in related transition metal complexes has been conducted successfully previously, but evidence of successful frequency calculations of other nickel thiophosphates is non-existent. For reference, there have been successful evaluations of frequency involving Ni and Fe where carbonyl ligands ligated to a Ni in a Ni-containing zeolite were predicted, or the full vibrational spectrum of the fayalite mineral Fe_2SiO_4 was calcuated.[75,76] Both models employ the use of Density Functional Theory (DFT) that operates with the use of functionals, models of electron density, to arrive at calculated results rather than approximated solutions to the full Schrödinger equation for the system.[77] The ability to vary the functional allows for greater tuning of the DFT method to the systems being modeled.

Experimental

General. Synthesis details and FT-IR analysis of all four compounds can be found in reference 46, Chapters 2 and 3, or Appendix 1. All calculations were performed using Gaussian 09[78] on Mac OS X 10.7.5 using DFT calculations with the LANL2DZ (Los Alamos National Laboratory second double-zeta) basis set. LANL2DZ uses a Dunning/Huzinaga full double-ξ basis set[79] on C, H, N, O and Si (though none are present) and the Hay and Wadt effective core potentials at Ni, P, and S.[80] A modified set of Ni^{II}: LANL2DZ and P, S: 6-31G(d,p)[81] was also used to observe if modeling the smaller P and S atoms with a conventional basis set would translate to a greater accuracy in the simulated spectrum. For the basic LANL2DZ and modified LANL2DZ, 6-31G(d,p) basis set calculations the functional was held as B3LYP, a combination of Becke's three-parameter hybrid exchange functional (B3) and the

correlation functional of Lee, Yang, and Parr (LYP).[82] A table of all calculations is included below this section (Table 7.1)

Frequency Calculations using XRD Geometry. XRD geometry of the molecular anions was attained by importing the .pdb (protein database format) files into Mercury 3.0 and removing all atoms of the EMIM cations until only atoms of the molecular anions remained.[83] Files were saved in a GaussView v5-compatible format and were subsequently opened in GaussView v5 to be converted into the standard Gaussian 09 input file. Reported frequencies were obtained from DFT calculations using B3LYP with the LANL2DZ and modified LANL2DZ,6-31G(d,p) basis sets. Calculations from XRD geometry were accomplished with for all four anions with B3LYP/LANL2DZ and B3LYP/LANL2DZ,6-31G(d,p) for all anions but $[EMIM]_7[(Ni^{II}P_3S_8)_4(PS_4)]^{7-}$. Calculations for $[EMIM]_7[(Ni^{II}P_3S_8)_4(PS_4)]^{7-}$ failed to converge when using the modified LANL2DZ basis set. Anion geometries were *not* yet optimized.

Frequency Calculations using Optimized Geometry. As Gaussian 09 computes frequency without the knowledge that the nickel thiophosphates in question are in the solid phase, calculating gas-phase geometry of each anion followed by frequency may allow Gaussian to better model the FT-IR spectra of the four anions. Calculations of optimized geometry (B3LYP/LANL2DZ) were accomplished for all four anions using and all but $[(Ni^{II}P_3S_8)_4(PS_4)]^{7-}$ using the modified B3LYP/LANL2DZ, 6-31G(d,p) basis set. Gaussian 09 was not able to converge to an minimum when applying the B3LYP/LANL2DZ, 6-31G(d,p) to $[(Ni^{II}P_3S_8)_4(PS_4)]^{7-}$, and without a reasonable geometry the frequencies could not be calculated. Frequency calculations from these results (B3LYP/LANL2DZ//B3LYP/LANL2DZ

and B3LYP/LANL2DZ, 6-31G(d,p)// B3LYP/LANL2DZ, 6-31G(d,p)) were completed for all successful geometry optimizations.

Variation of the Functional component of the LANL2DZ Basis Set. For the LANL2DZ calculations two additional functionals were investigated, B3PW91 and *m*PW1PW91, to observe the effect of a change of functional on the simulated spectra. B3PW91 is a combination of Becke's three-parameter hybrid exchange functional (B3) and Perdew and Wang's 1991 gradient-corrected correlation functional (PW91).[84] *m*PW1PW91 is a combination of the Perdew-Wang 1991 exchange functional as modified by Adamo and Barone (*m*PW1),[85] and the aforementioned PW91 gradient-corrected correlation functional.

Variation also served to probe for a better functional fit to the anions. For the XRD geometry, all functionals were able to simulate spectra. When using optimized geometry $[Ni^{II}(P_3S_9)_2]^{4-}$ failed with the use of B3PW91 and $[(Ni^{II}P_3S_8)_4(PS_4)]^{7-}$ failed with the use of *m*PW1PW91.

Table 7.1. Summary of All Attempted Frequency and Geometry Calculations.

		Anion			
	Method	$[Ni^{II}(P_2S_8)_2]^{2-}$	$[Ni^{II}(P_3S_9)(P_2S_8)]^{3-}$	$[Ni^{II}(P_3S_9)_2]^{4-}$	$[(Ni^{II}P_3S_8)_4(PS_4)]^{7-}$
XRD Geometry Frequency Calculations	B3LYP/ LANL2DZ	Complete	Complete	Complete	Complete
	B3PW91/ LANL2DZ	Complete	Complete	Complete	Complete
	*m*PW1PW91/ LANL2DZ	Complete	Complete	Complete	Complete
	Modified LANL2DZ*	Complete	Complete	Complete	Complete
Optimized Geometry Calculations	B3LYP/ LANL2DZ	Complete	Complete	Complete	Complete
	B3PW91/ LANL2DZ	Complete	Complete	Failed	Complete
	*m*PW1PW91/ LANL2DZ	Complete	Complete	Complete	Failed
	Modified LANL2DZ*	Complete	Complete	Complete	Failed
Optimized Geometry Frequency Calculations	B3LYP/ LANL2DZ	Complete	Complete	Complete	Complete
	B3PW91/ LANL2DZ	Complete	Complete	Failed	Complete
	*m*PW1PW91/ LANL2DZ	Complete	Complete	Complete	Failed
	Modified LANL2DZ*	Complete	Complete	Complete	Failed

*Modified LANL2DZ refers to the B3LYP/LANL2DZ, 6-31G(d,p) basis set.

Results and Discussion

XRD Geometry Frequency Calculations. The experimental FT-IR spectra for all anions are also provided (Figures 7.2 – 7.6). Results from all frequency calculations for XRD geometry are organized by the functional used (Figures 7.7 – 7.10). For both the LANL2DZ and modified LANL2DZ,6-31G(d,p) basis sets the calculated vibration spectra from XRD geometry were nearly identical in modeling the intense vibrational frequencies between 800 cm^{-1} and 400 cm^{-1} regardless of selected functional. Changes in functional lead to small shifts in the calculated frequencies above 400 cm^{-1} and significant changes in the calculated frequencies observed

below 100 cm^{-1}. However, this was irrelevant as no experimental data was ever collected in this range.

The B3LYP/LANL2DZ,6-31G(d,p) calculations contained the least amount of erroneous frequencies (Figure 7.10), thus they were set as the standard to compare to experimental spectra for all anions except $[(Ni^{II}P_3S_8)_4(PS_4)]^{7-}$. It will be noticed that the wavenumbers associated with the computational spectra do not resemble the experimental spectra. These values should be taken lightly; the relative intensities and pattern of the vibrational spectrum serve as an adequate fingerprint that allows for assignment of peaks for qualitative matching.

$[Ni(P_2S_8)_2]^{2-}$. The experimental vibrational frequencies for anion $[Ni^{II}(P_2S_8)_2]^{2-}$ are FT-IR from crystals isolated from $[EMIM]BF_4$: $\tilde{\nu}([Ni(P_2S_8)_2]^{2-})$ = 824 (m), 751 (w), 741 (w), 691 (m), 675 (s), 574 (m), 548 (m), 500 (m), 467 (m), 461 (m), 457 (w) cm^{-1} (Figure 7.2) and FT-IR from crystals isolated from $[EMIM]CF_3SO_3$: $\tilde{\nu}([Ni(P_2S_8)_2]^{2-})$ = 825 (m), 751 (w), 741 (w), 690 (m), 676 (s), 575 (s), 548 (m), 502 (m), 468 (m), 463 (m), 457 (w) cm^{-1}(Figure 7.3). Preliminary EMIM stretches had already been subtracted and the remaining frequencies assigned to the present anion. Calculated vibrational frequencies agreed with the assignment where $\tilde{\nu}([Ni(P_2S_8)_2]^{2-})_{calc}$ = 676 (s), 646 (s), 575 (s), 548 (m), 502 (m), 468 (m) cm^{-1} when qualitatively assessed. All peaks greater than 676 cm^{-1} that had previously been attributed to the anion are seen to be EMIM stretching, narrowing the window of comparison from anion to anion to approximately 200 cm^{-1}. The peak at 646 cm^{-1} is new and was only observed once simulation was complete due to its proximity to the strong 676 cm^{-1} vibration that masked it in the experimental spectra (Figures 7.2, 7.3 & 7.10).

$[Ni^{II}(P_3S_9)(P_2S_8)]^{3-}$. The experimental vibrational frequencies reported are $\tilde{\nu}([Ni(P_3S_9)(P_2S_8)]^{3-})$ = 983 (br), 924 (br), 818 (m), 741 (w), 730 (w), 686 (m), 666 (s), 656 (s), 607 (m) 590 (m), 579 (m), 556 (m), 544 (w), 493 (s), 464 (m), 460 (m), 458 (m) cm^{-1}. Like $[Ni^{II}(P_2S_8)_2]^{2-}$, preliminary removal of EMIM stretches had already been completed. Computational methods gave $\tilde{\nu}(Ni(P_3S_9)(P_2S_8)]^{3-})_{calc}$ = 686 (m), 666 (s), 590 (m), 579 (m), 556 (w), 493 (m) cm^{-1}. From the computational spectrum, it can be seen that two nearby peaks give rise to the 666 cm^{-1} vibration, but in the experimental FT-IR data there is no evidence of a second peak being resolved (Figures 7.4 & 7.10). Here these peaks are treated as a single entity.

$[Ni^{II}(P_3S_9)_2]^{4-}$: The experimental anion stretching is reported as FT-IR $\tilde{\nu}([Ni(P_3S_9)_2]^{4-})$ = 983 (br), 923 (br), 790 (vw), 658 (s), 647 (s), 607 (w), 586 (s), 576 (vw), 559 (m), 549 (w), 509 (w), 500 (s), 497 (s), 494 (s), 485 (m) cm^{-1}. Computational results give $\tilde{\nu}([Ni(P_3S_9)_2]^{4-})_{calc}$ = 658 (s), 647 (s), 586 (m), 559 (m), 494 (m) cm^{-1}. Like in the case of $[Ni^{II}(P_3S_9)(P_2S_8)]^{3-}$, the observed frequencies of 646 cm^{-1} and 494 cm^{-1} arise from two vibrations but are indistinguishable in the experimental FT-IR spectra (Figures 7.5 & 7.10). For the purpose of modeling the vibrational spectrum both vibrations are treated singularly as they were in $[Ni^{II}(P_3S_9)(P_2S_8)]^{3-}$.

$[(Ni^{II}P_3S_8)_4(PS_4)]^{7-}$.The reported frequencies are $\tilde{\nu}([(NiP_3S_8)_4(PS_4)]^{7-})$ = 983 (vw), 874 (vw), 875 (vw), 819 (br), 747 (w), 732 (w), 670 (s), 667 (s), 655 (s), 618 (m), 574 (s), 559 (s), 515 (m), 506 (w), 501 (w), 483 (s), 472 (w), 458 (w), 438 (s), 433 (m), 424 (w), 419 (w) cm^{-1} (Figure 7.6). Using the B3LYP/LANL2DZ calculations for $[(NiP_3S_8)_4(PS_4)]^{7-}$, (Figure 7.7) stretching was found to be $\tilde{\nu}([(NiP_3S_8)_4(PS_4)]^{7-})_{calc}$ = 670 (s), 574 (m), 516 (w), 483 (m), 438 (m) cm^{-1}. Due to the size of the anion,

many calculated frequencies make up the simulated FT-IR spectrum and preliminary stretching assignment was not viable for further analysis at the time. The anion was simply too large for valid application of simple stretching terminology.

Optimized Geometry. For all anions, geometry after optimization was significantly distorted and the calculated frequencies from the distorted geometry did not agree the experimental spectra or the XRD geometry calculations (Figures 7.11 -7.14). While it would seem that the calculation of frequency from distorted geometry is an expensive waste of processing time, the results do play a vital role. The incorrect frequency calculations serve as evidence that optimization of experimental geometry does not yield results that are consistent with the experimental data when modeling solid state structures. Thus for future transition metal compound calculations it should be understood that converting experimental geometry data for use in Gaussian 09 provides better results overall.

Preliminary Stretching Assignment. As group theory had not yet been learned at the time of these experiments, an in-depth spectroscopic analysis could not be completed. However, simple assignment of one or more of the modes of molecular vibration (wagging, twisting, symmetric stretching, asymmetric stretching, scissoring, rocking) served as a useful exercise in evaluating intramolecular motion and resultant energies. For this reason the $\tilde{\nu}_{\text{calc}}$ frequencies of $[Ni^{II}(P_2S_8)_2]^{2-}$ have been evaluated for the major vibrational modes. Vector diagrams for all stretches can be found in Figure 7.15. This method could also be applied to $[Ni^{II}(P_3S_9)(P_2S_8)]^{3-}$ and $[Ni^{II}(P_3S_9)_2]^{4-}$ where they would serve as a similar exercise.

$\tilde{\nu}([Ni(P_2S_8)_2]^{2-})_{calc}$ = 676 (s), 646 (s), 575 (s), 548 (m), 502 (m), 468 (m) cm^{-1}

676 cm^{-1}: Asymmetric stretching of 3P with 5S and 4S and wagging with 11S and 6S

Asymmetric stretching of 2P with 8S and 7S, and wagging with 9S and 5S

Asymmetric stretching of 13P with 21S and 17S, and wagging with 18S and 16S

Scissoring of 6S with 3P and 2P

646 cm^{-1}: Asymmetric stretching of 3P with 8S and 7S, and wagging with 6S and 11S

Asymmetric stretching of 2P with 5S and 4S, and wagging with 9S and 6S

Asymmetric stretching of 12P with 15S and 14S, and wagging with 19S and 16S

Rocking of 6S with 3P and 2P

575 cm^{-1}: Symmetric stretching of 3P with 11S, and 6S, 8S and 7S

Symmetric stretching of 2P with 5S, and 4S, 9S and 6S

Symmetric stretching of 12P with 14S, and 15S, 19S and 16S

Symmetric stretching of 13P with 21S, and 16S, 18S and 17S

Symmetric stretching/Wagging of 6S, with 3P and 2P

Symmetric stretching/Wagging of 16S, with 13P and 12P

548 cm^{-1}: Symmetric stretching of 3P with 11S, and 6S, 8S and 7S

Symmetric stretching of 2P with 5S, and 4S, 9S and 6S

Symmetric stretching of 12P with 15S, and 14S, 19S and 16S

Symmetric stretching of 13P with 21S, and 16S, 18S and 17S

Twisting of 6S with 3P and 2P

Twisting of 16S with 13P and 12P

502 cm^{-1}: Asymmetric stretching of 3P with 11S and 6S, and rocking with 8S and 7S

Asymmetric stretching of 2P with 9S and 6S, and rocking with 5S and 4S

Asymmetric stretching of 12P with 19S and 16S, and rocking with 15S and 14S

Asymmetric stretching of 13P with 21S and 16S, and rocking with 18S and 17S

Symmetric stretching/Wagging of 6S with 3P and 2P

Symmetric stretching/Wagging of 16S with 13P and 12P

468 cm^{-1}: Asymmetric stretching of 10S with 11S and 9S

Symmetric stretching of 11S with 3P and 10S

Asymmetric stretching of 3P with 11s and 6S, and wagging with 8S and 7S

Asymmetric stretching of 2P with 6s and 5S, and wagging with 8S and 7S

From the preliminary evaluation, it is evident that the most energetic vibrations at 676 cm^{-1} arise from the asymmetric stretching, wagging, and scissoring within one $(P_2S_8)^{2-}$ moiety while the other has one asymmetric stretching/wagging P and S atoms. This energy then drops at 646 cm^{-1} when the scissoring of the S atom switches to a lower energy rocking. Between 575 cm^{-1} and 548 cm^{-1} a similar drop in energy is observed when symmetric stretching and wagging centered on the 3P – 6S – 2P and 13P – 16S – 12P becomes twisting, while both P_2S_8 moieties contain the same symmetric stretching. The trend begins to dissolve at 502 cm^{-1} the symmetric stretching/wagging of the P – S – P regions returns and all symmetric stretching becomes asymmetric. At 468 cm^{-1} the calculated vibrations return to a single P_2S_8

and demonstrate vibrations beginning to involve the S – S – S structural entity. Further below 468 cm^{-1} no experimental data was gathered so preliminary assessment was not completed.

Conclusion

The modeling of FT-IR spectra by computational analysis for nickel thiophosphates demonstrates the versatility of computational modeling by interfacing inorganic synthesis, infrared spectroscopy, and X-ray diffraction. Further work should be done to evaluate the modes of vibration for all anions in order to determine the molecular components of the energies of the calculated and observed frequencies.

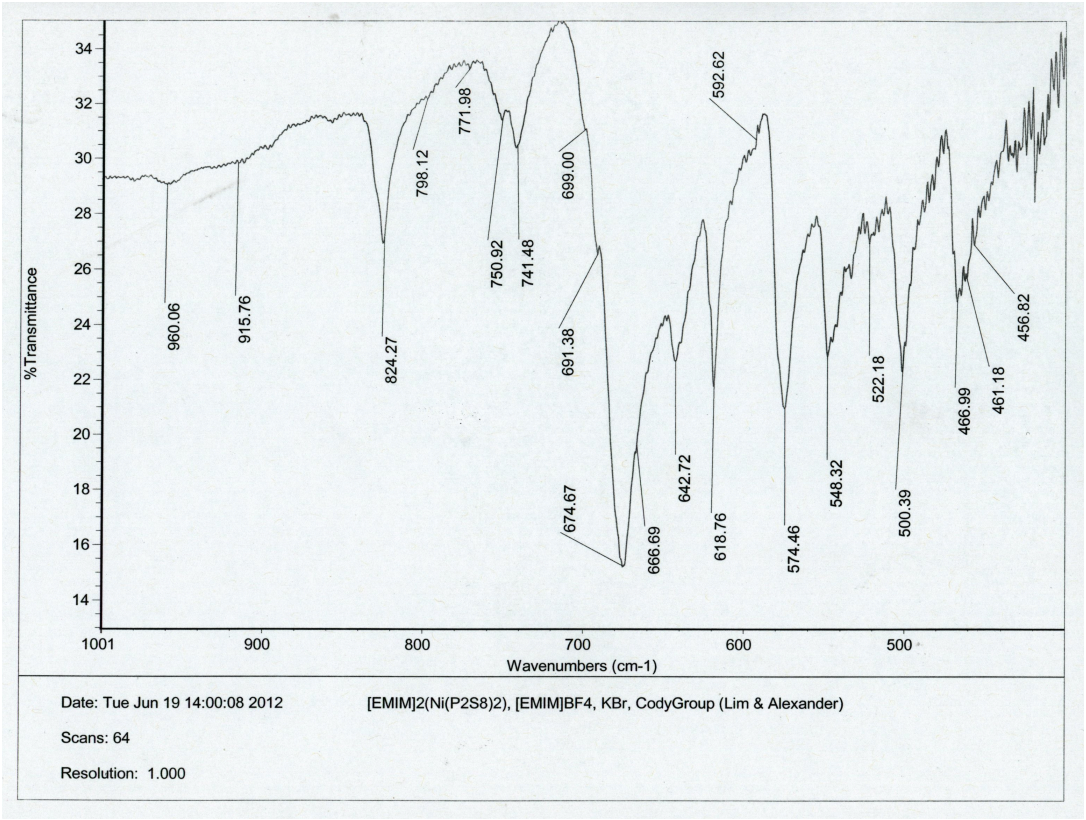

Figure 7.2. FT-IR spectrum of $[Ni^{II}(P_2S_8)_2]^{2-}$ from $[EMIM]BF_4$.

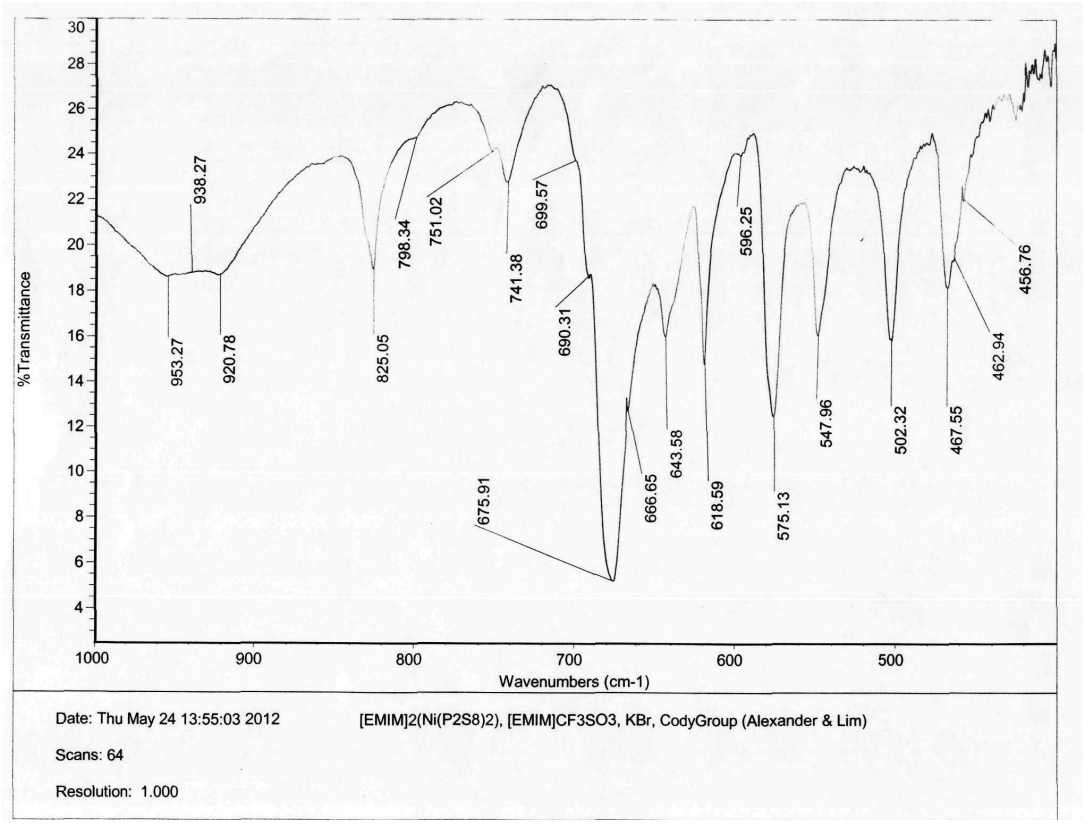

Figure 7.3. FT-IR spectrum of $[Ni^{II}(P_2S_8)_2]^{2-}$ from $[EMIM]CF_3SO_3$.

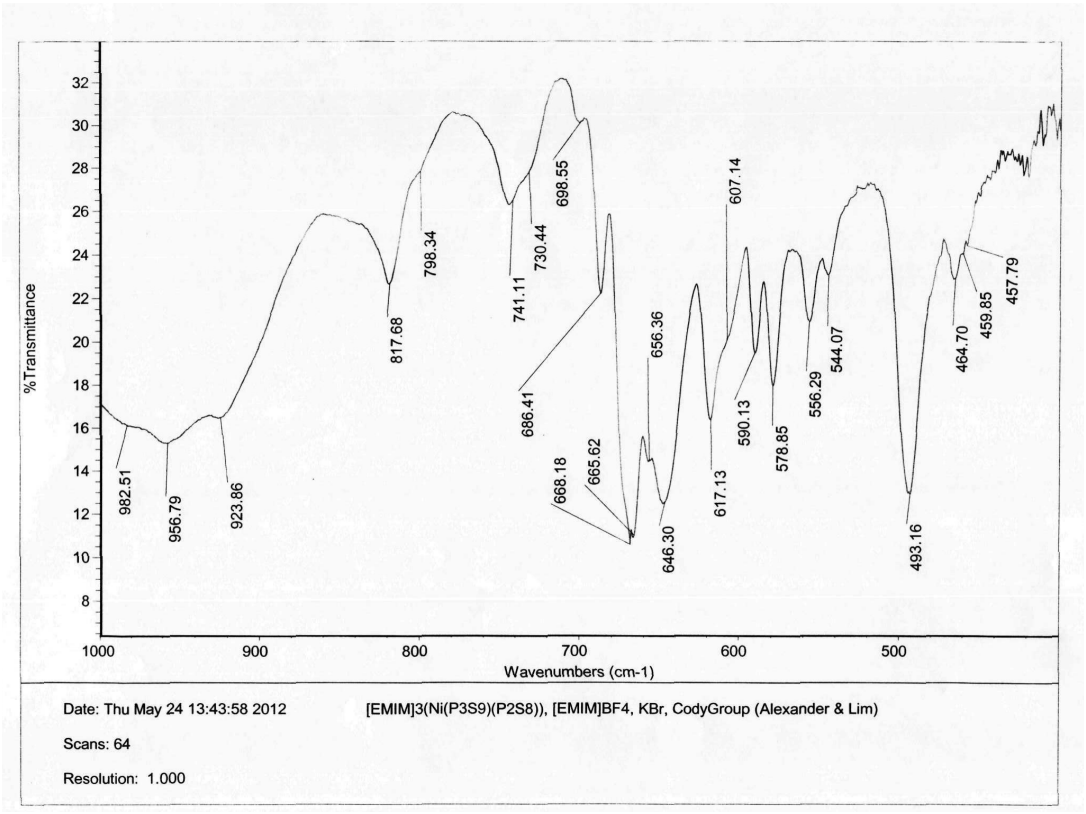

Figure 7.4. FT-IR spectrum of $[Ni^{II}(P_2S_8)(P_3S_9)_2]^{3-}$ from $[EMIM]BF_4$.

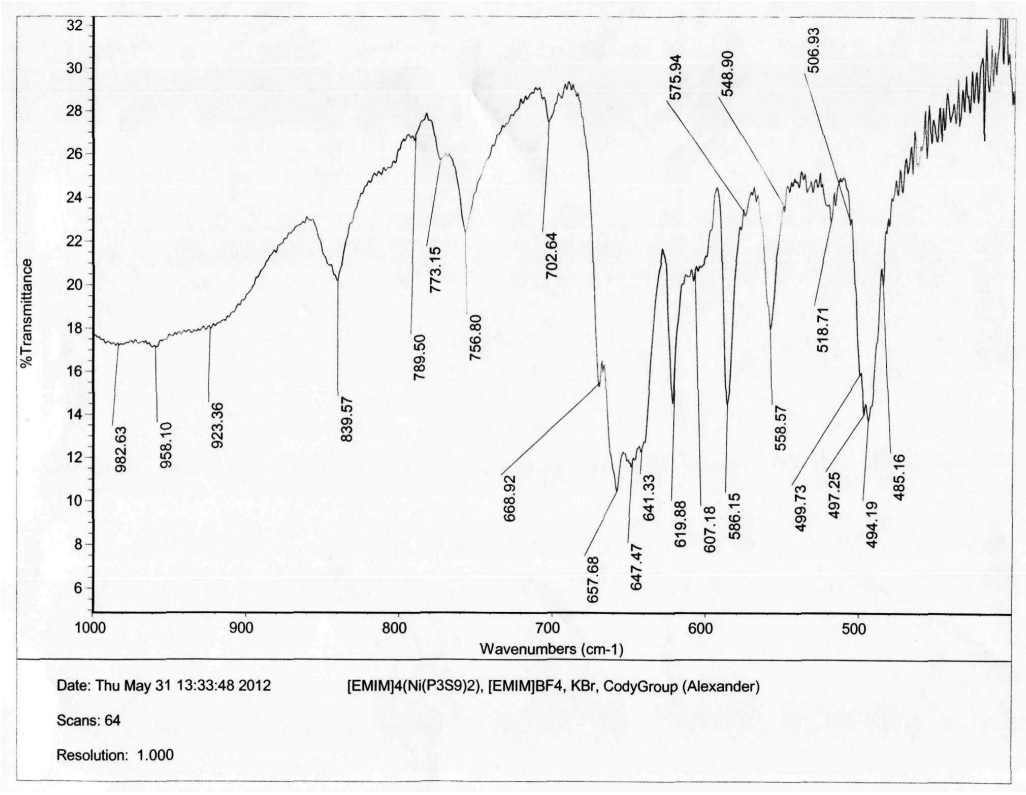

Figure 7.5. FT-IR spectrum of $[Ni^{II}(P_3S_9)_2]^{4-}$ from $[EMIM]BF_4$.

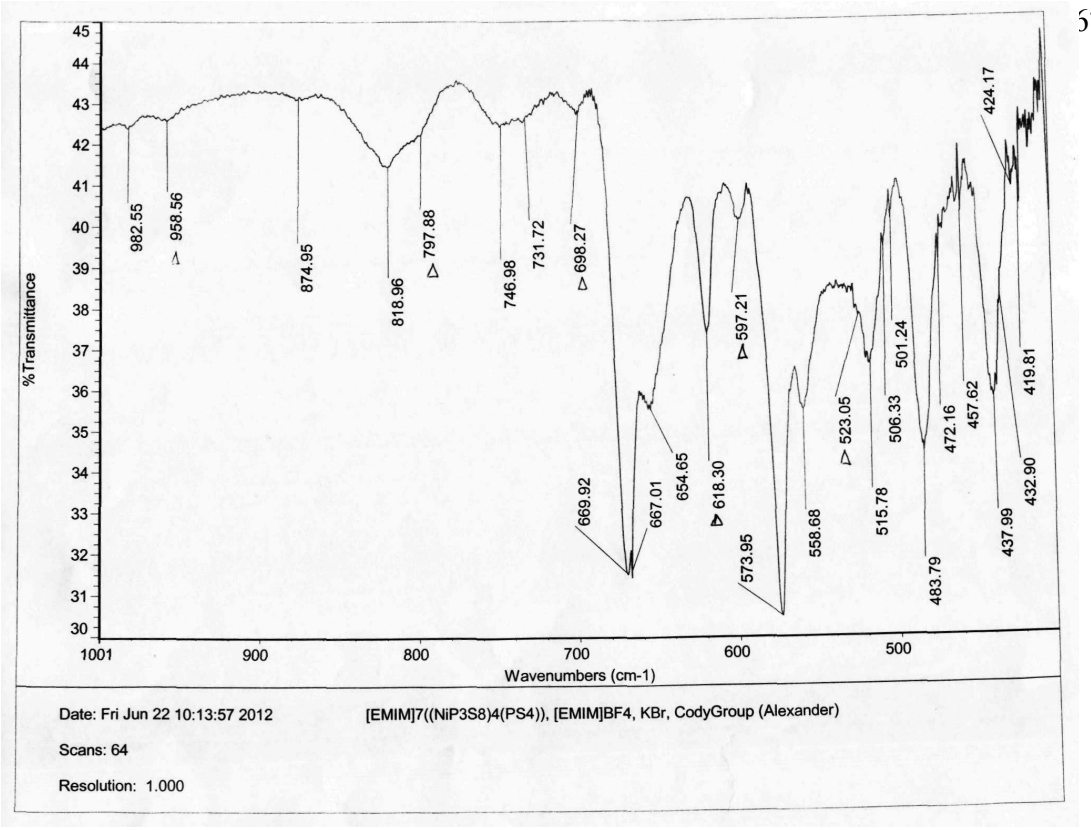

Figure 7.6. FT-IR spectrum of $[(NiP_3S_8)_4(PS_4)]^{7-}$ from $[EMIM]BF_4$.

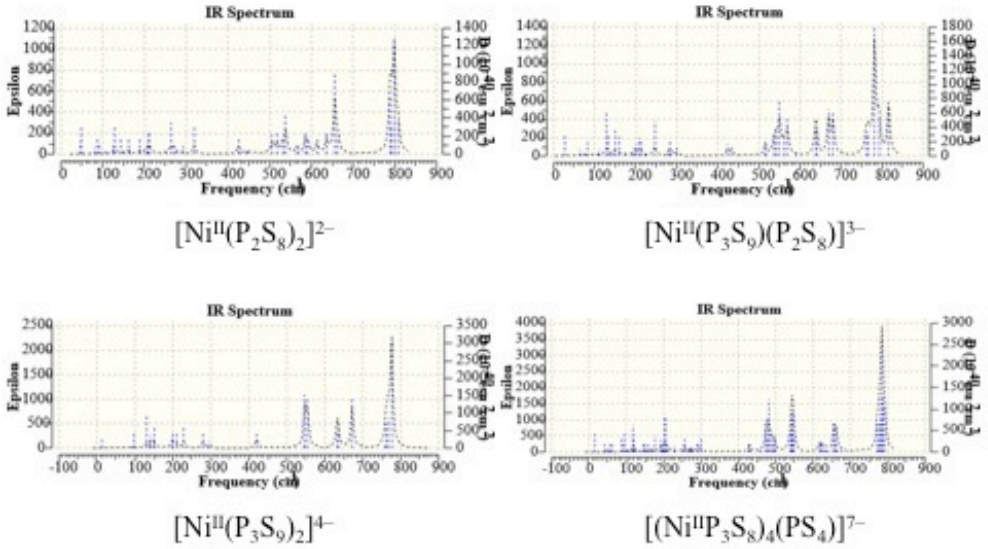

Figure 7.7. Frequency calculation results: XRD geometry (B3LYP /LANL2DZ).

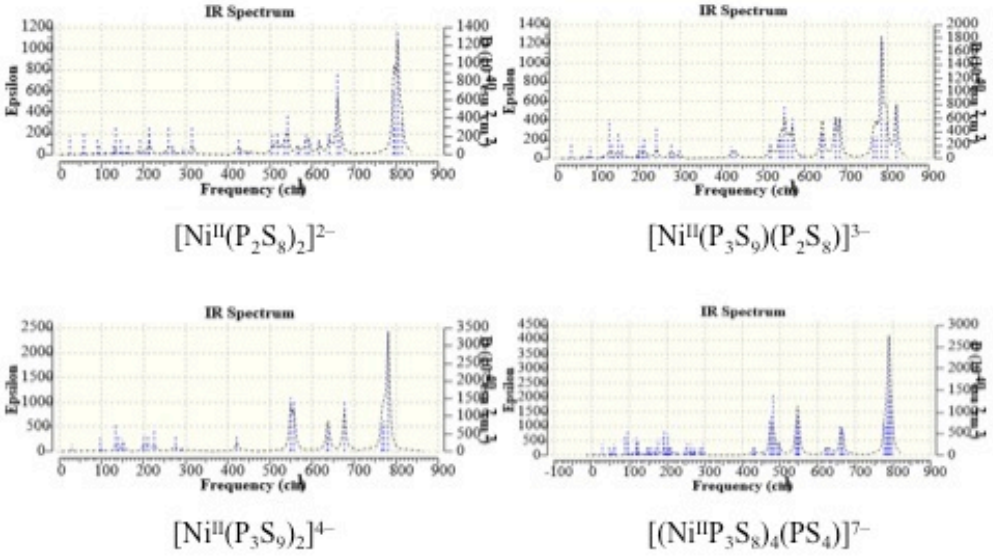

Figure 7.8. Frequency calculation results: XRD geometry (B3PW91/ LANL2DZ).

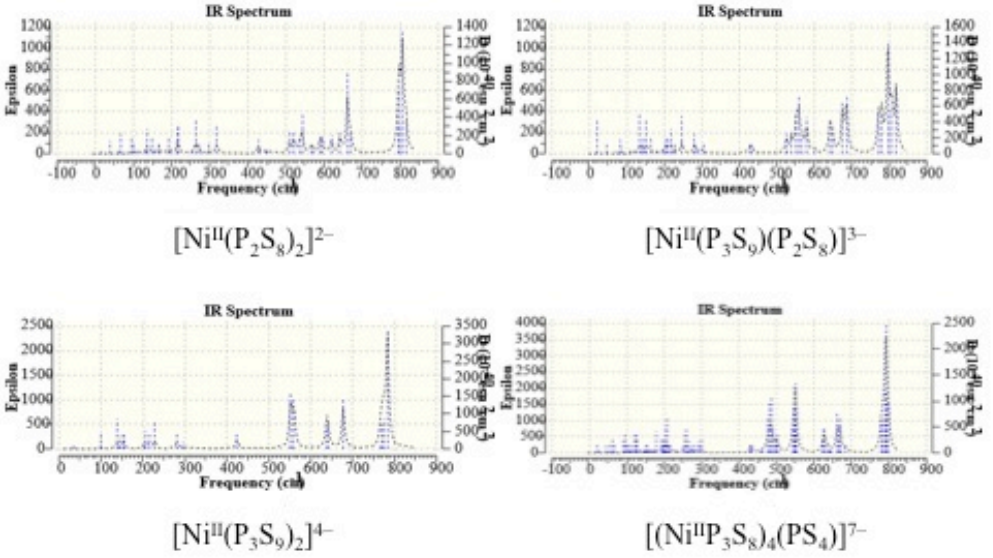

Figure 7.9. Frequency calculation results: XRD geometry (*m*PW1PW91/LANL2DZ).

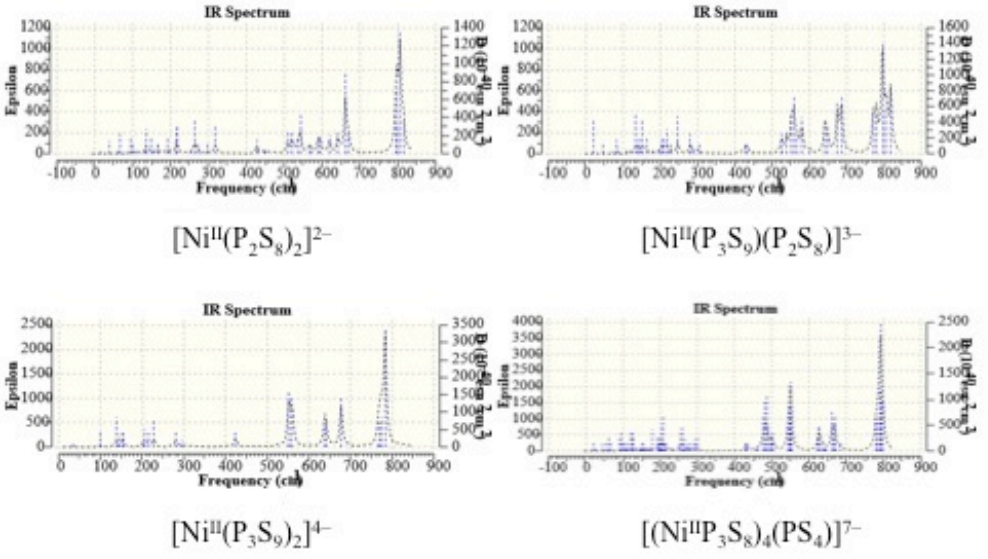

Figure 7.10. Frequency calculation results: XRD geometry (B3LYP/LANL2DZ, 6-31G(d,p)).

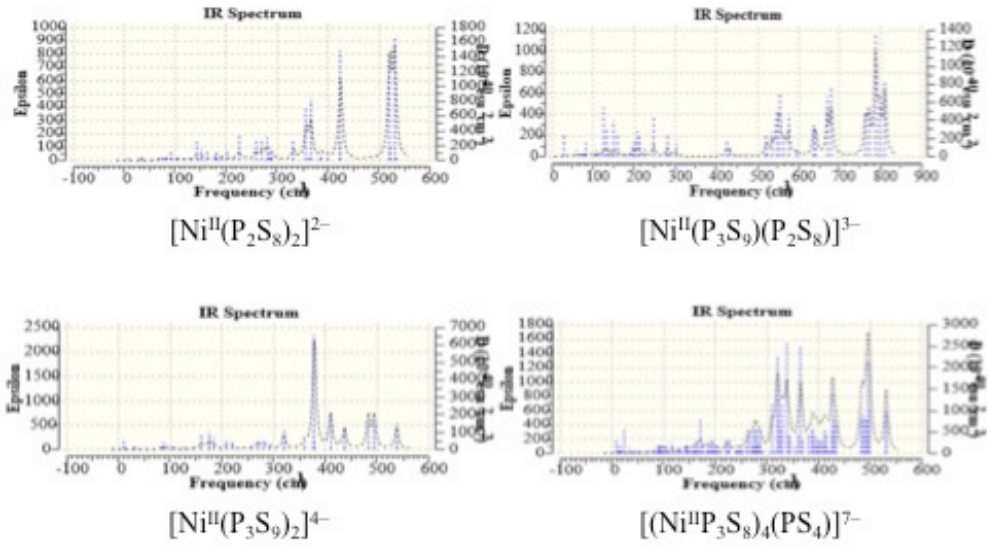

Figure 7.11. Frequency calculation results: Optimized geometry (B3LYP/LANL2DZ//B3LYP/LANL2DZ).

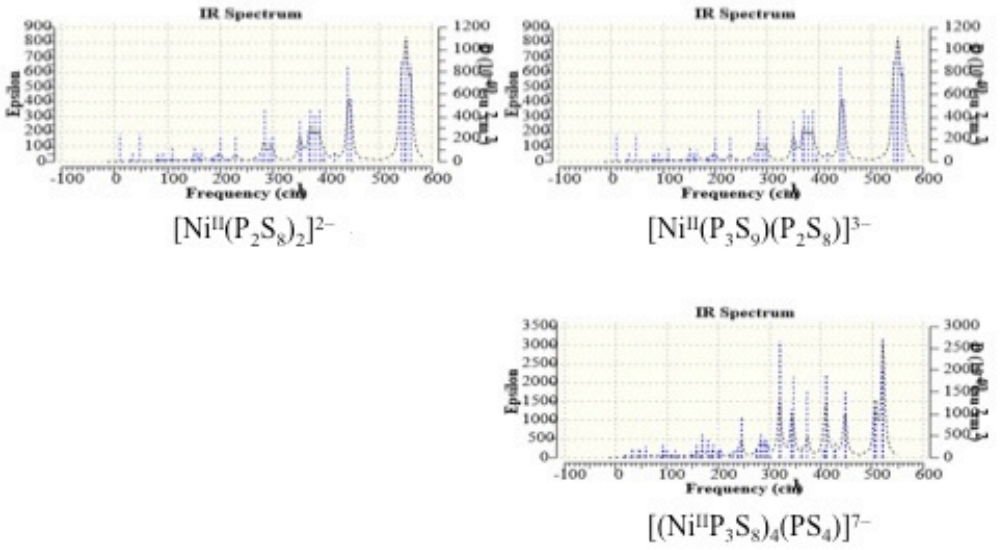

Figure 7.12. Frequency calculation results: Optimized geometry (B3PW91/LANL2DZ//B3PW91/LANL2DZ).

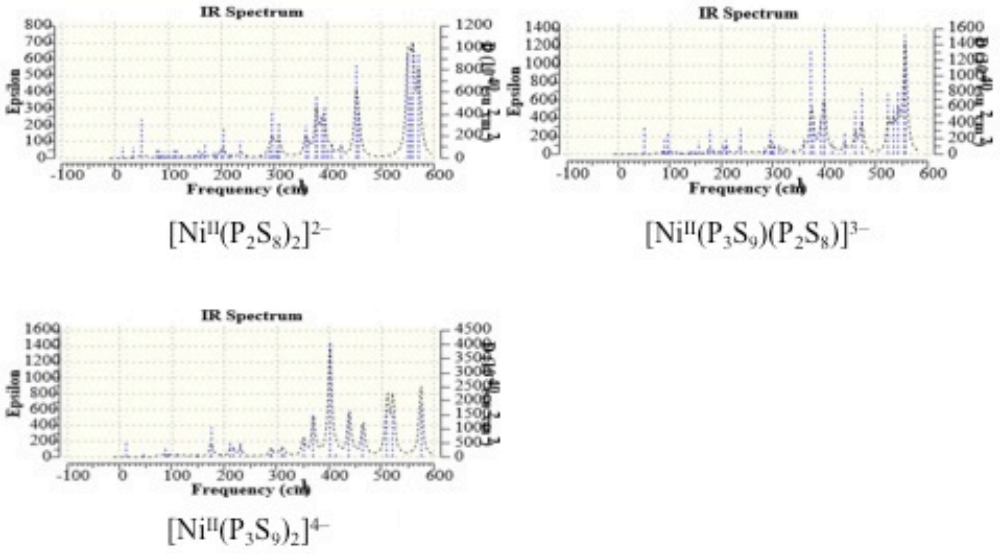

Figure 7.13. Frequency calculation results: Optimized geometry (*m*PW1PW91/LANL2DZ//*m*PW1PW91/LANL2DZ).

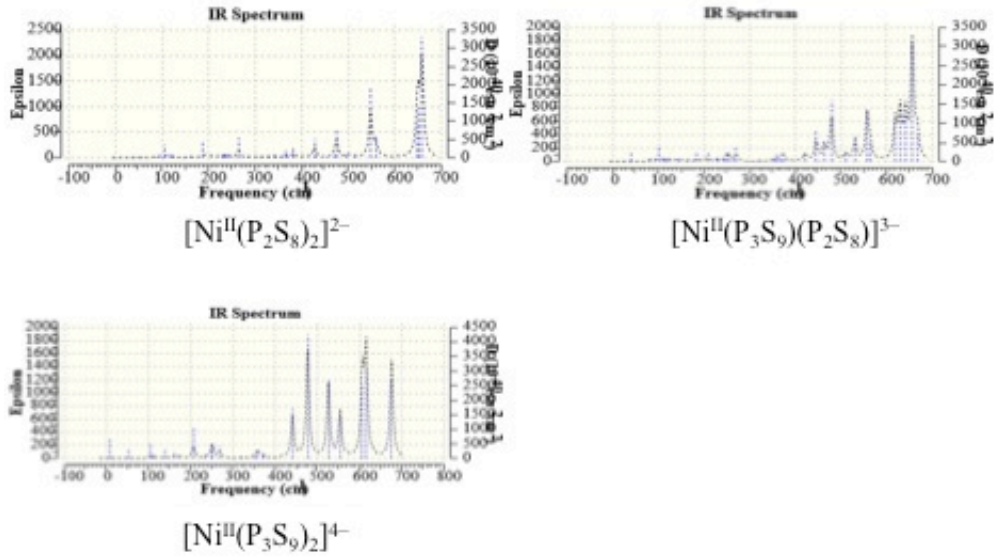

Figure 7.14. Frequency calculation results: Optimized geometry (B3LYP/LANL2, 6-31G(d,p)//B3LYP/LANL2, 6-31G(d,p))

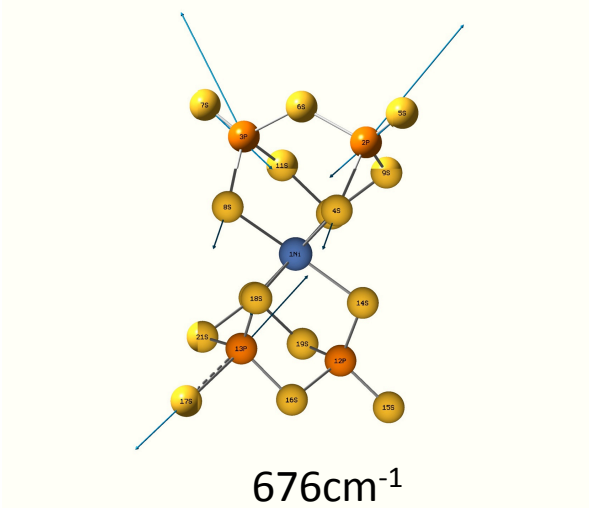

676cm^{-1}

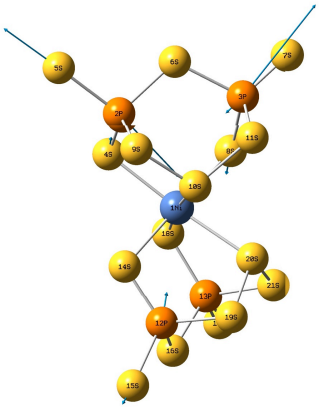

646cm^{-1}

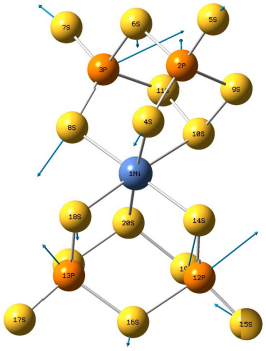

575cm^{-1}

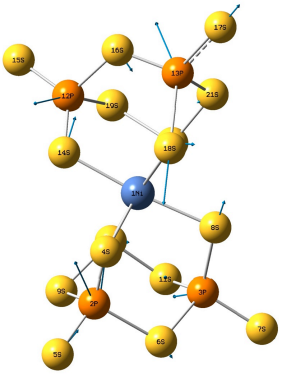

548cm^{-1}

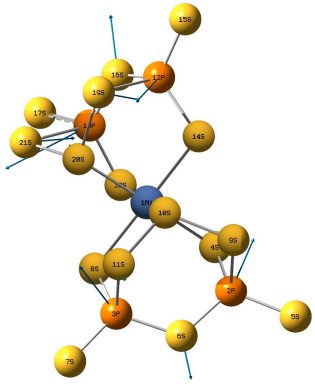

502cm^{-1}

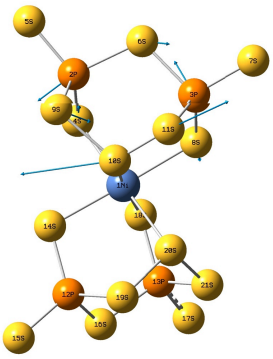

468cm^{-1}

Figure 7.15. Vector Diagrams for $\tilde{\nu}_{calc}$ frequencies of $[Ni^{II}(P_2S_8)_2]^{2-}$.

Chapter 8. Discussion, Conclusions, and Remaining Mysteries

Discussion and Conclusions

When this thesis research started, only two nickel thiophosphates were known and both were unable to be consistently reproduced. From there, the initial observation of orange precipitate in the early summer of 2011 has since blossomed into the isolation of three new metal thiophosphates with strong evidence for two more, the isolation of a new salt of a thioselenate, and a sophisticated computational modeling project.

Because of its ubiquity in the results, it is clear that the $P_2S_8^{2-}$ moiety is very stable and is easily produced by the elemental reaction of a metal, phosphorus, and sulfur in an ionic liquid. It is now known that Ni^{II}, Mo^{II}, and Mn^{II} can be isolated as anions coordinated to $P_2S_8^{2-}$ ligands. The major differences come with solubility. Ni^{II} complexes precipitate above room temperature allowing for facilitated slow cooling down to ambient temperature resulting in the growth of large sample crystals. Mo^{II} and Mn^{II} anions show a higher solubility and require mild refrigeration to begin precipitating due to a greater solubility of the coordination complex in $[EMIM]BF_4$, the only ionic liquid from which they have been isolated so far. With this knowledge, the other reactions that were carried out with Cr, W, Ti, and Nb may also have product that has remained dissolved since they were removed from the oven in the fall of 2012.

Although $P_2S_8^{2-}$ is a soft ligand coordinated to an intermediate-hardness Ni^{II} metal center, the $[Ni^{II}(P_2S_8)_2]^{2-}$ is sufficiently air stable for enough time to complete full characterization on the CAD4 diffractometer. When the Ni atom is replaced by Mn or Mo, there is a dramatic decrease in stability of the product, possibly due to the change in polarizability (hardness) of the metal center as the newer analogs contain

elements from farther left in the d-block of the Periodic Table. With this in mind, the possible Cr, W, Ti, and Nb analogs may also be similarly air sensitive.

What may be one of the more interesting facets of the chemistry surrounding the $P_2S_8^{2-}$ ligand are the two different monoclinic polymorphs of the same anion that have been isolated. The most commonly-isolated polymorph based on recovery of Ni^{II} is α-$[EMIM]_2[Ni^{II}(P_2S_8)_2]$ (cell parameters outlined in Chapter 3). However, due to the thermal cycling during the summer of 2011, the β- $[EMIM]_2[Ni^{II}(P_2S_8)_2]$ form is also known, and the Mo and Mn species prepared have almost identical unit cell parameters to this form (as noted in Chapter 6 they deviate by no more than 3%). This polymorph has not been recreated for the nickel-containing salt, as more thermal cycling experiments were never conducted intentionally.

Unlike $P_2S_8^{2-}$, the $P_3S_9^{3-}$ was known prior to beginning this thesis. It has since appeared in the compound $[Ni^{II}(P_2S_8)(P_3S_9)]^{3-}$ that was affectionately known as "mixed" since it contained both the new $P_2S_8^{2-}$ and $P_3S_9^{3-}$ ligands. Interestingly, the $[Ni^{II}(P_2S_8)(P_3S_9)]^{3-}$ anion was only produced with the 1 : 3.25 : 9 ratio of Ni : P : S from which the $[Ni^{II}(P_3S_9)_2]^{4-}$ anion had originally been isolated. The rapid drop in temperature during the heating profile may be a key feature in the isolation of the $P_3S_9^{3-}$ moiety in the presence of Ni^{II}, as the isolation of $[Cr^{III}(P_3S_9)_2]^{3-}$ was carried out with the longest cooling profile possible and only yielded the $P_3S_9^{3-}$ form despite starting from the molar ratio for $P_2S_8^{2-}$ synthesis. Additionally, the $P_3S_9^{3-}$ moiety may only exist at higher temperatures where the ligand is still a viable product of species present in solution, as when temperature drops it is clear that $P_2S_8^{2-}$ is favored.

Another interesting feature of the results has been the role of the RTIL anion in the product of a given reaction. When trying to prepare either the

$[Ni^{II}(P_2S_8)(P_3S_9)]^{3-}$ or $[Ni^{II}(P_2S_8)_2]^{2-}$ anion, when using $CF_3SO_3^-$ *only* $[Ni^{II}(P_2S_8)_2]^{2-}$ is formed regardless of the molar ratios being used. Only the use of BF_4^- has allowed for the isolation of the $[Ni^{II}(P_2S_8)(P_3S_9)]^{3-}$ anion. Also the different nature of the product crystals between the two anion systems is dramatic with respect to α-$[EMIM]_2[Ni^{II}(P_2S_8)_2]$. BF_4^- will allow for much bulkier crystal growth whereas $CF_3SO_3^-$ promotes the growth of very long, thin fibers of α-$[EMIM]_2[Ni^{II}(P_2S_8)_2]$ that fill the tube such that any remaining $[EMIM]CF_3SO_3$ is trapped in the crystal mass. $[EMIM]CF_3SO_3^-$ has also been the only successful solvent in isolating $[Cr^{III}(P_3S_9)_2]^{3-}$ anion since when $[EMIM]BF_4$ was used, only cubic S_8 was isolated. However, $[EMIM]BF_4$ has been the only successful solvent at preparing the Mo^{II} and Mn^{II} complexes. A better understanding of each solvent system may be necessary so that future reactions can employ the appropriate solvent.

The effort to substitute S with Se did not yield a Ni^{II} based product; however the $P_2Se_8^{2-}$ is analogous to a known $P_2S_8^{2-}$ isomer isolated during the summer of 2012 (but not reported herein since it was nothing new). The sulfur anion was isolated from reaction tube that also included the main product of the reaction, $[Ni^{II}(P_2S_8)_2]^{2-}$, so the replacement of S with Se may still be possible for both ligand systems $P_2S_8^{2-}$ and $P_3S_9^{3-}$ despite initial results.

Remaining Mysteries and Future Directions

In every reaction, regardless of metal, a black solid is found in the bottom of each reaction tube. Although many different cooling schemes have been used, no significant crystallization of the black solid has occurred yet either. Previously black solid from Ni^{II} trials has been analyzed by EDX but no conclusive results of composition have been found. The black solid is not very soluble. It might be an extended solid material analogous to zeolites, the type of product expected of this project from its outset since many solvothermal reactions form such extended solids. It was thought that reaction products would consist of rings of the $P_3S_9^{3-}$ anion with square planar Ni^{II} atoms (rather than octahedral) bridging in three directions to create infinite 2D sheets. However, the chemistry of Ni^{II} might not be the most important factor since the other metals that have been tried will not have the same chemistry yet they exhibit similar black solid production. To probe the nature of these solids full elemental analysis of more than just C, H, and N must be carried out to gather more information about the composition of the solid.

Another possibility is that the black powder precipitates immediately upon formation due to low solubility in the ionic liquids being used, possibly because it has a neutral charge. While other ionic liquids have been used in the past they have not been probed for the black solid solubility properties. This will need to be completed if the black solid is going to be a major target of investigation in the near future. The current ionic liquids may even be sufficient, however they are not currently being heated at a high enough temperature so that slow cooling will allow black solid to slowly crystallize out of solution. Before moving to higher temperatures however, a thorough literature investigation of the thermal stability of

both [EMIM]BF_4 and [EMIM]CF_3SO_3 will have to be conducted. Another option would be to run a series benchtop experiments under vacuum or very low pressures to attempt to dissolve the black solid in either ionic liquid at elevated temperature. If any degradation were to occur NMR or FT-IR would reveal any dramatic changes in solvent structure, though visible changes should also be dramatic.

In contrast to the insoluble, mysterious black solid, the recently-isolated chromium, manganese and molybdenum thiophosphate anions are very soluble and persist in solution until refrigerated or a long period of curing time allowed small crystals to form. Refrigeration has proven successful at isolating crystals of manganese and molybdenum, however chromium trials have not yet been cooled below ambient temperature. Currently only one approach to sub-ambient cooling has been implemented where reaction tubes are suspended in a large beaker of water and placed a departmental refrigerator. This and other methods should be probed further to investigate the degree of control that can be exercised while cooling. Using isolating dewars rather than Pyrex beakers may serve to slow the cooling rate even more and thus facilitate larger crystal growth.

As mentioned before, trials with W, Ti, and Nb were attempted but no crystals were isolated despite a very slow cooling rate to room temperature. Understanding now that anion solubility seems to increase when the included metal is farther to the left of the d-block and that refrigeration has worked for Mn and Mo, remaining reaction tubes of what were thought to be unsuccessful metal trials should be cooled slowly by the dewar method described above to see if any crystals can be isolated.

Deviating from sulfur chemistry, future investigations of selenophosphates as possible ligands should be continued despite the lack of metal-containing products from the Ni : P : Se trials. If isolated, crystals would probably be as air sensitive as current thiophosphates but they would demonstrate that the chalcogenide could be swapped and Se analogs prepared. Furthermore, a move from sulfur as the chalcogenide to oxygen and $P_xO_y^{z-}$ ligands would be of more interest from the standpoint of stability and overall applications. These ligands should bind with much more affinity to the harder metal centers due to the harder nature of the oxygen as Lewis base. The resulting greater stability would allow for more methods of characterization and possible application of products if they demonstrate interesting properties. Polyoxometalates such as $[PW_{12}O_{40}]^{3-}$ (As noted in Chapter 1) may also be interesting products to target by ionothermal routes to further expand the applicability of the ionothermal method.[16]

Overall, the results of this project have opened many avenues of investigation that future students should tackle with newfound curiosity and enthusiasm for the subject of chemistry. As a student at the recent Student Symposium poster session remarked, “There is so much left to be done.”

Appendix 1

Inorganic Chemistry

Article

pubs.acs.org/IC

Ionothermal Synthesis of Four New Nickel Thiophosphate Anions: $[Ni(P_2S_8)_2]^{2-}$, $[Ni(P_3S_9)(P_2S_8)]^{3-}$, $[Ni(P_3S_9)_2]^{4-}$, and $[(NiP_3S_8)_4(PS_4)]^{7-}$

Jason A. Cody,*[†] Kenneth B. Finch,[†] Gilbert J. Reynders, III,[†] Grant C. B. Alexander,[†] Hyung G. Lim,[†] Christian Näther,[‡] and Wolfgang Bensch[‡]

[†]Department of Chemistry, Lake Forest College, 555 North Sheridan Road, Lake Forest, Illinois 60045, United States

[‡]Institute of Inorganic Chemistry, Christian-Albrechts-University of Kiel, Max-Eyth Strasse 2, 24118 Kiel, Germany

Supporting Information

ABSTRACT: Four new nickel thiophosphate anions have been isolated as 1-ethyl-3-methylimidazolium (EMIM) salts: $[EMIM]_2[Ni(P_2S_8)_2]$ (**1**), $[EMIM]_3[Ni(P_3S_9)(P_2S_8)]$ (**2**), $[EMIM]_4[Ni(P_3S_9)_2]$ (**3**), and $[EMIM]_7[(NiP_3S_8)_4(PS_4)]$ (**4**). Single crystals of each were prepared by ionothermal reaction of the elements in $[EMIM][BF_4]$. **1** can also be obtained from $[EMIM][CF_3SO_3]$. In all four anions, Ni atoms are octahedrally coordinated and P atoms are tetrahedrally coordinated. In the anion found in **1**, two tridentate 1,3-$P_2S_8^{2-}$ ligands are cis to each other. The anion in **2** contains two different tridentate thiophosphate ligands, 1,3-$P_2S_8^{2-}$ and $P_3S_9^{3-}$, whereas the anion in **3** consists of two $P_3S_9^{3-}$ ligands coordinated to the central Ni atom. The anion in **4** is complex, consisting of four $NiP_3S_8^-$ clusters surrounding a central PS_4 tetrahedron; within the $NiP_3S_8^-$ groups, one P atom is directly bound to Ni. The discovery of these four new compounds demonstrates the versatility of ionothermal methods for the synthesis of novel thiophosphates.

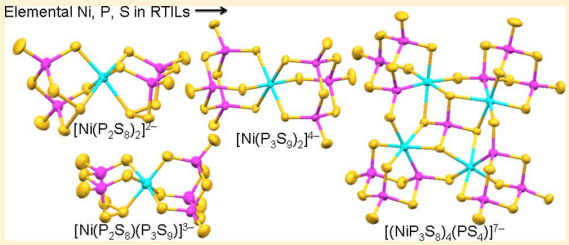

INTRODUCTION

The unique properties of ionic liquids (ILs), including high thermal stability, wide liquidus ranges, negligible vapor pressure, and their ability to dissolve a variety of materials, make them favorable media for both organic and inorganic reactions.[1−4] Recently, ILs have been successfully used as media for the preparation of zeolites,[5] metal-containing nanoparticles,[1] metal−organic frameworks,[6,7] polyoxometalates,[8] as well as coordination polymers.[9,10] Thus, ILs, specifically room-temperature ILs (RTILs),[11−13] have been studied in detail in order to replace more hazardous or environmentally harmful solvents. However, while ILs themselves have been known for decades, inorganic synthesis using ionothermal methods is a developing field of study.[14,15]

Among research on inorganic compounds using ILs, chalcogenide synthesis has been of particular interest because of the potential thermoelectric[16,17] and solar energy conversion[18] properties of the resulting products. However, of the handful of reports on chalcogenide syntheses in ILs found in the literature,[16,19−21] many result in simple binary structures.[22,23] More specifically, thiophosphates have shown important properties such as luminescence[24] but have yet to be explored with ILs.[15]

Because access to new properties often comes through the preparation of new materials, ionothermal synthesis provides an important avenue for exploration because most thiophosphates prepared via more traditional molten flux routes tend to contain smaller P/S groups such as isolated tetrahedral PS_4^{3-} or ethane-like $[P_2S_6]^{4-}$ anions.[25] For example, the compounds $A_3Nd[PS_4]_2$ (A = K, Cs)[26] and $Ba_3Ln_2[P_4S_{16}]$ (Ln = Gd−Er)[27] contain isolated PS_4^{3-} tetrahedra, whereas $A_3Zr_2P_5S_{18}$ (A = Rb, Cs)[28] and $Cs_2Ti_2(P_2S_8)(PS_4)_2$[29] have only slightly larger $[P_2S_7]^{4-}$ and $[P_2S_8]^{4-}$ anions, respectively.

Recent reports of new chalcogenide complexes prepared in ILs are the cationic species such as $[Bi_2TeBr](AlCl_4)$[16] and $[Sb_7S_8Br_2](AlCl_4)_3$.[20] These complex cations, the former crystallized as two-dimensional sheets and the latter as a double-cubane molecular cation, were isolated from an acidic IL, [EMIM]Br/$AlCl_3$.

Among known thiophosphate compounds, $KNiPS_4$ piqued our interest because of its unusual combination of solid-state and solution-phase reactivity.[30] When the $^1_\infty[NiPS_4^-]$ chains of the solid-state reaction product are dissolved in *N*,*N*-dimethylformamide (DMF), a liquid-crystalline phase is observed that, in turn, ultimately forms discrete $[Ni_3P_3S_{12}]^{3-}$ rings.[31,32] These crownlike rings exhibit pseudo-C_{3v} symmetry, and each contains three square-planar Ni^{II} d^8 atoms and three tetrahedrally coordinated P^V atoms; the counterions in the solid salts can be cryptand-encased alkali metals, alkaline-earth ions, or even other transition-metal coordination complexes.[33] This chemistry is quite different from that of the simpler solid-state $NiPS_3$ compound that contains ethane-like $P_2S_6^{2-}$ anions that coordinate octahedral Ni atoms.[34]

Here, we report the discovery of four new nickel thiophosphate anions using two different 1-ethyl-3-methylimi-

Received: September 30, 2012
Published: November 29, 2012

   dx.doi.org/10.1021/ic302112g | Inorg. Chem. 2012, 51, 13357−13362

dazolium RTILs as the solvent (with tetrafluoroborate, BF_4^-, and triflate, $CF_3SO_3^-$, anions) for reactions of elemental Ni, P, and S. We also present the structures and spectroscopy of the novel anions.

EXPERIMENTAL SECTION

General Procedures. Elemental Ni, P, and S were combined in a nitrogen-filled MBraun Lab Master 130 glovebox. According to the ratios given in Scheme 1, the mass sums for 6−10 reactions were combined, ground together, and distributed by mass into the corresponding number of reaction tubes, and then 1.25 mL of the appropriate IL was added to each tube in a nitrogen-filled glovebag. The ILs [EMIM][BF_4] and [EMIM][CF_3SO_3] (EMIM = 1-ethyl-3-methylimidazolium) were synthesized according to the literature procedure shown in Schemes 2[35] and 3.[36] The tubes were evacuated, sealed, and heated in a temperature-controller-equipped drying oven according to the heating profiles discussed in the respective synthesis sections. Once heating and cooling were completed, the reaction tubes were opened, the ILs were decanted, and the solids were vacuum-filtered and washed with dry acetone prior to characterization.

Scheme 1. Summary of the Synthetic Routes Used for Nickel Thiophosphate Anions 1−4[a]

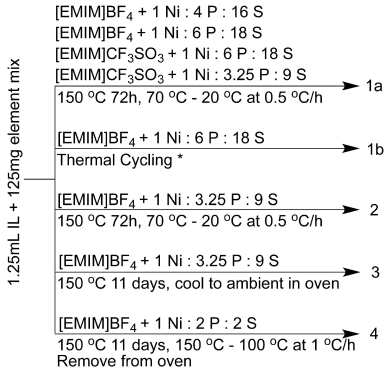

[a]Thermal cycling involved heating at 150 °C for 5 days. A power outage allowed the oven to cool to ambient temperature, and then when the power was restored, the oven returned to 150 °C before slowly cooling from 70 °C at 0.5 °C/h.

Scheme 2. Preparation of [EMIM]BF_4 from Reference 35

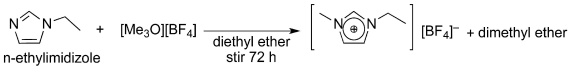

Scheme 3. Preparation of [EMIM]CF_3SO_3 from Reference 36

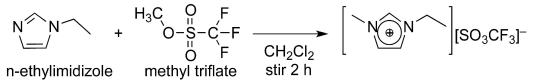

Energy-Dispersive X-ray (EDX). The chemical compositions of all samples were analyzed using an EDX-equipped scanning electron microscope (Hitachi S-3400N-II). These analyses were performed on single crystals mounted with double-sided conducting tape on aluminum stubs. The average percent compositions for all compounds agree very well with the expected molar ratios from the single-crystal diffraction studies.

Elemental Analysis. The carbon, nitrogen, and hydrogen compositions of compounds **1** and **2** were analyzed by ALS Environmental, formerly Columbia Analytical Services.

X-ray Crystallography. The structures of all compounds were determined by single-crystal X-ray diffraction studies. Data collections were carried out using an IPDS-1 or IPDS-2 Imaging Plate Diffraction System from STOE & CIE using graphite-monochromated Mo Kα radiation. For all compounds, a face-indexed absorption correction was performed using *X-red* and *X-Shape* from STOE & CIE. All structures were solved with *SHELXS-97*, and refinement was done against F^2 using *SHELXL-97*.[37] All non-H atoms, except some of the disordered C atoms of lower occupancy as well as the C and N atoms in compound **2**, were refined anisotropically. The H atoms were positioned with idealized geometry and refined isotropically with $U_{iso}(H) = 1.2U_{eq}(C)$ (1.5 for methyl H atoms). In compound **1a**, the ethyl and methyl orientations of one EMIM cation are disordered and were refined using a split model (occupancies 0.6 and 0.4, respectively). In compound **2**, all organic cations were refined using restraints. In compound **3**, one organic cation is disordered in two orientations and was refined using a split model. This cation is additionally disordered around a crystallographic mirror plane. Therefore, the structure was additionally refined in space groups *C*2 and *Cc*, but the disordering remains constant. In compound **4**, one organic cation has a disordered ethyl group that was refined using a split model, and another organic cation is disordered over two overlapping positions with refined occupancies of 0.7 and 0.3 for the two orientations. Selected crystal data and details on the structure refinements are given in Table 1.

^{31}P NMR Spectroscopy. The ^{31}P resonances of compound **1** were recorded on Varian Inova 400 MHz Fourier transform (FT)-NMR equipped with a multinuclear variable-temperature probe. Dimethyl sulfoxide (DMSO)-d_6 was used as the solvent for all scans; the samples decompose in DMSO, as evidenced by the gradual decrease in the intensity of the characteristic peaks of the anions and the concurrent appearance of additional peaks in less than 1 h.

IR Spectroscopy. The IR stretches of all compounds were recorded on a Thermo Nicolet Avatar 360 FT-IR spectrometer in pressed KBr disks.

Synthesis of 1a and 1b, [EMIM]$_2$[Ni(P_2S_8)$_2$]. A total mass of 1.25 g of elemental Ni, P, and S was assembled and ground in a glovebox in the molar ratios of 1:6:18 and 1:4:16, as shown in Scheme 1. Then, 125 mg portions of the mixture were weighed into reaction tubes, and 1.25 mL of the IL, either [EMIM][BF_4] or [EMIM][CF_3SO_3], was added. The original molar ratio of 1:6:18 was used in an attempt to remake **3**; however, after characterization of **1a** and **1b**, the direct elemental ratio of 1:4:16 was used and resulted in higher yield. The tubes were heated for 4 days at 150 °C, followed by rapid cooling to 70 °C, and then were further cooled at 0.5 °C/h to 20 °C. **1b** was isolated from a single set of reaction tubes that underwent uncontrolled thermal cycling due to a power outage. Yields based on Ni were 37.6% (62.0 mg) from [EMIM][BF_4] and 55.8% (92.1 mg) from [EMIM][CF_3SO_3]. Elem anal. Calcd for **1** ($C_{12}H_{22}N_4NiP_4S_{16}$): C, 15.7; H, 2.42; N, 6.10. Found: C, 15.3; H, 2.91; N, 5.89. ^{31}P NMR (400 MHz, DMSO-d_6, 20 °C): δ 82.0. FT-IR from [EMIM][BF_4]: ν(EMIM$^+$) 960 (w), 916 (w), 798 (w), 772.98 (vw), 699 (w), 667 (sh), 642 (s), 618 (m), 592 (vw), 522 (w), ν([Ni(P_2S_8)$_2$]$^{2-}$) 824 (m), 751 (w), 741 (w), 691 (m), 675 (s), 574 (m), 548 (m), 500 (m), 467 (m), 461 (m), 457 (w) cm^{-1}. FT-IR from [EMIM][CF_3SO_3]: ν(EMIM$^+$) 953 (w), 916 (w), 798 (w), 700 (w), 667 (sh), 644 (s), 618 (s), 596 (vw), ν([Ni(P_2S_8)$_2$]$^{2-}$) 825 (m), 751 (w), 741 (w), 690 (m), 676 (s), 575 (s), 548 (m), 502 (m), 468 (m), 463 (m), 457 (w) cm^{-1}.

Synthesis of 2, [EMIM]$_3$[Ni(P_3S_9)(P_2S_8)]. **2** was prepared in the same manner as **1**; however, it was only isolated from [EMIM][BF_4] from the molar ratio 1:3.25:9 Ni/P/S (see Scheme 1). Large, dark-orange crystals formed in long, hollow hexagonal tubes, encasing the IL within. The yield was found to be 38% (115.9 mg) based on Ni. Elem anal. Calcd for **2** ($C_{18}H_{33}N_6NiP_5S_{17}$): C, 19.8; H, 3.05; N, 7.69. Found: C, 21.5; H, 2.88; N, 7.89. FT-IR: ν(EMIM$^+$) 956 (br), 798 (w), 699 (w), 668 (sh), 646 (s), 617 (s), ν([Ni(P_3S_9)(P_2S_8)]$^{3-}$) 983

dx.doi.org/10.1021/ic302112g | *Inorg. Chem.* 2012, 51, 13357−13362

Table 1. Crystallographic Data for 1−4

	1a	1b	2	3	4
chemical formula	$[Ni(P_2S_8)_2]^{2-}$	β-$[Ni(P_2S_8)_2]^{2-}$	$[Ni(P_3S_9)(P_2S_8)]^{3-}$	$[Ni(P_3S_9)_2]^{4-}$	$[(NiP_3S_8)_4(PS_4)]^{7-}$
a, Å	22.5477(9)	7.2317(5)	11.8394(2)	22.0276(14)	10.5512(7)
b, Å	7.2491(2)	17.7138(9)	20.0693(3)	12.2186(7)	16.0948(10)
c, Å	24.0143(9)	13.4488(9)	56.7194(13)	22.3472(12)	32.066(2)
α, deg	90	90	90	90	100.936(8)
β, deg	116.410(3)	93.637(8)	90	119.397(6)	91.108(8)
γ, deg	90	90	90	90	105.420(7)
V, Å^3	2515.9(2)	1719.33(19)	13476.8(4)	5240.2(5)	5140.0(6)
Z	4	2	12	4	2
fw, g mol^{-1}	917.89	917.89	1092.08	1266.28	2569.79
space group	$P\,2_1/n$	$P\,2_1$	$P\,2_1\,2_1\,2_1$	$C\,2/c$	$P\,\bar{1}$
T, °C	20	−73	20	−100	20
λ, Å	0.71073	0.71073	0.71073	0.71073	0.71073
D_{calcd}	1.734	1.773	1.615	1.605	1.661
μ, mm^{-1}	1.701	1.739	1.425	1.303	1.695
R1(F_o)[a]	0.0356	0.0478	0.0444	0.0380	0.0554
wR2(F_o^2)	0.0838	0.1194	0.1222	0.0916	0.1309

[a] $R1 = \sum||F_o| - |F_c||/\sum|F_o|$; $wR2 = [\sum w(F_o^2 - F_c^2)^2/\sum w(F_o^2)^2]^{1/2}$.

Table 2. Selected Bond Distances (Å) and Angles (deg) for 1−4

	1a	1b	2	3	4
Ni−S	2.354(1) −2.5821(8)	2.369(2) −2.554(2)	2.369(3) −2.563(3)	2.4337(7) −2.4580(6)	2.381(2) −2.602(2)
P−S	1.931(2) −2.137(1)	1.945(3) −2.130(2)	1.936(5)− 2.128(3)	1.953(1) −2.1266(9)	1.941(3) −2.195(2)
S−S	2.056(1) −2.064(1)	2.060(2) −2.068(3)	2.056(4) −2.063(4)		
cis-S−Ni−S	78.01(2) −95.34(3)	80.44(6) −95.90(6)	78.9(1) −101.5(1)	82.96(2) −97.04(2)	80.99(6) −98.55(7)
trans-S−Ni−S	172.82(3) −177.78(3)	175.94(7) −176.81(7)	169.4(1) −179.4(2)	180.00(2)	167.41(8) −175.99(8)
cis-P−Ni−S					79.48(7) −98.55(7)
trans-P−Ni−S					170.17(8) −175.48(8)
S−P−S	102.94(5) −118.08(5)	103.5(1) −119.8(1)	102.7(2) −120.1(2)	102.37(4) −116.79(5)	100.4(1) −117.9(2)
P−S−P	109.89(4) −110.81(5)	110.0(1) −110.2(1)	109.1(2) −110.4(2)	109.18(4) −110.08(4)	97.6(1) −110.9(1)
P−S−S	99.64(5) −101.60(5)	99.8(1) −101.63(9)	99.7(1) −100.9(2)		
S−S−S	106.20(5) −106.75(5)	105.2(1) −106.1(1)	106.1(2) −106.7(2)		
Ni−P−S					109.9(1) −127.8(1)
Ni−S−Ni					120.09(8) −123.18(8)

(br), 924 (br), 818 (m), 741 (w), 730 (w), 686 (m), 666 (s), 656 (s), 607 (m), 590 (m), 579 (m), 556 (m), 544 (w), 493 (s), 464 (m), 460 (m), 458 (m) cm^{-1}.

Synthesis of 3, $[EMIM]_4[Ni(P_3S_9)_2]$. **3** was prepared in the same fashion as **2** except for the heating profile (see Scheme 1). The tubes were heated at 150 °C for 11 days and then removed from the oven without slow cooling. After no initial crystal formation, the tubes were left for 1 month without disturbance; opaque orange crystals formed. The yield was not calculated. FT-IR: ν(EMIM$^+$) 958(br), 840 (m), 773 (w), 757 (m), 703 (vw), 669 (sh), 641 (s), 620 (s), 519 (w) cm^{-1}, $\nu([Ni(P_3S_9)_2]^{4-})$ 983 (br), 923 (br), 790 (vw), 658 (s), 647 (s), 607 (w), 586 (s), 576 (vw), 559 (m), 549 (w), 509 (w), 500 (s), 497 (s), 494 (s), 485 (m) cm^{-1}.

Synthesis of 4, $[EMIM]_7[(NiP_3S_8)_4(PS_4)]$. **4** was prepared in the same manner as **1** using the molar ratio described in Scheme 1. The tubes were heated for 11 days at 150 °C and then slowly cooled to 100 °C at 1 °C/h, at which point the tubes were removed from the oven to cool rapidly to room temperature. A few black needles were produced in sufficient amounts to perform EDX (see the Supporting Information) and single-crystal X-ray diffraction studies (Table 1). The yield was not calculated. FT-IR: ν(EMIM$^+$) 959 (w), 798 (w), 618 (m), 597 (w), 523 (w), $\nu([(NiP_3S_8)_4(PS_4)]^{7-})$ 983 (vw), 874 (vw), 875 (vw), 819 (br), 747 (w), 732 (w), 670 (s), 667 (s), 655 (s), 618 (m), 574 (s), 559 (s), 515 (m), 506 (w), 501 (w), 483 (s), 472 (w), 458 (w), 438 (s), 433 (m), 424 (w), 419 (w) cm^{-1}.

RESULTS AND DISCUSSION

Syntheses. All title compounds were obtained as single crystals using the reactions shown in Scheme 1. All preparations of the title thiophosphate anions were carried out in ILs synthesized according to literature procedures as shown in Schemes 2 and 3. Because of the preparation routes chosen, we avoided the two largest challenges of using ILs in synthesis: the high purchase price by preparing the ILs ourselves and the difficulty in purification of prepared ILs because the only byproducts of the syntheses were solvents that were easily removed via vacuum. In addition to the crystals of the new anions, all reactions in $[EMIM][BF_4]$ yielded various amounts of amorphous black powder; all reactions carried out in $[EMIM][CF_3SO_3]$ yielded only orange needles of **1**. Despite its role as our initial impetus for the exploration, $[Ni_3P_3S_{12}]^{3-}$ was not observed in any crystalline products.

Crystal Structures. In **1**−**4**, there are several structural similarities: all Ni^{II} atoms are octahedrally coordinated, all P atoms are tetrahedrally coordinated, and S atoms are found in several different bonding modes ranging from terminal to μ_3. In addition, the only cations observed in the crystalline products were EMIM$^+$ cations, regardless of whether $[EMIM][BF_4]$ or $[EMIM][CF_3SO_3]$ was used as the IL for the synthesis. The Ni−S distances of 2.354(1)−2.602(2) Å, P−S distances of

dx.doi.org/10.1021/ic302112g | Inorg. Chem. 2012, 51, 13357−13362

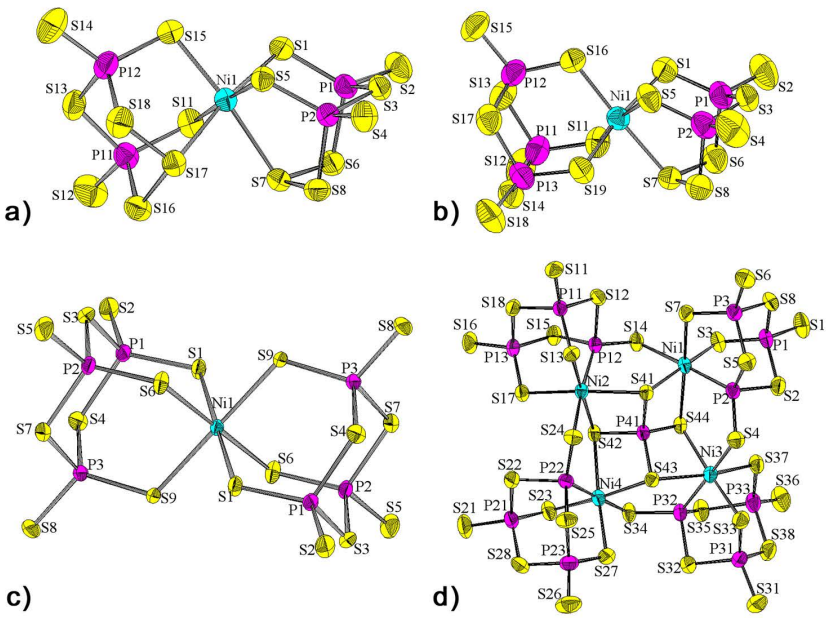

Figure 1. Thermal ellipsoid plots (50%) of the structures of nickel thiophosphate anions: (a) **1a**, $[Ni(P_2S_8)_2]^{2-}$ identical with that found in **1b**; (b) **2**, $[Ni(P_3S_9)(P_2S_8)]^{3-}$; (c) **3**, $[Ni(P_3S_9)_2]^{4-}$, (d) **4**, $[(NiP_3S_8)_4(PS_4)]^{7-}$. Ni atoms are teal, P atoms are magenta, and S atoms are yellow.

1.931(2)−2.195(2) Å, and S−S distances of 2.056(1)−2.068(3) Å (see Table 2) all agree with other published thiophosphate compounds in the literature.[38−40] Structures **1a**, **3**, and **4** contain disordered cations, but simple modeling of the two major orientations was sufficient for reasonable accounting of the available electron density. Despite the low value for sin θ/λ of the data collected for **3**, owing to the very large unit cell dimension of 56.7194(13) Å, the single-crystal structure solution clearly resolves the inorganic portions of the structure that were refined anisotropically; the lighter atoms were refined only isotropically. In all other structure solutions, all atoms were refined anisotropically.

The same nickel thiophosphate anion is found in both **1a** and **1b**. It contains a central Ni atom with two tridentate 1,3-$P_2S_8^{2-}$ ligands (see Figure 1a). On each, only S atoms coordinate with the Ni; two of these are coordinated to the P atoms of the 1,3-$P_2S_8^{2-}$ moiety, and the third is the central S atom of the trisulfide group of the P_2S_4 ring of the 1,3-$P_2S_8^{2-}$ group. The trisulfide bridges of the two 1,3-$P_2S_8^{2-}$ ligands are arranged cis rather than trans relative to one another, giving the anion pseudo-C_2 symmetry. The structural differences between uncoordinated and coordinated 1,3-$P_2S_8^{2-}$ ligands are small enough to be attributed to the difference in temperature between X-ray data collection experiments.

The 1,3-$P_2S_8^{2-}$ ligand found in **1a** and **1b** is not new, but the tridentate coordination mode has never been observed. The first appearance of 1,3-$P_2S_8^{2-}$ is as an isolated anion prepared as a PPh_4^+ salt from the reaction of PPh_4S_5 and white phosphorus in acetonitrile.[38] The only report of this anion as a ligand to transition-metal centers is $[(TiCl_2)(P_2S_8)]_2$ prepared from $TiCl_4$ and P_4S_{10} in CS_2.[41] In this ring-shaped neutral molecule, the P_2S_8 groups bridge two octahedrally coordinated Ti atoms; the four terminal S atoms of each P_2S_8 group coordinate to the Ti atoms, and two Cl atoms complete the coordination sphere. The trisulfide group of the P_2S_4 ring of the 1,3-$P_2S_8^{2-}$ group does not coordinate to the Ti atoms.

The bond angles and distances found in **1a** and **1b** are essentially the same (Table 2). Apparently, unintentional thermal cycling due to a thunderstorm power outage caused dissolution of the $[Ni(P_2S_8)_2]^{2-}$ anion and precipitation in the different monoclinic crystalline form. However, only the morphology of the crystals is different: **1a** grows as long, orange, rectangular needles, and **1b** appears as cubes of the same orange color.

The new anion in **2** contains two different tridentate thiophosphate ligands: the same 1,3-$P_2S_8^{2-}$ unit found in **1** and a nonathiocyclotriphosphate, $P_3S_9^{3-}$, moiety (see Figure 1b). Upon coordination to the Ni atom, the geometrical features of the $P_3S_9^{3-}$ group change very little; differences observed in the P−S distances of the coordinating S atoms are sufficiently small as to arise from the temperature difference in data acquisition: from an average of 1.963 Å (120 K)[39] to an average of 1.988 Å (173 K) in **2**.

Similar to the $P_2S_8^{2-}$ group, the $P_3S_9^{3-}$ moiety is not new, but it has never been observed in the coordination mode exhibited in **2**. This anion, first reported in 1982,[42] was prepared from P_4S_{10} in liquid ammonia at −33 °C, and the structure was first reported in 1992 from a crystal prepared from the direct reaction of the elements with amines in various traditional solvents (i.e., chloroform and DMF).[39] More recently, it was prepared from the reaction of P_4S_{10} and *N*,*N*′-diphenylurea and isolated as the pyridinium salt $[pyH]_3[P_3S_9]$.[40]

There are only two reports of $P_3S_9^{3-}$ serving as a ligand, one compound with Ga atoms and the other with Cu atoms. In $(t\text{-}Bu)_6Ga_3P_3S_9$,[43] one central P_3S_9 group participates in bidentate bonding through terminal S atoms to three Ga atoms, forming a large trimetallic ring. This compound was prepared from *t*-Bu_3Ga and P_4S_{10} in pentane at ambient temperature. The P_3S_9 groups found in $K_2CuP_3S_9$[44] were prepared from K_2S, P_2S_5, and Cu under reactive flux conditions. In this case, the thiophosphate ligands bridge Cu atoms to form a coordination

dx.doi.org/10.1021/ic302112g | *Inorg. Chem.* 2012, 51, 13357−13362

polymer, binding in a tridentate mode to one Cu atom on one side and in a monodentate mode to a Cu atom on the other.

The molecular anion found in **3** comprises a central Ni atom coordinated to two tridentate $P_3S_9^{3-}$ ligands, assuming pseudo-D_{3h} symmetry (see Figure 1c). The geometrical parameters for the ligand are essentially the same as those found in **2**.

The structure of the nickel thiophosphate anion found in **4** is complex (see Figure 1d). It can be described as a central PS_4^{3-} group surrounded by four interconnecting $NiP_3S_8^-$ groups, thus forming a disk-shaped 7− polyatomic anion. In fact, there is a distorted square of Ni_4S_4 circumscribed around the central PS_4^{3-} group. The Ni-atom coordination sphere is thus comprised of two S atoms from the central square, two S and one P atom from the P_3S_8 groups, and one S atom from a neighboring $NiP_3S_8^-$ moiety.

The coordination within the $NiP_3S_8^-$ groups is unusual because one P atom is directly bound to Ni; we know of no other thiophosphate compounds that exhibit P atoms that coordinate to metal atoms in *two modes*: directly, acting as a phosphine ligand, and through bridging S atoms. The four $NiP_3S_8^-$ groups resemble β-P_4S_8, wherein one P−P bond is found in the midst of many P−S−P linkages.[45] The P atoms coordinated to the Ni atoms must be formally P^{III} atoms, whereas the P atoms surrounded by four S atoms are formally P^V. This is consistent with the overall charge on the molecular anion; the empirical formula for the anion can be written as $Ni^{II}_4P^{III}_4P^V_9S^{II-}_{36}$ for an overall ionic charge of 7−. Moreover, the P^{III}−S distances are longer, on average, than those observed for P^V−S.

Of the four anions presented herein, **4** exhibits the most distortion from idealized tetrahedral coordination for P atoms and octahedral coordination for Ni atoms. In particular, the 100.38(11)° S34−P32−S35 angle from the phosphine-coordinated P atom is the smallest observed. Moreover, the Ni atoms have S−Ni−S angles that range from 80.99(6)° S41−Ni1−S44 to 98.55(7)° S33−Ni3−S43 (Table 2).

^{31}P NMR Spectroscopy. Finding a suitable solvent for NMR spectroscopy was a challenge because the thiophosphate anions were soluble in few non-oxygen-containing solvents. Compounds **1**−**3** are insoluble in chloroform, acetone, and acetonitrile. DMSO-d_6 was used for all scans, but slow decomposition of all products was observed, beginning after only ~30 min. The observed chemical shift of δ 81.98 for **1** is consistent with the shift (δ 83) observed for the isolated $P_3S_9^{3-}$ anion.[42]

IR Spectroscopy. Most features of the IR spectra of **1**−**4** are observed below 800 cm^{-1}. After removal of the many peaks from the EMIM cations present in all salts, distinctive patterns for the 1,3-$P_2S_8^{2-}$ and $P_3S_9^{3-}$ ligands are observed (see the Supporting Information). Several of the peaks from the homoleptic anions found in **1** and **3** are observed in the mixed-anion **2**. The IR spectrum of **4** has many peaks in the same low-energy range, but these do not match peaks from **1**−**3** (see Table S1 in the Supporting Information). Uniquely identified absorbances are observed for all four compounds: **1**, 825 and 675 cm^{-1}; **2**, 818 cm^{-1}; **3**, 647 and 497 cm^{-1}; **4**, 670, 618, and 438 cm^{-1}.

CONCLUSION

This work demonstrates the versatility of ionothermal synthesis for preparing new thiophosphate compounds directly from the elements. We are currently exploring the reactivity of other metals with thiophosphate ligands under ionothermal conditions.

ASSOCIATED CONTENT

Supporting Information

IR spectra, CIF files, and EDX analysis for compounds **1**−**4**. This material is available free of charge via the Internet at http://pubs.acs.org.

AUTHOR INFORMATION

Corresponding Author

*E-mail: cody@lakeforest.edu. Phone: 847-735-5093. Fax: 847-735-6194.

Notes

The authors declare no competing financial interest.

ACKNOWLEDGMENTS

We thank Lake Forest College, the NUANCE EPIC center at Northwestern University for use of the EDX facilities, Dr. Robert Sommer for use of the X2S diffractometer at DePaul University, and the state of Schleshwig-Holstein. We also thank Lake Forest College undergraduate students N. Larson, K. Ric, J. Brown, and A. (Constantinescu) Ondreicsik for contributions to this work.

REFERENCES

(1) Li, Z.; Jia, Z.; Luan, Y.; Mu, T. *Curr. Opin. Solid State Mater. Sci.* **2008**, *12*, 1−8.
(2) Morris, R. E. *Chem. Commun.* **2009**, 2990−2998.
(3) Ma, Z.; Yu, J.; Dai, S. *Adv. Mater.* **2010**, *22*, 261−285.
(4) Ahmed, E.; Ruck, M. *Angew. Chem., Int. Ed.* **2012**, *51*, 308−309.
(5) Cooper, E. R.; Andrews, C. D.; Wheatley, P. S.; Webb, P. E.; Wormald, P.; Morris, R. E. *Nature* **2004**, *430*, 1012−1016.
(6) Parnham, E. R.; Morris, R. E. *Acc. Chem. Res.* **2007**, *40*, 1005−1013.
(7) Xe, Z.; Feng, M.; Li, J.; Huang, X. *Inorg. Chem. Commun.* **2008**, *11*, 1143−1146.
(8) Zou, N.; Chen, W.; Li, Y.; Liu, W.; Wang, E. *Inorg. Chem. Commun.* **2008**, *11*, 1367−1370.
(9) Lin, Z.; Wragg, D. S.; Wright, P. A.; Warren, J. E.; Morris, R. E. *J. Am. Chem. Soc.* **2007**, *129*, 10334−10335.
(10) Zhang, N.; Liu, Q.; Wan, Y. *Inorg. Chem. Commun.* **2010**, *13*, 706−710.
(11) Buzzeo, M. C.; Evans, R. G.; Compton, R. G. *ChemPhysChem* **2004**, *5*, 1106−1120.
(12) Hayamizu, K.; Aihara, Y.; Nakagawa, H.; Nukuda, T.; Price, W. S. *J. Phys. Chem. B* **2004**, *108*, 19527−19532.
(13) Mizuuchi, H.; Jaitely, V.; Murdan, S.; Florence, A. T. *Eur. J. Pharm. Sci.* **2008**, *33*, 326−331.
(14) Castner, E. W., Jr.; Wishart, J. F. *J. Chem. Phys.* **2010**, *132*, 120901−120910.
(15) Freudenmann, D.; Wolf, S.; Wolff, M.; Feldmann, C. *Angew. Chem., Int. Ed.* **2011**, *50*, 11050−11060.
(16) Biswas, K.; Zhang, Q.; Chung, I.; Song, J.; Androulakis, J.; Freeman, A. J.; Kanatzidis, M. G. *J. Am. Chem. Soc.* **2010**, *132*, 14760−14762.
(17) Ding, N.; Kanatzidis, M. G. *Angew. Chem., Int. Ed.* **2006**, *45*, 1397−1401.
(18) Hsu, K. F.; Loo, S.; Guo, F.; Chen, W.; Dyck, J. S.; Uher, C.; Hogan, T.; Polychroniadis, E. K.; Kanatzidis, M. G. *Science* **2004**, *303*, 818−821.
(19) Lin, Y.; Dehnen, S. *Inorg. Chem.* **2011**, *50*, 7913−7915.
(20) Zhang, Q.; Chung, I.; Jang, J. I.; Ketterson, J. B.; Kanatzidis, M. G. *J. Am. Chem. Soc.* **2009**, *131*, 9896−9897.
(21) Li, J.; Xie, Z.; He, X.; Li, L.; Huang, X. *Angew. Chem., Int. Ed.* **2011**, *50*, 11395−11399.

(22) Mahjoor, P.; Latturner, S. E. *Cryst. Growth Des.* **2009**, *9*, 1385–1389.
(23) Jiang, Y.; Zhu, Y. *J. Phys. Chem. B* **2005**, *109*, 4361–4364.
(24) Huang, Z.; Cajipe, V. B.; Le Rolland, B.; Colombet, P.; Schipper, W. J.; Blasse, G. *Eur. J. Solid State Inorg. Chem.* **1992**, *29*, 1133–1144.
(25) Wu, Y.; Bensch, W. *CrystEngComm* **2010**, *12*, 1003–1015.
(26) Wu, Y.; Bensch, W. *Inorg. Chem.* **2008**, *47*, 7523–7534.
(27) Klawitter, Y.; Bensch, W.; Wickleder, C. *Chem. Mater.* **2006**, *18*, 187–197.
(28) Gutzmann, A.; Näther, C.; Bensch, W. *Solid State Sci.* **2006**, *6*, 205–211.
(29) Wu, Y.; Bensch, W. *Inorg. Chem.* **2007**, *46*, 6170–6177.
(30) Sayettat, J.; Bull, L. M.; Gabriel, J. P.; Jobic, S.; Camerel, F.; Marie, A.; Fourmigué, M.; Batail, P.; Brec, R.; Inglebert, R. *Angew. Chem., Int. Ed.* **1998**, *37*, 1711–1714.
(31) Sayettat, J.; Bull, L. M.; Jobic, S.; Gabriel, J. P.; Fourmigué, M.; Batail, P.; Brec, R.; Inglebert, R.; Sourisseau, C. *J. Mater. Chem.* **1999**, *9*, 143–153.
(32) Bujoli-Doeuff, M.; Coste, S.; Evain, M.; Brec, R.; Massiot, D.; Jobic, S. *New J. Chem.* **2002**, *26*, 910–914.
(33) Collin, I.; Bujoli-Doeuff, M.; Dessapt, R.; Champeaux, M.; Danot, M.; Paris, M.; Jobic, S. *C. R. Chim.* **2005**, *8*, 1029–1033.
(34) Brec, R. *Solid State Ionics* **1986**, *22*, 3–30.
(35) Egashira, M.; Yamamoto, Y.; Fukutake, T.; Yoshimoto, N.; Morita, M. *J. Fluorine Chem.* **2006**, *127*, 1261–1264.
(36) Bonhôte, P.; Dias, A.; Papageorgiou, N.; Kalyanasundaram, K.; Grätzel, M. *Inorg. Chem.* **1996**, *35*, 1168–1178.
(37) Sheldrick, G. M. *SHELXS-97 and SHELXL-97*; Siemens Analytical X-ray Instruments, Inc.: Madison, WI, 1997.
(38) Gruber, H.; Müller, U. *Z. Anorg. Allg. Chem.* **1997**, *623*, 957–961.
(39) Falius, H.; Schliephake, A. *Z. Anorg. Allg. Chem.* **1992**, *611*, 141–148.
(40) Dastychová, L.; Sotolářová, M.; Dastych, D.; Taraba, J.; Nečas, M.; Příhoda, J. *Polyhedron* **2007**, *26*, 4250–4256.
(41) Hoppe, D.; Pfitzner, A. *Z. Anorg. Allg. Chem.* **2009**, *635*, 1986–1990.
(42) Wolf, G.; Meisel, M. *Z. Anorg. Allg. Chem.* **1982**, *494*, 49–54.
(43) Cowley, A. H.; Hellert, D.; Gabbai, F. P.; Olbrich, F. *Inorg. Chem.* **1995**, *34*, 3127–3129.
(44) Hanko, J. A.; Sayettat, J.; Jobic, S.; Brec, R.; Kanatzidis, M. G. *Chem. Mater.* **1998**, *10*, 3040–3049.
(45) Jason, M. E.; Ngo, T.; Rahman, S. *Inorg. Chem.* **1997**, *36*, 2633–2640.

Appendix 2

Acta Crystallographica Section E
Structure Reports Online
ISSN 1600-5368

Bis(1-ethyl-3-methylimidazolium) 3,6-diselanylidene-1,2,4,5-tetraselena-3,6-diphosphacyclohexane-3,6-diselenolate

Jason A. Cody,[a]* Grant C. B. Alexander[a] and Catherine Guillot-Deudon[b]

[a]Lake Forest College, 555 N. Sheridan Rd, Lake Forest, IL 60045, USA, and [b]Institut des Matériaux Jean Rouxel (IMN), UMR 6502 CNRS-Université de Nantes, 2 rue de la Houssinière, BP 32229, 44322 Nantes Cedex 03, France
Correspondence e-mail: cody@lakeforest.edu

Received 10 July 2013; accepted 22 July 2013

Key indicators: single-crystal X-ray study; T = 293 K; mean σ(C–C) = 0.007 Å; R factor = 0.029; wR factor = 0.063; data-to-parameter ratio = 31.5.

In the title compound, $2C_6H_{11}N_2^+\cdot P_2Se_8^{2-}$ or $[EMIM]_2P_2Se_8$ (EMIM = 1-ethyl-3-methylimidazolium), the anions, located about inversion centers between EMIM cations, exhibit a cyclohexane-like chair conformation. The cations are found in columns along the a axis, with centroid–centroid distances of 3.8399 (3) and 4.7530 (2) Å. The observed P—Se distances and Se—P—Se angles agree with other salts of this anion.

Related literature

For similar selenophosphate compounds, see: Biswas *et al.* (2010); Lin *et al.* (2012). For ionothermal reactions in room-temperature ionic liquids, see: Morris (2009); Parnham & Morris (2007); Cody *et al.* (2012). For the preparation of EMIM(BF_4), see: Egashira *et al.* (2006). For the structure of the $P_2Se_8^{2-}$ anion, see: Zhao *et al.* (1992); Rotter *et al.* (2008). For π–π interactions between imidazolium cations, see: Wilkes & Zaworotko (1993).

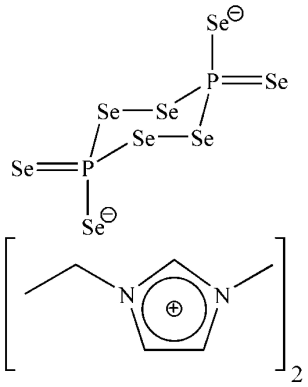

Experimental

Crystal data

$2C_6H_{11}N_2^+\cdot P_2Se_8^{2-}$
M_r = 915.96
Triclinic, $P\overline{1}$
a = 7.8885 (4) Å
b = 9.3783 (4) Å
c = 9.8039 (5) Å
α = 110.390 (3)°
β = 96.395 (4)°
γ = 102.992 (5)°
V = 648.00 (5) Å^3
Z = 1
Mo $K\alpha$ radiation
μ = 11.41 mm^{-1}
T = 293 K
0.19 × 0.07 × 0.03 mm

Data collection

Nonius KappaCCD diffractometer
Absorption correction: Gaussian [*JANA2006* (Petříček *et al.*, 2006) and *X-SHAPE* (Stoe & Cie, 1998)]
T_{min} = 0.204, T_{max} = 0.754
22118 measured reflections
3719 independent reflections
2622 reflections with $I > 2\sigma(I)$
R_{int} = 0.072

Refinement

$R[F^2 > 2\sigma(F^2)]$ = 0.029
$wR(F^2)$ = 0.063
S = 1.02
3719 reflections
118 parameters
H-atom parameters constrained
$\Delta\rho_{max}$ = 0.47 e Å^{-3}
$\Delta\rho_{min}$ = −0.55 e Å^{-3}

Table 1
Selected geometric parameters (Å, °).

P1—Se4	2.1104 (8)	P1—Se2^{i}	2.2809 (8)
P1—Se3	2.1334 (8)	Se1—Se2	2.3442 (5)
P1—Se1	2.2794 (9)		
Se4—P1—Se3	122.19 (4)	Se3—P1—Se2^{i}	100.49 (3)
Se4—P1—Se1	113.49 (4)	Se1—P1—Se2^{i}	104.32 (3)
Se3—P1—Se1	100.04 (3)	P1—Se1—Se2	102.89 (2)
Se4—P1—Se2^{i}	113.90 (4)	P1^{i}—Se2—Se1	102.37 (2)

Symmetry code: (i) $-x+1, -y, -z$.

Data collection: *COLLECT* (Hooft, 2009); cell refinement: *COLLECT*; data reduction: *COLLECT*; program(s) used to solve structure: *SHELXS97* (Sheldrick, 2008); program(s) used to refine structure: *SHELXL97* (Sheldrick, 2008); molecular graphics: *DIAMOND* (Brandenburg & Putz, 2012); software used to prepare material for publication: *SHELXL97*.

We thank Lake Forest College and Pays de la Loire for sabbatical support for JAC at the Institut des Matériaux Jean Rouxel (IMN) in Nantes, France. We also thank Stéphane Jobic for his assistance with this structure and sabbatical.

Supplementary data and figures for this paper are available from the IUCr electronic archives (Reference: NC2314).

References

Biswas, K., Zhang, Q., Chung, I., Song, J., Androulakis, J., Freeman, A. J. & Kanatzidis, M. G. (2010). *J. Am. Chem. Soc.* **132**, 14760–14762.
Brandenburg, K. & Putz, H. (2012). *DIAMOND*. Crystal Impact GbR, Bonn, Germany.
Cody, J. A., Finch, K. B., Reynders, G. J. III, Alexander, G. C. B., Lim, H. G., Näther, C. & Bensch, W. (2012). *Inorg. Chem.* **51**, 13357–13362.
Egashira, M., Yamamoto, Y., Fukutake, T., Yoshimoto, N. & Morita, M. (2006). *J. Fluorine Chem.* **127**, 1261–1264.
Hooft, R. W. W. (2009). *COLLECT*. Nonius BV, Delft, The Netherlands.
Lin, Y., Massa, W. & Dehnen, S. (2012). *Chem. Eur. J.* **18**, 13427–, 13434.
Morris, R. E. (2009). *Chem. Commun.* pp. 2990–2998.
Parnham, E. R. & Morris, R. E. (2007). *Acc. Chem. Res.* **40**, 1005–1013.

Petříček, V., Dušek, M. & Palatinus, L. (2006). *JANA2006*. Institute of Physics, Praha, Czech Republic.
Rotter, C., Schuster, M., Kidik, M., Schön, O., Klapötke, T. M. & Karaghiosoff, K. (2008). *Inorg. Chem.* **47**, 1663–1673.
Sheldrick, G. M. (2008). *Acta Cryst.* A**64**, 112–122.
Stoe & Cie (1998). *X-SHAPE*. Stoe & Cie, Darmstadt, Germany.
Wilkes, J. S. & Zaworotko, M. J. (1993). *Supramol. Chem.* **1**, 191–193.
Zhao, J., Pennington, W. T. & Kolis, J. W. (1992). *J. Chem. Soc. Chem. Commun.* pp. 265–266.

supplementary materials

Acta Cryst. (2013). E**69**, o1359–o1360 [doi:10.1107/S1600536813020308]

Bis(1-ethyl-3-methylimidazolium) 3,6-diselanylidene-1,2,4,5-tetraselena-3,6-diphosphacyclohexane-3,6-diselenolate

Jason A. Cody, Grant C. B. Alexander and Catherine Guillot-Deudon

Comment

Thiophosphate and selenophosphate compounds are sought for their interesting and fine-tunable electronic properties (Lin *et al.*, 2012). As new synthetic methods are often needed to gain access to new compounds with interesting properties, ionothermal reactions of thio- and selenophosphates were explored. Recently, room-temperature ionic liquids have received much interest for the preparation of inorganic materials (Morris, 2009; Parnham & Morris, 2007; Cody, *et al.*, 2012).

The structure of the anion in the title compound was first reported by Zhao *et al.* (1992) and the EMIM cation is well known. All interatomic distances and angles found in the current study (Fig. 1) are within normal ranges (Rotter *et al.*, 2008). Although the EMIM cations are found in columns in the title compound, the centroid-to-centroid distances of 3.8399 (3) Å and 4.7530 (2) Å (Fig. 2) indicate only weak pi-pi interactions (Wilkes & Zaworotko, 1993).

Experimental

The title compound was prepared by the literature method (Cody *et al.*, 2012) for ionothermal synthesis of related sulfur compounds. A total mass of 125 mg of the elements with a stoichiometry of Ni: 4P: 16Se was ground together in a glove box and then placed in a Pyrex tube. An aliquot of 1.25 ml of the ionic liquid $EMIMBF_4$, prepared according to the literature (Egashira, *et al.*, 2006), was added to the tube in a glove bag. The tube was then evacuated and sealed. The reaction mixture was heated at 150 °C for 96 h and then slowly cooled to room temperature at a rate of 0.5 °C/min. The tube was opened, the product mixture was filtered, and individual crystals were selected for analysis by hand. The products included black powder, large red blocks, and small yellow plates. The latter were both the title compound; the color difference is attributed to absorption effects from the thickness of the crystals. Although elemental nickel was included in the reaction mixture, it was not observed in the isolated crystalline products.

Refinement

All H atoms were positioned with idealized geometry and were refined isotropically with $U_{iso}(H) = 1.2\ U_{eq}(C)$ (1.5 for methyl H atoms) using a riding model with C—H = 0.93 Å for aromatic, 0.97 Å for methylene and 0.96 Å for methyl H-atoms.

Computing details

Data collection: *COLLECT* (Hooft, 2009); cell refinement: *COLLECT* (Hooft, 2009); data reduction: *COLLECT* (Hooft, 2009); program(s) used to solve structure: *SHELXS97* (Sheldrick, 2008); program(s) used to refine structure: *SHELXL97* (Sheldrick, 2008); molecular graphics: *DIAMOND* (Brandenburg & Putz, 2012); software used to prepare material for publication: *SHELXL97* (Sheldrick, 2008).

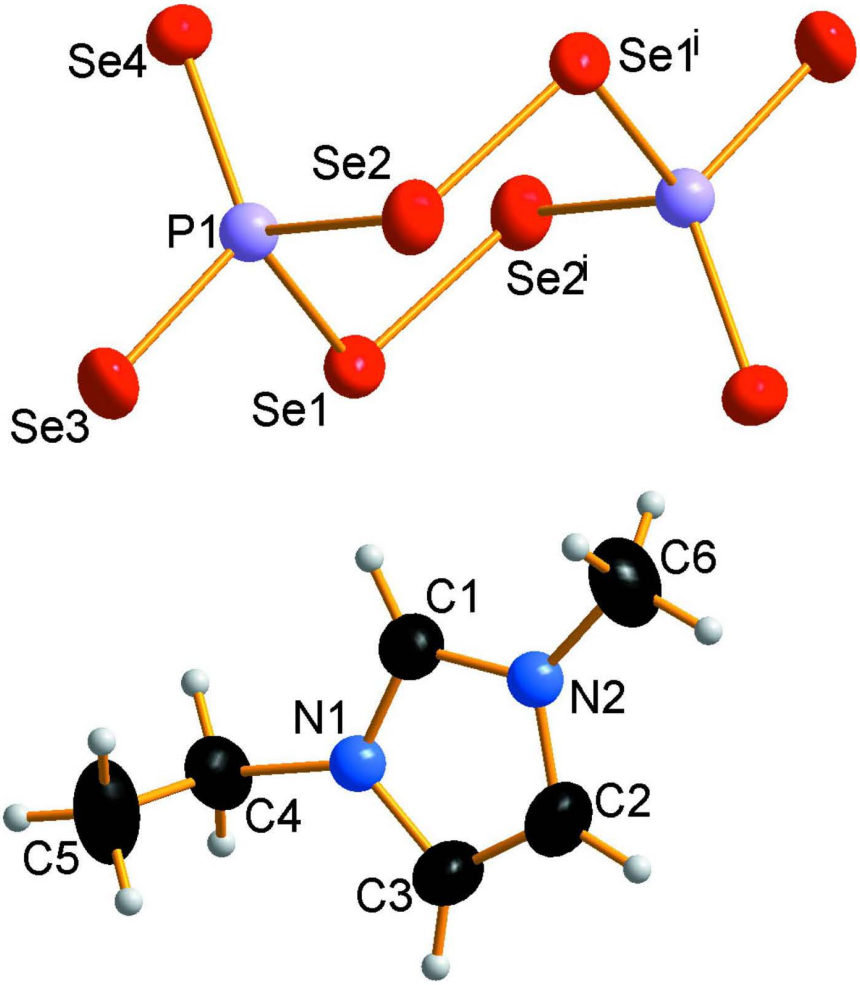

Figure 1

Molecular structure and atomic labeling scheme for the title compound. Thermal elipsoids are shown at the 50% level. Symmetry code for the generation of equivalent atoms: i = 1 - *x*, -*y*, -*z*.

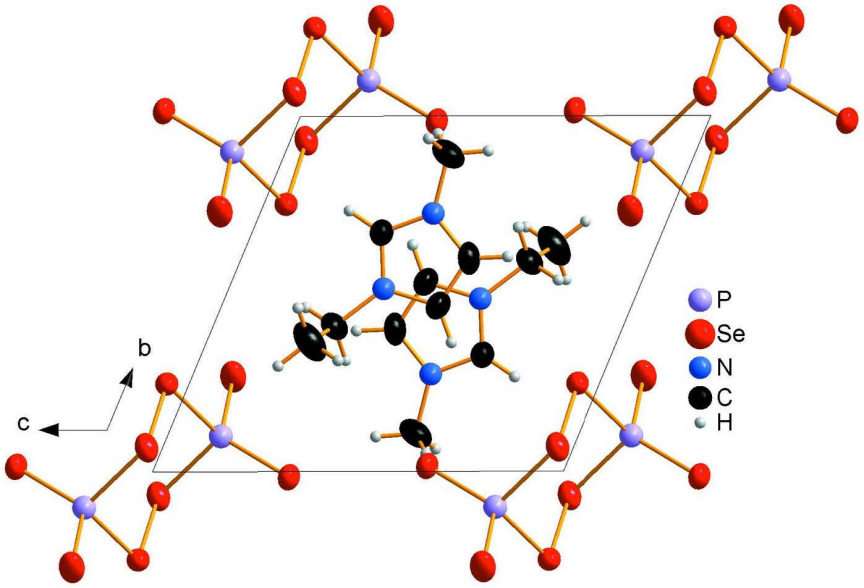

Figure 2

A packing diagram of the title compound showing the column of EMIM cations along the *a* axis.

Bis(1-ethyl-3-methylimidazolium) 3,6-diselanylidene-1,2,4,5-tetraselena-3,6-diphosphacyclohexane-3,6-diselenolate

Crystal data

$2C_6H_{11}N_2^+\cdot P_2Se_8^{2-}$
$M_r = 915.96$
Triclinic, $P\overline{1}$
Hall symbol: -P 1
$a = 7.8885$ (4) Å
$b = 9.3783$ (4) Å
$c = 9.8039$ (5) Å
$\alpha = 110.390$ (3)°
$\beta = 96.395$ (4)°
$\gamma = 102.992$ (5)°
$V = 648.00$ (5) Å^3
$Z = 1$
$F(000) = 424$
$D_x = 2.347$ Mg m^{-3}
Mo $K\alpha$ radiation, $\lambda = 0.71073$ Å
Cell parameters from 3719 reflections
$\theta = 6.5$–30.0°
$\mu = 11.41$ mm^{-1}
$T = 293$ K
Plate, yellow
0.19 × 0.07 × 0.03 mm

Data collection

Nonius KappaCCD diffractometer
Radiation source: fine-focus sealed tube
Unknown monochromator
ω scans
Absorption correction: gaussian [JANA2006 (Petříček *et al.*, 2006) and *X-SHAPE* (Stoe & Cie, 1998)]
$T_{min} = 0.204$, $T_{max} = 0.754$
22118 measured reflections
3719 independent reflections
2622 reflections with $I > 2\sigma(I)$
$R_{int} = 0.072$
$\theta_{max} = 30.0°$, $\theta_{min} = 6.5°$
$h = -10 \rightarrow 11$
$k = -13 \rightarrow 13$
$l = -13 \rightarrow 13$

Refinement

Refinement on F^2
Least-squares matrix: full
$R[F^2 > 2\sigma(F^2)] = 0.029$
$wR(F^2) = 0.063$
$S = 1.02$
3719 reflections
118 parameters
0 restraints
Primary atom site location: structure-invariant direct methods
Secondary atom site location: difference Fourier map
Hydrogen site location: inferred from neighbouring sites
H-atom parameters constrained
$w = 1/[\sigma^2(F_o^2) + (0.0252P)^2 + 0.2292P]$ where $P = (F_o^2 + 2F_c^2)/3$
$(\Delta/\sigma)_{max} < 0.001$
$\Delta\rho_{max} = 0.47$ e Å^{-3}
$\Delta\rho_{min} = -0.55$ e Å^{-3}

Special details

Experimental. A set of 280 frames were collected with a rotation of 2° per frame and an exposure time of 190 s; the crystal to detector distance was 25.00 mm. Refinements were done with the *SHELXTL97* (Sheldrick, 2008) software package; absorption correction was made with the program Jana2006 (Petricek *et al.*, 2006) using the program *X-SHAPE* (Stoe & Cie, 1998).

Geometry. All e.s.d.'s (except the e.s.d. in the dihedral angle between two l.s. planes) are estimated using the full covariance matrix. The cell e.s.d.'s are taken into account individually in the estimation of e.s.d.'s in distances, angles and torsion angles; correlations between e.s.d.'s in cell parameters are only used when they are defined by crystal symmetry. An approximate (isotropic) treatment of cell e.s.d.'s is used for estimating e.s.d.'s involving l.s. planes.

Refinement. Refinement of F^2 against ALL reflections. The weighted R-factor wR and goodness of fit S are based on F^2, conventional R-factors R are based on F, with F set to zero for negative F^2. The threshold expression of $F^2 > \sigma(F^2)$ is used only for calculating R-factors(gt) *etc.* and is not relevant to the choice of reflections for refinement. R-factors based on F^2 are statistically about twice as large as those based on F, and R- factors based on ALL data will be even larger.

Fractional atomic coordinates and isotropic or equivalent isotropic displacement parameters (Å^2)

	x	y	z	U_{iso}*/U_{eq}
P1	0.62769 (11)	−0.10004 (9)	0.13027 (9)	0.03455 (17)
Se1	0.38273 (4)	−0.24755 (3)	−0.05425 (4)	0.04208 (9)
Se2	0.21381 (4)	−0.06847 (4)	−0.03916 (4)	0.04234 (9)
Se3	0.77764 (6)	−0.26777 (5)	0.09996 (4)	0.05519 (11)
Se4	0.56642 (5)	0.01558 (4)	0.33743 (4)	0.04503 (10)
N1	0.2827 (4)	0.4858 (3)	0.3773 (3)	0.0413 (6)
N2	0.2005 (3)	0.2740 (3)	0.4218 (3)	0.0422 (6)
C1	0.2281 (4)	0.3279 (4)	0.3154 (4)	0.0415 (7)
H1	0.2122	0.2661	0.2148	0.050*
C2	0.2379 (5)	0.4007 (5)	0.5542 (4)	0.0530 (9)
H2	0.2298	0.3961	0.6465	0.064*
C3	0.2884 (5)	0.5333 (4)	0.5270 (4)	0.0525 (9)
H3	0.3210	0.6372	0.5965	0.063*
C4	0.3182 (5)	0.5911 (4)	0.2952 (4)	0.0486 (8)
H4A	0.3597	0.5382	0.2068	0.058*
H4B	0.4115	0.6869	0.3572	0.058*
C5	0.1558 (6)	0.6340 (6)	0.2513 (6)	0.0735 (13)
H5A	0.1832	0.7026	0.1986	0.110*
H5B	0.1156	0.6877	0.3388	0.110*
H5C	0.0641	0.5395	0.1883	0.110*
C6	0.1325 (5)	0.1069 (4)	0.3983 (5)	0.0606 (10)
H6A	0.1248	0.0980	0.4922	0.091*

H6B	0.2114	0.0496	0.3527	0.091*
H6C	0.0165	0.0634	0.3345	0.091*

Atomic displacement parameters (Å²)

	U^{11}	U^{22}	U^{33}	U^{12}	U^{13}	U^{23}
P1	0.0454 (4)	0.0353 (4)	0.0258 (4)	0.0132 (3)	0.0065 (3)	0.0144 (3)
Se1	0.0560 (2)	0.03274 (15)	0.03188 (17)	0.00568 (13)	0.00294 (14)	0.01201 (13)
Se2	0.03936 (17)	0.05217 (19)	0.03963 (19)	0.00924 (13)	0.00866 (14)	0.02474 (16)
Se3	0.0774 (3)	0.0598 (2)	0.0454 (2)	0.0411 (2)	0.01621 (19)	0.02586 (19)
Se4	0.0639 (2)	0.04233 (17)	0.02882 (17)	0.01506 (15)	0.01340 (15)	0.01247 (14)
N1	0.0472 (15)	0.0410 (14)	0.0361 (15)	0.0097 (11)	0.0087 (12)	0.0172 (12)
N2	0.0435 (14)	0.0439 (15)	0.0431 (16)	0.0089 (11)	0.0079 (12)	0.0239 (13)
C1	0.0461 (18)	0.0424 (16)	0.0338 (17)	0.0084 (13)	0.0078 (14)	0.0147 (14)
C2	0.063 (2)	0.066 (2)	0.036 (2)	0.0179 (18)	0.0138 (17)	0.0268 (19)
C3	0.071 (2)	0.0468 (18)	0.0329 (18)	0.0121 (17)	0.0126 (17)	0.0101 (16)
C4	0.054 (2)	0.0459 (18)	0.052 (2)	0.0092 (15)	0.0174 (17)	0.0277 (17)
C5	0.065 (3)	0.095 (3)	0.095 (4)	0.030 (2)	0.025 (2)	0.069 (3)
C6	0.064 (2)	0.051 (2)	0.075 (3)	0.0095 (17)	0.013 (2)	0.038 (2)

Geometric parameters (Å, º)

P1—Se4	2.1104 (8)	C2—C3	1.345 (5)
P1—Se3	2.1334 (8)	C2—H2	0.9300
P1—Se1	2.2794 (9)	C3—H3	0.9300
P1—Se2^{i}	2.2809 (8)	C4—C5	1.489 (5)
Se1—Se2	2.3442 (5)	C4—H4A	0.9700
Se2—P1^{i}	2.2809 (8)	C4—H4B	0.9700
N1—C1	1.332 (4)	C5—H5A	0.9600
N1—C3	1.370 (4)	C5—H5B	0.9600
N1—C4	1.477 (4)	C5—H5C	0.9600
N2—C1	1.327 (4)	C6—H6A	0.9600
N2—C2	1.366 (4)	C6—H6B	0.9600
N2—C6	1.463 (4)	C6—H6C	0.9600
C1—H1	0.9300		
Se4—P1—Se3	122.19 (4)	C2—C3—H3	126.6
Se4—P1—Se1	113.49 (4)	N1—C3—H3	126.6
Se3—P1—Se1	100.04 (3)	N1—C4—C5	111.4 (3)
Se4—P1—Se2^{i}	113.90 (4)	N1—C4—H4A	109.3
Se3—P1—Se2^{i}	100.49 (3)	C5—C4—H4A	109.3
Se1—P1—Se2^{i}	104.32 (3)	N1—C4—H4B	109.3
P1—Se1—Se2	102.89 (2)	C5—C4—H4B	109.3
P1^{i}—Se2—Se1	102.37 (2)	H4A—C4—H4B	108.0
C1—N1—C3	108.8 (3)	C4—C5—H5A	109.5
C1—N1—C4	125.1 (3)	C4—C5—H5B	109.5
C3—N1—C4	126.0 (3)	H5A—C5—H5B	109.5
C1—N2—C2	108.5 (3)	C4—C5—H5C	109.5
C1—N2—C6	125.1 (3)	H5A—C5—H5C	109.5
C2—N2—C6	126.3 (3)	H5B—C5—H5C	109.5

N2—C1—N1	108.3 (3)	N2—C6—H6A	109.5
N2—C1—H1	125.9	N2—C6—H6B	109.5
N1—C1—H1	125.9	H6A—C6—H6B	109.5
C3—C2—N2	107.8 (3)	N2—C6—H6C	109.5
C3—C2—H2	126.1	H6A—C6—H6C	109.5
N2—C2—H2	126.1	H6B—C6—H6C	109.5
C2—C3—N1	106.7 (3)		

Symmetry code: (i) $-x+1, -y, -z$.

References

1. Kanatzidis, M. G.; Poeppelmeier, K. R. *Prog. Solid State Chem.* **2007,** 1-133.

2. Davis, M. E. *Chem. Mater.* **2013,** *26*, 239-245.

3. Housecroft, C. E.; Sharpe, A. G. *Inorganic Chemistry,* 4th ed.; Pearson: Essex, U. K., 2012; p 469-470.

4. Cook, T. R.; Zheng, Y. R.; Stang, P. J. *Chem. Rev.* **2013,** *113*, 734-777.

5. Buser, H. J.; Schwarzenbach, D.; Petter, W.; Ludi, A. *Inorg. Chem.* **1977,** *16*, 2704-2710.

6. Iwamoto, T.; Miyoshi, T.; Sasaki, Y. *Acta. Crystallogr.* **1974,** *B30*, 292-295.

7. Hoskins, B. F.; Robson, R. J. *J. Am. Chem. Soc.* **1989,** *111*, 5962-5964.

8. Fujita, M.; Kwon, Y.; Washizu, S.; Ogura, K. *J. Am. Chem. Soc.* **1994,** *116*, 1151-1152.

9. Sumida, K.; Rogow, D. L.; Mason, J. A.; McDonald, T. M.; Bloch, E. D.; Herm, Z. R.; Bae, T. H.; Long, J. R. *Chem. Rev.* **2012,** *112*, 724-781.

10. Suh, M. P.; Park, H. J.; Prasad, T. K.; Lim. D. W. *Chem. Rev.* **2012,** *112*, 782-835.

11. Kreno, L. E.; Leong, K.; Farha, O. K.; Allendorf, M.; Van Duyne, R. P.; Hupp, J. T. *Chem. Rev.* **2012,** *112*, 1105-1125.

12. Li, J. R.; Sculley, J.; Zhou, H. C. *Chem. Rev.* **2012,** *112*, 869-932.

13. Wang, C.; Zheng, M.; Lin, W. *J. Phys. Chem. Lett.* **2011**, *2*, 1701-1709.

14. Rosi, N. L.; Eckert, J.; Eddaoudi, M.; Vodak, D. T.; Kim, J.; O'Keeffe, M.; Yaghi, O. M. *Science*, **2003,** *300*, 1127-1129.

15. Dolbecq, A.; Dumas, E.; Mayer, C. R.; Mialane, P. *Chem. Rev.* **2010,** *110*, 6009-6048.

16. Ishii, Y.; Takenaka, Y.; Konishi, K. *Angew. Chem., Int. Ed.* **2004,** *43*, 2702-2705.

17. Férey, G.; Mellot-Draznicks, C.; Serre, C.; Millange, F.; Dutour, J.; Surble, S.; Margiolaki, I. *Science*, **2005,** *309*, 2040-2042.

18. Maksimchuk, N. V.; Timofeeva, M. N.; Melgunov, M. S.; Shmakov, O. A. *J. Catal*. **2008,** *257*, 315-323.

19. Clemente-Juan, J. M.; Coronado, E. *Coord. Chem. Rev.* **1999,** *193-195*, 361-394.

20. Kögerler, P.; Tsukerblat, B.; Müller, *Dalton Trans*. **2010,** *39*, 21-36.

21. Keita, B.; Liu, T. B.; Nadjo, L. *J. Mater. Chem.* **2009,** *19*, 19-33.

22. Rhule, J. T.; Craig, L. H.; Judd, D. A. *Chem. Rev.* **1998,** *98*, 327-357.

23. Hasenknopf, B. *Biosci.* **2005,** *10*, 275-287.

24. Walden, P. *Bull. Acad. Impér. Sci. St. Pétersbourg.* **1914,** *8*, 405-422.

25. Plechkova, N. V.; Seddon, K. R. *Chem. Soc. Rev.* **2008,** *37*, 123-150.

26. Housecroft, C. E.; Sharpe, A. G. *Inorganic Chemistry;* 4th ed.; Pearson: Essex, U. K., 2012; p 288.

27. Parnham, E. R.; Morris, R. E. *Acc. Chem. Res.* **2007,** *40*, 1005-1013.

28. Hallet, J. P.; Welton, T. *Chem. Rev.* **2011,** *111*, 3508-3576.

29. Lee. S. G. *Chem. Commun.* **2006,** 1049-1063.

30. Parvulescu, V. I.; Hardacre, C. *Chem. Commun.* **2007,** *107*, 2615-2665.

31. Morris, R. E. *Chem. Commun.* **2009,** 2990-2298.

32. Zhang, S. J.; Sun, N.; He, S. H.; Lu, X. M.; Zhang, X. P. *J. Phys. Chem. Ref. Data.* **2005,** 35, 1475-1517.

33. Ahmed, E.; Ruck, M. *Angew. Chem., Int. Ed.* **2012,** *51*, 308-309.

34. Cooper, E. R.; Andrews, C. D.; Wheatley, P. S.; Webb, P. E.; Wormald, P.; Morris, R. E. *Nature* **2004,** *430*, 1012-1016.

35. Lin, Z.; Wragg, D. S.; Wright, P. A.; Warren, J. E.; Morris, R. E. *J. Am. Chem. Soc.* **2007,** *129*, 10334-10335.

36. Zhang, N.; Liu, Q.; Wan, Y. *Inorg. Chem. Commun.* **2010,** *13*, 706-710.

37. Xe, Z.; Feng, M.; Li, J.; Huang, X. *Inorg. Chem. Commun.* **2008,** *11*, 1143-1146.

38. Zou, N.; Chen, W.; Li, Y.; Liu, W.; Wang, E. *Inorg. Chem. Commun.* **2008,** *11*, 1367-1370.

39. Biswas, K.; Zhang, Q.; Chung, I.; Song, J.; Androulakis, J.; Freeman, A. J.; Kanatzidis, M. G. *J. Am. Chem. Soc.* **2010,** *132*, 14760-14762.

40. Ding, N.; Kanatzidis, M. G. *Angew. Chem., Int. Ed.* **2006,** *45*, 1397-1401.

41. Hsu, K. F.; Loo, S.; Guo, F.; Chen, W.; Dyck, J. S.; Uher, C.; Hogan, T.; Polychroniadis, E. K.; Kanatzidis, M. G. *Science* **2004,** *303*, 818-821.

42. Wu, Y.; Bensch, W. *Cryst. Eng. Comm.* **2010,** *12*, 1003-1015.

43. Sayettat, J.; Bull, L. M.; Gabriel, J. P.; Jobic, S.; Camerel, F.; Marie, A.; Fourmigué, M.; Batail, P.; Brec, R.; Inglebert, R. *Angew. Chem., Int. Ed.* **1998,** *37*, 1711-1714.

44. Sayettat, J.; Bull, L. M.; Jobic, S.; Gabriel, J. P.; Fourmigué, M.; Batail, P.; Brec, R.; Inglebert, R.; Sourisseau, C. *J. Mater. Chem.* **1999,** *9*, 143-153..

45. Cody, J. A.; Finch, K. B.; Reynders, G. J. III; Alexander, G. C. B.; Lim, H. G.; Näther, C.; Bensch, W. *Inorg. Chem.* **2012,** *51*, 13357-13362.

46. Finch, K. Ionic Liquids for Materials Synthesis: Preparation and Characterization of $[EMIM]_7[Ni_4P_{13}S_{36}]$ (EMIM = 1-ethyl-3-methyl-imidazoilum). Senior Thesis, Lake Forest College, **2007**.

47. Brown, J. Toward the Synthesis of New Zinc Thiophosphate Compounds in Ionic Liquids. Senior Thesis, Lake Forest College, **2008**.

48. Constantinescu, A. S. Nickel Thiophosphate Synthesis in Ionic Liquids. Senior Thesis, Lake Forest College, **2008**.

49. Larson, N. R. An Investigation into the use of the Ionic Liquids EMIM Methyl Sulfate and EMIM Triflate for Ionothermal Synthesis. Senior Thesis, Lake Forest College, **2010**.

50. Reynders, G. J. III. Ionothermal Synthesis of Novel Nickel Thiophosphates: $[EMIM]_7Ni_4P_{13}S_{36}$ and $[EMIM]_4NiP_6S_{18}$. Senior Thesis, Lake Forest College, **2011**.

51. Egashira, M.; Yamamoto, Y.; Fukutake, T.; Yoshimoto, N.; Morita, M. *J. Fluorine Chem.* **2006,** *127*, 1261-1264.

52. Bonhôte, P.; Dias, A.; Papageorgiou, N.; Kalyanasundaram, K.; Grätzel, M. *Inorg. Chem.* **1996,** *35*, 1168-1178.

53. Gruber, H.; Müller, U. *Z. Anorg. Allg. Chem.* **1997,** *623*, 957-961.

54. Falius, H.; Schliephake, A. *Z. Anorg. Allg. Chem.* **1992,** *611*, 141-148.

55. Dastychová, L.; Sotolářová, M.; Dastych, D.; Taraba, J.; Nečas, M.; Příhoda, J. *Polyhedron* **2007,** *26*, 4250-4256.

56. Wolf, G.; Meisel, M. *Z. Anorg. Allg. Chem.* **1982,** *494*, 49-54.

57. Cowley, A. H.; Hellert, D.; Gabbai, F. P.; Olbrich, F. *Inorg. Chem.* **1995,** *34*, 3127-3129.

58. Hanko, J. A.; Sayettat, J.; Jobic, S.; Brec, R.; Kanatzidis, M. G. *Chem. Mater.* **1998,** *10*, 3040-3049.

59. Holder, A. A. *Annu. Rep. Chem., Sect. A: Inorg. Chem.* **2012,** *108*, 166-175.

60. Bonamico, M. *Ric. Sci.*. **1968,** *38*, 1106-1107.

61. Merlino, S.; Satori, F. *Acta. Crystallogr.* **1972,** *B28*, 972.

62. Goh, Y. G.; Weng, Z.; Leong, W. K.; Leung, H. L. *Angew. Chem. Int. Ed.* **2001,** *40*, 3236-3239.

63. Cody, J. A. Alexander, G. C. B.; Guillot-Deudon, C. *Acta. Crystallogr.* **2013,** *E69*, 1359-1360.

64. Zhao, J.; Pennington, W. T.; Kolis, J. W. *J. Chem. Soc. Chem. Commun.* **2012,** pp. 265-266.

65. Rotter, C.; Schuster, M.; Kidik, M.; Schön, O.; Klapötke, T. M.; Karaghiosoff, K. *Inorg. Chem.* **2008,** *47*, 1663-1673.

66. Shannon, R. D. *Acta. Crystalollogr.* **1976,** *A32*, 751-767.

67. Maganas, D.; Staniland, S. S.; Grigoropoulos, A.; White, F.; Parsons, S.; Robertson, N.; Kyritsis, P.; Pneumatikakis, G. *Dalton Trans.* **2006,** *19*, 2301-2315.

68. Jian, F. F.; Wang, J.; Xaio, H. L.; Zhao, P. S.; Sun, P. P.; Huang, L. H. *Dalton Trans.* **2010,** *39*, 11045-11052.

69. Ratnani, R.; Srivastava, G.; Mehrotra, R. C. *Trans. Met. Chem. (Dordrecht, Neth.).* **1992,** *17*, 137-140.

70. Borgs, G.; Keck, H.; Kuchen, W.; Mootz, D.; Wiskemann, R.; Wunderlich, H. *Z. Naturforsch., B: J. Chem. Sci.* **1991,** *46*, 1525-1531.

71. Lin, Z. *Acc. Chem. Res.* **2010,** *43*, 602-611.

72. Bencini, A. *Inorg. Chem. Acta.* **2008,** *361*, 3280-3831.

73. Teng, F.; Jiang, N.; Wang, Z.; Cui, Y.; Wang, J. *J. Serb. Chem. Soc.* **2012,** *77*, 1-16.

74. Fey, N.; Orpen, A. G.; Harvey, J. N. *Coord. Chem. Rev.* **2009,** *253*, 704-722.

75. Aleksandrov, H. A.; Zdravkova, V. R.; Mihaylov, M. Y.; Petkov, P. S.; Vayssilov, G. N.; Hadjivanov, K. I. *J. Phys. Chem. C.* **2012,** *116*, 22823-22831.

76. Noel, Y.; De, L. P., M.; Maschio, L; Rerat, M.; Zicovich-Wilson, C. M.; Dovesi, R. *Int. J. Quantum Chem.* **2012,** *112*, 2098-2108.

77. Foresman, J. B.; Frisch. Æ. *Exploring Chemistry with Electronic Structure Methods*, 2nd ed.; Gaussian: Pittsburgh PA, 1996.

78. Frisch, M. J.; Trucks, G. W.; Schlegel, H. B.; Scuseria, G. E.; Robb, M. A.; Cheeseman, J. R.; Scalmani, G.; Barone, V.; Mennucci, B.; Petersson, G. A.; Nakatsuji, H.; Caricato, M.; Li, X.; Hratchian, H. P.; Izmaylov, A. F.; Bloino, J.; Zheng, G.; Sonnenberg, J. L.; Hada, M.; Ehara, M.; Toyota, K.; Fukuda, R.; Hasegawa, J.; Ishida, M.; Nakajima, T.; Honda, Y.; Kitao, O.; Nakai, H.; Vreven, T.; Montgomery, J. A., Jr.; Peralta, J. E.; Ogliaro, F.; Bearpark, M.; Heyd, J. J.; Brothers, E.; Kudin, K. N.; Staroverov, V. N.; Kobayashi, R.; Normand, J.; Raghavachari, K.; Rendell, A.; Burant, J. C.; Iyengar, S. S.; Tomasi, J.; Cossi, M.; Rega, N.; Millam, N. J.; Klene, M.; Knox, J. E.; Cross, J. B.; Bakken, V.; Adamo, C.; Jaramillo, J.; Gomperts, R.; Stratmann, R. E.; Yazyev, O.; Austin, A. J.; Cammi, R.; Pomelli, C.; Ochterski, J. W.; Martin, R. L.; Morokuma, K.; Zakrzewski, V. G.; Voth, G. A.; Salvador, P.; Dannenberg, J. J.; Dapprich, S.; Daniels, A. D.; Farkas, Ö.; Foresman, J. B.; Ortiz, J. V.; Cioslowski, J.; Fox, D. J. *Gaussian 09.* Gaussian, Inc.: Wallingford CT, 2009.

79. Dunning, T. H.; Hay, P. J. *Modern Theoretical Chemistry*; Schaefer, H. F., III, Ed.; Plenum: New York, 1976; Vol. 3, p 1.

80. Hay, P. J.; Wadt, W. R. *J. Chem. Phys.* **1985,** *82*, 270-283.

81. Francl, M. M.; Pietro W. J.; Hehre, W. J.; Binkley, J. S.; Gordon, M. S.; DeFrees, D. J.; Pople, J. A. *J.Chem.Phys.* **1982**, *77*, 3654-3665

82. (a) Becke, A. D. *Phys. Rev. A: At., Mol., Opt. Phys.* **1988,** *38*, 3098-3010 (b) Lee, C.; Yang, W.; Parr, R. G. *Phys. Rev. B: Condens. Matter Mater. Phys.* **1988,** *37*, 785-789 (c) Stephens, P. J.; Devlin, F. J.; Chabalowski, C. F.; Frisch, M. J. *J. Phys. Chem.* **1994,** *98*, 11623-11627.

83. Macrae, C. F.; Bruno, I. J.; Chisholm, J. A.; Edgington, P. R.; McCabe, P.; Pidcock, E.; Rodriguez-Monge, L.; Taylor, R.; van de Streek, J.; Wood, P. A. *J. Appl. Cryst.* **2008,** *41*, 466-470.

84. (a) Becke, A. D. *Phys. Rev. A: At., Mol., Opt. Phys.* **1988,** *38*, 3098-3010 (b) Perdew, J. P. *Electronic Structure of Solids '91*; Ziesche, P., Eschig, H., Eds.; Akademie Verlag: Berlin, 1991; p 11 (c) Becke, A. D. *J. Chem. Phys.* **1993,** *98*, 5648-5652.

85. (a) Perdew, J. P. *Electronic Structure of Solids '91*; Ziesche, P., Eschig, H., Eds.; Akademie Verlag: Berlin, 1991; p 11 (b) Adamo, C.; Barone, V. J. *Chem. Phys.* **1998,** *108*, 664-675.